The Development of a Lead-Free Replacement for the Lindlar Catalyst for Alkyne Semi-Hydrogenation Using Silica Supported, N-doped Carbon Modified Cobalt Nanoparticles

Peter McNeice,[a] Marc-André Müller,[b] Jonathan Medlock,[b] Werner Bonrath,[b] Nils Rockstroh,[a] Stephan Bartling,[a] Henrik Lund,[a] Kathrin Junge,*[a] and Matthias Beller*[a]

[a]Leibniz-Institut für Katalyse e.V., Albert-Einstein-Straße 29a, 18059 Rostock, Germany

[b] DSM Nutritional Products Ltd. P.O. Box 2676, 4002 Basel (Switzerland)

57 Pages S1-S57

61 Figures S1-S61

12 Tables S1-S12

Contents

S1 General Remarks

Unless otherwise stated, reactions were performed in autoclaves. Solvents were used directly without further purification. NMR spectra were recorded on Bruker AV 300 and 400 spectrometers. All chemical shifts (δ) are reported in parts per million (ppm) and coupling constants (J) in Hz. All chemical shifts are reported relative to tetramethylsilane (δ = 0.0 for 1H NMR in CDCl) and d-solvent peaks (δ = 77.00 for 13C NMR, chloroform), respectively. Gas chromatography was performed on a HP 6890 with a HP5 column (Agilent).

XRD (X-ray diffraction) powder pattern were recorded either on a Panalytical X'Pert diffractometer equipped with a Xcelerator detector used with automatic divergence slits and Cu Kα radiation (40 kV, 40 mA). Cu beta radiation was excluded by using nickel filter foil. The measurements were performed with 0.005 $°s^{-1}$. Samples were mounted on silicon zero background holders. Obtained intensities were converted from automatic to fixed divergence slits (0.25°) for further analysis. Peak positions and profile were fitted with Pseudo-Voigt function using the HighScore Plus software package (Panalytical). Phase identification was done by using the PDF-2 database of the International Center of Diffraction Data (ICDD).

Crystallite size is calculated by applying the Scherrer equation using the integral breadth under the assumption of spherically shaped crystallites. K is set to 1.0747. For fcc Co 111, 200 and 220, for hcp Co 100, 002 and 101 Bragg peak parameter are used for calculation of sizes. The average value is presented.

Scanning Transmission Electron Microscopy (STEM) measurements were performed at 200kV with an aberration-corrected JEM-ARM200F (JEOL, Corrector: CEOS). Energy-dispersive X-ray (EDX) analysis is done with a JED-2300 (JEOL) energy-dispersive X-ray spectrometer having a silicon drift detector (dry SD60GV). The microscope is further equipped with an Enfinium ER (Gatan) electron energy loss spectrometer (EELS). For STEM imaging a High-Angle Annular Dark Field (HAADF) and an Annular Bright Field (ABF) detector were used, while an Annular Dark Field (ADF) detector was used during EELS acquisition. A holey carbon supported Cu-grid (mesh 300) was used for the dry deposition of the solid samples without any pre-treatment. Subsequently, the grid was transferred to the microscope.

The XPS (X-ray Photoelectron Spectroscopy) measurements were performed on a ESCALAB 220iXL (ThermoFisher Scientific) with monochromated Al-Kα radiation (E = 1486.6 eV). The electron binding energies EB were obtained with charge compensation using a flood electron source. The binding energies were referenced to the C1s peak of C-C and C-H bonds at 284.8 eV. For quantitative analysis the peaks were deconvoluted with Gaussian-Lorentzian curves, the peak areas were divided by a sensitivity factor obtained from the element specific Scofield factor and the transmission function of the spectrometer.

The metal precursors $Co(OAc)_2.4H_2O$ (98 %), $Fe(OAC)_2$ (99.99 %), and $Cu(OAc)_2$.H2O (98 %) were obtained from Sigma Aldrich. $Mn(OAc)_2.4H_2O$ (99+ %) was purchased from Strem. Melamine (99%) was purchased from Alfa Aesar. SiO_2 (Aerosil OX-50) was obtained from Evonik. DIP was provided by DSM. All semi-hydrogenation substrates were purchased from commercial sources. All reagents were used directly without further purification prior to use.

S2 Catalyst Synthesis

The syntheses of Co/Mel@SiO_2 catalysts are available in the main manuscript.

S2.1 1:1-Fe/Mel@SiO_2

In a 250 mL round bottomed flask $Fe(OAc)_2$ (0.16 g, 0.91 mmol), melamine (0.11 g, 0.91 mmol) and EtOH (30 mL) were stirred at RT for 15 mins. An orange-brown solution with some suspended melamine formed. The flask was placed in an oil bath pre-heated to 60 °C and stirred for 1 h. A bright yellow solution formed. SiO_2 (Aerosil OX50, 1.27 g) was added so that the Fe was ca. 4 wt. % SiO_2. The suspension was stirred at RT overnight (22 h). Solvent was removed *via* rotary evaporation (45 °C, 80 mbar) to leave a yellow powder which was dried overnight (19 h) at RT under high vacuum. The dry solid was ground to a fine powder and 0.918 g placed in a crucible with a lid. The crucible was placed in an oven (Dekema Austromat 624) which was evacuated to ca. 5 mbar and then flushed with argon. The oven was heated to 800 °C with a heating rate of 25 °C/min. The oven was held at the final temperature for 2 h, purging with argon the entire time. The oven was allowed to cool to room temperature, the crucible removed, and the catalyst (black powder, 0.788 g) yield transferred to a sample *via*l for storage.

S2.2 1:1-Mn/Mel@SiO_2

In a 250 mL round bottomed flask $Mn(OAc)_2.4H_2O$ (0.19 g, 0.79 mmol), melamine (0.10 g, 0.79 mmol) and EtOH (30 mL) were stirred at RT for 15 mins. A colourless solution with some suspended melamine formed. The flask was placed in an oil bath pre-heated to 60 °C and stirred for 1 h. A brown solution formed. SiO_2 (Aerosil OX50, 1.08 g) was added so that the Mn was ca. 4 wt. % SiO_2. The suspension was stirred at RT overnight (22 h). Solvent was removed *via* rotary evaporation (45 °C, 80 mbar) to leave a pale pink powder which was dried overnight (19 h) at RT under high vacuum. The dry solid was ground to a fine powder and 0.842 g was placed in a crucible with a lid. The crucible was placed in an oven (Dekema Austromat 624) which was evacuated to ca. 5 mbar and then flushed with argon. The oven was heated to 800 °C with a heating rate of 25 °C/min. The oven was held at the final temperature for 2 h, purging with argon the entire time. The oven was allowed to cool to room temperature, the crucible removed, and the catalyst (grey powder, 0.715 g) transferred to a sample *via*l for storage.

S2.3 1:1-Cu/Mel@SiO_2

In a 250 mL round bottomed flask $Cu(OAc)_2$ (0.123 g, 0.67 mmol), melamine (0.850 g, 0.67 mmol), EtOH (40 mL) and distilled water (1 mL) were stirred at RT for 15 mins. A blue-green solution with some suspended melamine formed. The flask was placed in an oil bath pre-heated to 60 °C and stirred for 1 h. Some melamine remained undissolved. SiO_2 (Aerosil OX50, 1.07 g) was added so that the Cu was ca. 4 wt. % relative to SiO_2. The suspension was stirred at RT overnight (22 h). Solvent was removed *via* rotary evaporation (45 °C, 80 mbar) to leave a green powder which was dried overnight (19 h) at RT under high vacuum. The dry solid was ground to a fine powder and 0.985 g was placed in a crucible with a lid. The crucible was placed in an oven (Dekema Austromat 624) which was evacuated to ca. 5 mbar and then flushed with argon. The oven was heated to 800 °C with a heating rate of 25 °C/min. The oven was held at the final temperature for 2 h, purging with argon the entire time. The oven was allowed to cool to room temperature, the crucible removed, and the catalyst (white powder, 0.530 g) transferred to a sample *via*l for storage.

S2.4 1:1-Co/Phenanthroline@SiO_2

In a 250 mL round bottomed flask $Co(OAc)_2.4H_2O$ (0.14 g, 0.56 mmol), 1,10-phenanthroline monohydrate (0.10 g, 0.57 mmol) and EtOH (20 mL) were stirred for 15 mins at RT and an orange-pink solution formed. The flask was placed in an oil bath pre-heated to 60 °C and stirred for 1 h. SiO_2 (Aerosil OX50, 0.82 g) was added so that the Co was ca. 4 wt. % SiO_2. The suspension was stirred at

RT overnight (22 h). Solvent was removed *via* rotary evaporation (45 °C, 80 mbar) to leave an pink powder which was dried overnight (19 h) at RT under high vacuum. The dry solid was ground to a fine powder and 0.367 g placed in a crucible with a lid. The crucible was placed in an oven (Dekema Austromat 624) which was evacuated to ca. 5 mbar and then flushed with argon. The oven was heated to 800 °C with a heating rate of 25 °C/min. The oven was held at the final temperature for 2 h, purging with argon the entire time. The oven was allowed to cool to room temperature, the crucible removed, and the catalyst (0.340 g) transferred to a sample *via*l for storage.

S2.5 Co/Chitin@SiO_2

In a 250 mL round bottomed flask $Co(OAc)_2.4H_2O$ (0.17 g, 0.69 mmol), chitin (1.02 g, Co is ca. 4 wt. % chitin) and EtOH (30 mL) were stirred for 15 mins at RT to form a bright pink-purple solution with some insoluble chitin suspended. The flask was placed in an oil bath pre-heated to 60 °C and stirred for 1 h. The chitin remained insoluble. SiO_2 (Aerosil OX50, 1.08 g) was added so that the Co was ca. 4 wt. % SiO_2. The suspension was stirred at RT overnight (22 h). Solvent was removed *via* rotary evaporation (45 °C, 80 mbar) to leave a pink powder which was dried overnight (19 h) at RT under high vacuum. The dry solid was ground to a fine powder and 0.505 g placed in a crucible with a lid. The crucible was placed in an oven (Dekema Austromat 624) which was evacuated to ca. 5 mbar and then flushed with argon. The oven was heated to 800 °C with a heating rate of 25 °C/min. The oven was held at the final temperature for 2 h, purging with argon the entire time. The oven was allowed to cool to room temperature, the crucible removed, and the catalyst (0.299 g) transferred to a sample *via*l for storage.

S3 Co/Mel@SiO_2 Catalyst Characterisation

S3.1 Elemental Analysis

Table S1: Elemental analysis (C, H, N, Co) and XPS analysis (Co) of Co/Mel@SiO_2 catalysts.

		Elemental analysis				XPS
Entry	**Catalyst**	**C (wt. %)**	**H (wt. %)**	**N (wt. %)**	**Co (wt. %)[a]**	**Co (wt. %)[b]**
1	1:0.5-Co/Mel@SiO_2	0.49	0.09	0.21	4.15	2.86
2	1:1-Co/Mel@SiO_2	1.34	0.22	0.15	4.49	3.07
3	1:5-Co/Mel@SiO_2	1.37	0.06	0.17	5.22	1.27
4	1:10-Co/Mel@SiO_2	2.28	0.17	1.22	5.01	0.27

[a]Determined by atomic absorption. [b]Determined by XPS and converted from atomic %.

S3.2 X-Ray Diffraction (XRD) Analysis

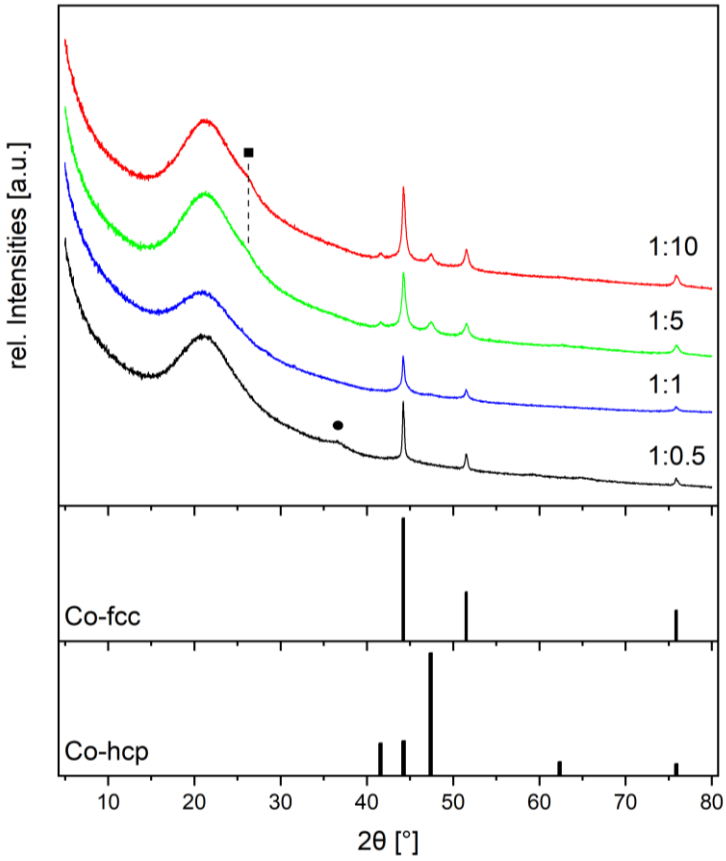

Figure S1: Powder diffraction pattern of prepared catalysts applying different cobalt to melamine ratios, respectively. Reference Bragg peak positions given below: ICDD pdf-2 00-015-086 (Co-fcc) and ICDD pdf-2 00-089-4308 (Co-hcp). Black circle represents Co_3O_4, black square graphitic carbon respectively.

Table S2: Calculated crystallite sizes according to Scherrer equation.

Entry	sample	Co modification	average size [nm]
1	1:0.5-Co/Mel@SiO_2	fcc	31
2	1:1-Co/Mel@SiO_2	fcc	4/37[a]
3	1:5-Co/Mel@SiO_2	fcc	13
		hcp	7
4	1:10-Co/Mel@SiO_2	fcc	15
		hcp	9

[a]Presented values are obtained from peak parameters under the assumption of a bi-modal size distribution. Peak position in deconvolution process was constrained for both peaks, each used to describe one of the size modes.

S3.3 X-Ray Photoelectron Spectroscopy (XPS) Analysis

Table S3: XPS elemental quantification table.

Entry	Catalyst	C [at.%]	O [at.%]	Si [at.%]	N [at.%]	Co [at.%]
1	1:0.5-Co/Mel@SiO_2	4.2	60.2	34.5	0.1	1.0
2	1:1-Co/Mel@SiO_2	6.5	57.5	34.2	0.7	1.1
3	1:5-Co/Mel@SiO_2	5.2	58.4	33.9	2.1	0.4
4	1:10-Co/Mel@SiO_2	8.9	56.2	32.0	2.8	0.1

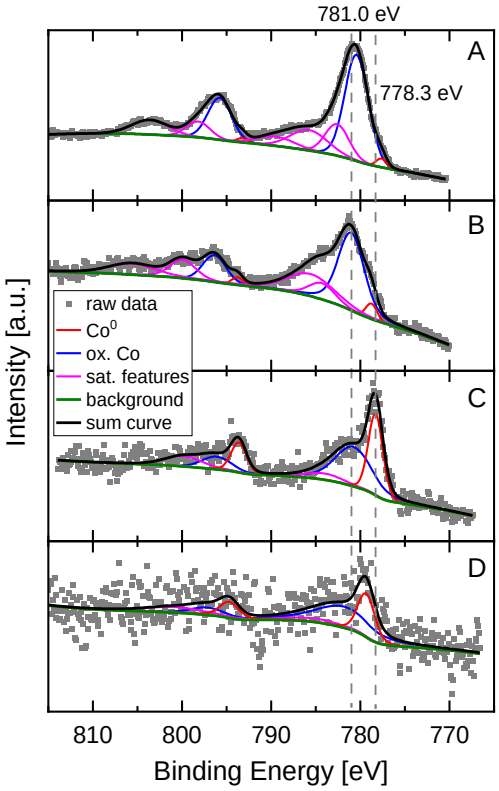

Figure S2: The Co 2p XPS region of A) 1:0.5-Co/Mel@SiO_2. B) 1:1-Co/Mel@SiO_2. C) 1:5-Co/Mel@SiO_2. D) 1:10-Co/Mel@SiO_2.

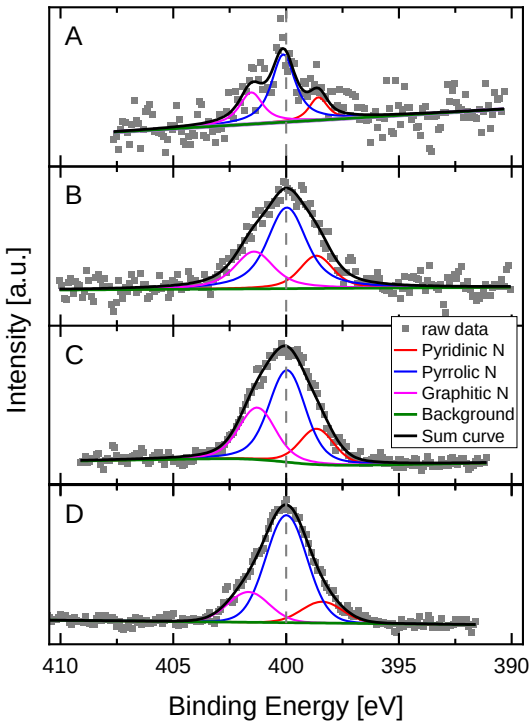

Figure S3: The N 1s XPS region of A) 1:0.5-Co/Mel@SiO_2. B) 1:1-Co/Mel@SiO_2. C) 1:5-Co/Mel@SiO_2. D) 1:10-Co/Mel@SiO_2.

S3.4 Scanning Transmission Electron Microscopy (STEM)

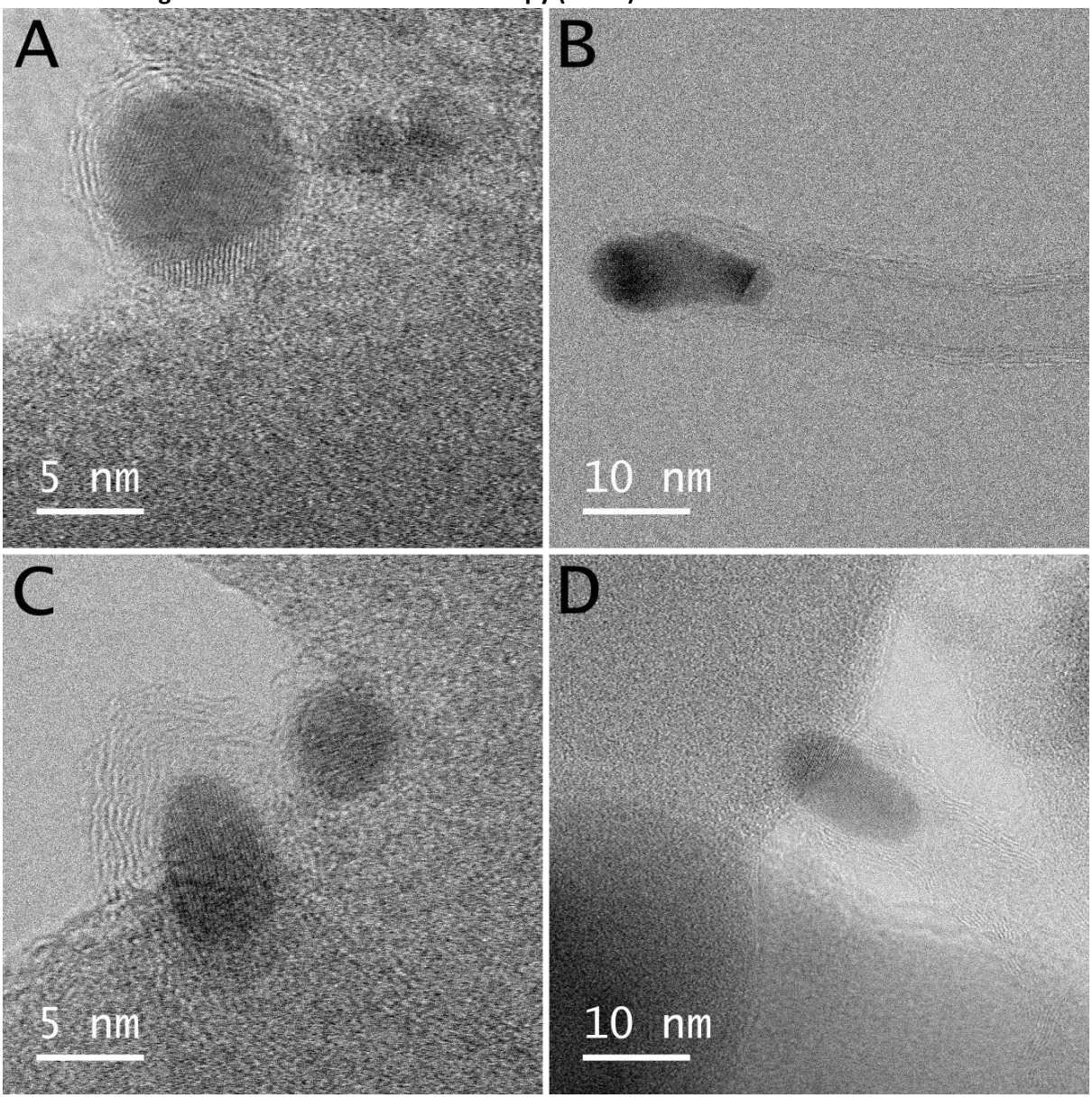

Figure S4: Bright field (BF) images of freshly prepared 1:1-Co/Mel@SiO_2 (A, B) and the same catalyst recovered after 5 runs of DIP hydrogenation at 120 °C, 30 bar H_2, 15 h in MeCN (C, D) showing the presence of graphitic layers around Co. Also, in a few cases the formation of carbon nanotubes at the Co particles was observed (B and D, more visible in B).

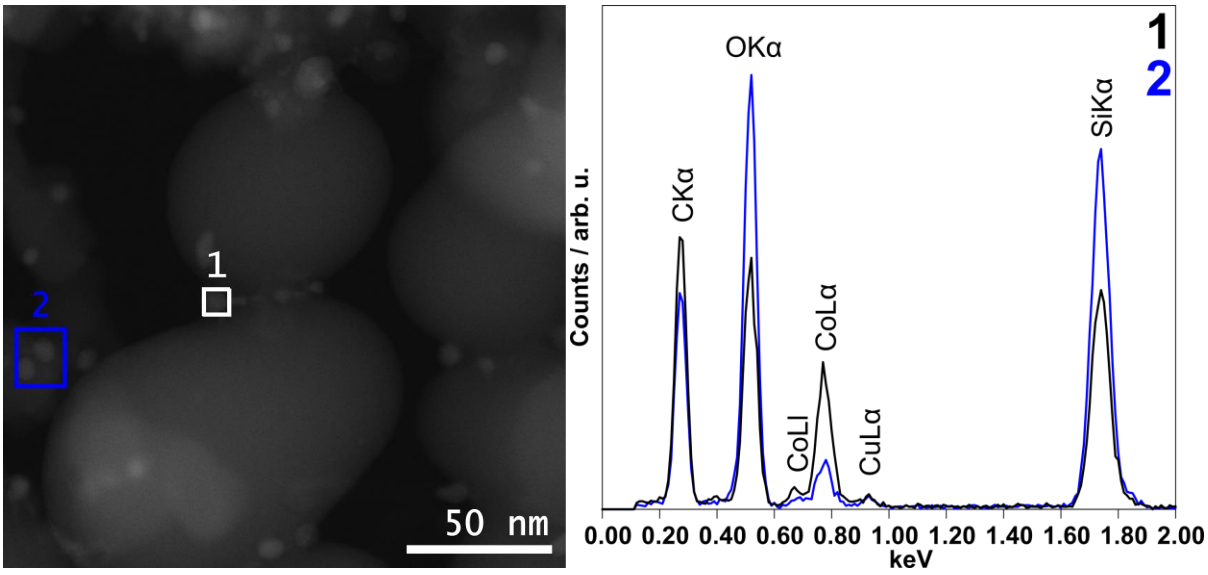

Figure S5: Selected EDX spectra (right) of the marked areas in the STEM-HAADF image (left) of freshly prepared 1:1-Co/Mel@SiO_2. Comparison of the signals for O K_α, Co L_α and Si K_α implies the presence of metallic cobalt (see also Figure S6).

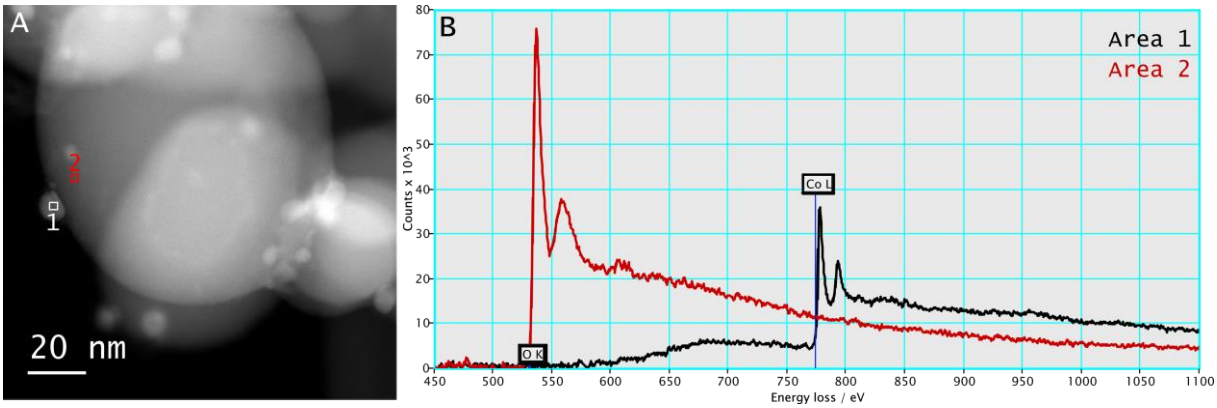

Figure S6: An annular dark field (ADF) image of freshly prepared 1:1-Co/Mel@SiO_2 is shown in A with the corresponding electron energy-loss (EEL) spectra of the highlighted areas being displayed in image B. Area 1 shows clearly the absence of oxygen due to the favorable location of the Co particle at the surface of SiO_2. Additionally, the L3/L2 ratio of the Co edge reveals the presence of metallic Co.[1,2] Area 2 shows pure SiO_2 as indicated by the oxygen signal and the missing Co signal.

S3.5 Brunauer-Emmett-Teller (BET) analysis

Table S4: Surface area and porosity of the catalysts and unmodified silica support.

Entry	Catalyst	Surface Area (m^2/g)[a]	Pore Size (nm)[b]
1	SiO_2	43.3	8.3
2	1:1-Co/Mel@SiO_2	41.9	9.4
3	1:5-Co/Mel@SiO_2	41.1	10.4
4	1:10-Co/Mel@SiO_2	35.8	12.1

[a]BET surface area. [b]BJH desorption average.

The decrease in surface area may be as a result of the increased thickness of the nitrogen doped carbon layer when more melamine is used to prepare the catalysts.

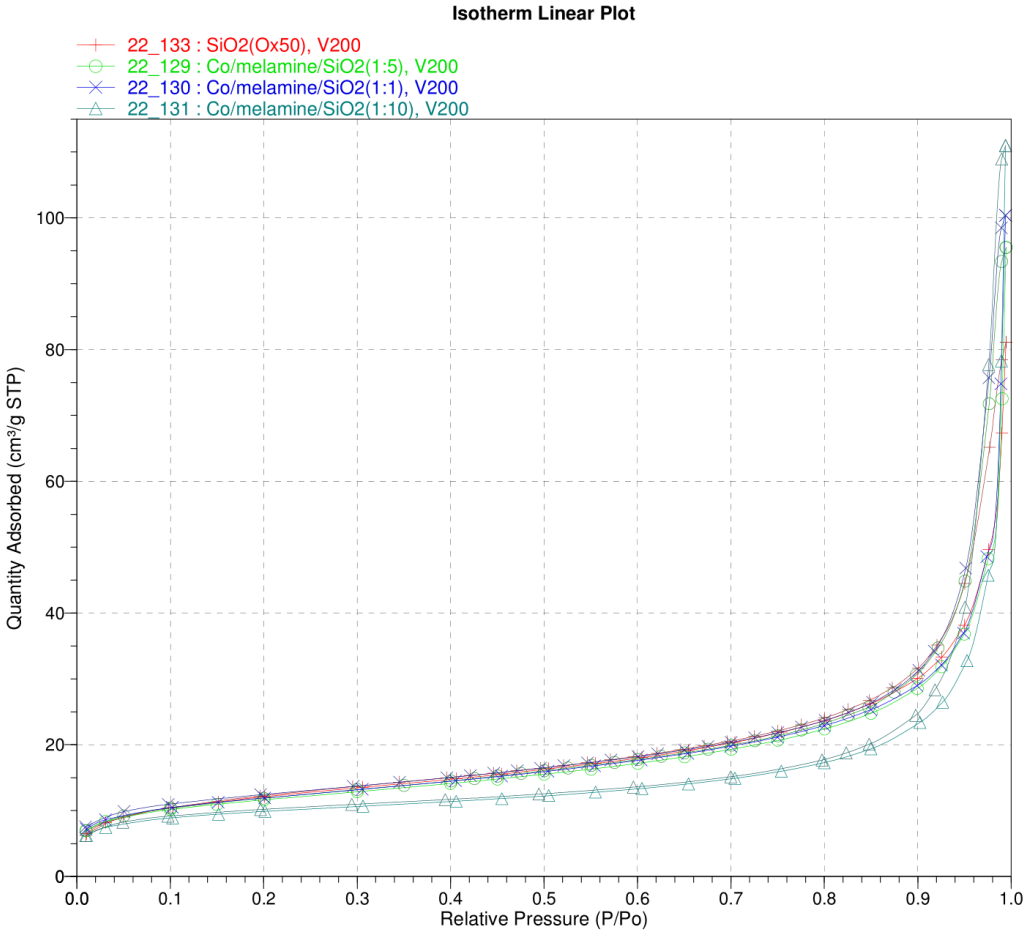

Figure S7: Combined isotherm linear plot of the prepared cobalt on silica catalysts and unmodified silica.

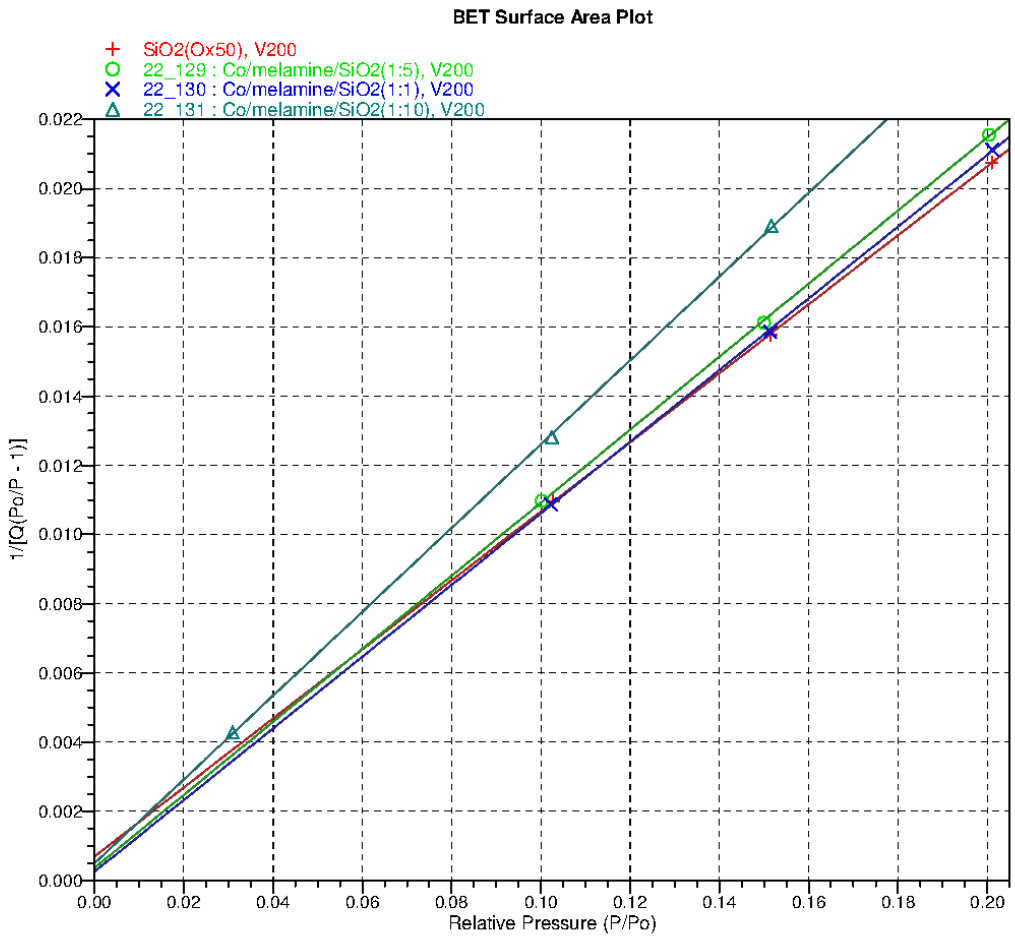

Figure S8: Combined BET surface area plot of the prepared cobalt on silica catalysts and unmodified silica.

Summary Report

Surface Area

Single point surface area at P/Po = 0.200962852: 42.1554 m²/g

BET Surface Area: 43.3304 m²/g

Pore Volume

BJH Desorption cumulative volume of pores
between 1.0000 nm and 100.0000 nm width: 0.094790 cm³/g

Pore Size

BJH Desorption average pore width (4V/A): 8.3425 nm

Figure S9: BET summary report for SiO_2.

BJH Desorption Pore Distribution Report

Faas Correction
Halsey
t = 3.54 [-5 / ln(P/Po)] ^ 0.333

Width Range: 1.0000 nm to 100.0000 nm
Adsorbate Property Factor: 0.95300 nm
Density Conversion Factor: 0.0015468
Fraction of Pores Open at Both Ends: 0.00

Pore Width Range (nm)	Average Width (nm)	Incremental Pore Volume (cm^3/g)	dV/dlog(w) Pore Volume (cm^3/g)	Incremental Pore Area (m^2/g)	dA/dlog(w) Pore Area (m^2/g)
85.0 - 40.3	48.2	0.035738	1.1032×10^{-1}	2.966	9.1551×10^{0}
40.3 - 25.5	29.6	0.016022	8.0454×10^{-2}	2.166	1.0875×10^{1}
25.5 - 20.4	22.3	0.005937	6.1015×10^{-2}	1.063	1.0927×10^{1}
20.4 - 16.0	17.6	0.004952	4.6867×10^{-2}	1.125	1.0643×10^{1}
16.0 - 13.4	14.4	0.003158	4.0921×10^{-2}	0.876	1.1345×10^{1}
13.4 - 11.7	12.4	0.002194	3.6894×10^{-2}	0.708	1.1910×10^{1}
11.7 - 10.2	10.8	0.002144	3.6160×10^{-2}	0.793	1.3383×10^{1}
10.2 - 9.0	9.5	0.001643	3.1196×10^{-2}	0.691	1.3114×10^{1}
9.0 - 8.1	8.5	0.001490	3.1811×10^{-2}	0.702	1.4976×10^{1}
8.1 - 7.3	7.7	0.001300	2.9839×10^{-2}	0.679	1.5579×10^{1}
7.3 - 6.6	6.9	0.001374	2.9975×10^{-2}	0.795	1.7355×10^{1}
6.6 - 6.0	6.3	0.001032	2.7832×10^{-2}	0.656	1.7699×10^{1}
6.0 - 5.6	5.8	0.000962	2.7702×10^{-2}	0.665	1.9129×10^{1}
5.6 - 5.2	5.4	0.000887	2.6911×10^{-2}	0.662	2.0083×10^{1}
5.2 - 4.8	5.0	0.000787	2.4963×10^{-2}	0.632	2.0061×10^{1}
4.8 - 4.5	4.6	0.000767	2.5628×10^{-2}	0.662	2.2101×10^{1}
4.5 - 4.2	4.3	0.000702	2.4322×10^{-2}	0.648	2.2440×10^{1}
4.2 - 3.9	4.1	0.000654	2.3441×10^{-2}	0.644	2.3086×10^{1}
3.9 - 3.7	3.8	0.000629	2.3082×10^{-2}	0.660	2.4220×10^{1}
3.7 - 3.5	3.6	0.000570	2.1504×10^{-2}	0.636	2.4003×10^{1}
3.5 - 3.3	3.4	0.000639	2.4736×10^{-2}	0.758	2.9323×10^{1}
3.3 - 3.1	3.2	0.000493	1.9366×10^{-2}	0.621	2.4354×10^{1}
3.1 - 2.9	3.0	0.000513	2.0379×10^{-2}	0.683	2.7165×10^{1}
2.9 - 2.6	2.7	0.001041	2.0575×10^{-2}	1.521	3.0063×10^{1}
2.6 - 2.3	2.4	0.001039	2.0772×10^{-2}	1.704	3.4074×10^{1}
2.3 - 1.8	2.0	0.002340	2.2398×10^{-2}	4.679	4.4773×10^{1}
1.8 - 1.4	1.5	0.003291	2.5714×10^{-2}	8.706	6.8023×10^{1}
1.4 - 1.1	1.2	0.002491	2.6684×10^{-2}	8.350	8.9457×10^{1}

Figure S10: BJH desorption pore distribution plot for SiO_2.

Summary Report

Surface Area

Single point surface area at P/Po = 0.201122532: 41.4424 m²/g

BET Surface Area: 41.9115 m²/g

Pore Volume

BJH Desorption cumulative volume of pores
between 1.0000 nm and 100.0000 nm width: 0.154545 cm³/g

Pore Size

BJH Desorption average pore width (4V/A): 9.4019 nm

Figure S11: BET summary report for 1:1-Co/MeI@SiO_2.

BJH Desorption Pore Distribution Report

Faas Correction
Halsey
$t = 3.54\ [\ -5\ /\ \ln(P/Po)\ ]\ ^{\wedge}\ 0.333$

Width Range: 1.0000 nm to 100.0000 nm
Adsorbate Property Factor: 0.95300 nm
Density Conversion Factor: 0.0015468
Fraction of Pores Open at Both Ends: 0.00

Pore Width Range (nm)	Average Width (nm)	Incremental Pore Volume (cm^3/g)	dV/dlog(w) Pore Volume (cm^3/g)	Incremental Pore Area (m^2/g)	dA/dlog(w) Pore Area (m^2/g)
187.2 - 82.8	99.3	0.038185	1.0771×10^{-1}	1.538	4.3373×10^{0}
82.8 - 41.3	49.3	0.050015	1.6593×10^{-1}	4.058	1.3465×10^{1}
41.3 - 24.6	28.8	0.021628	9.6153×10^{-2}	3.000	1.3337×10^{1}
24.6 - 20.6	22.3	0.004775	6.2197×10^{-2}	0.858	1.1174×10^{1}
20.6 - 16.5	18.1	0.004669	4.8312×10^{-2}	1.032	1.0677×10^{1}
16.5 - 13.8	14.9	0.003068	3.9856×10^{-2}	0.822	1.0680×10^{1}
13.8 - 11.8	12.7	0.002307	3.4134×10^{-2}	0.728	1.0772×10^{1}
11.8 - 10.3	11.0	0.001821	3.0864×10^{-2}	0.663	1.1243×10^{1}
10.3 - 9.2	9.7	0.001543	2.9794×10^{-2}	0.638	1.2308×10^{1}
9.2 - 8.2	8.7	0.001271	2.7128×10^{-2}	0.587	1.2541×10^{1}
8.2 - 7.5	7.8	0.001162	2.7517×10^{-2}	0.594	1.4082×10^{1}
7.5 - 6.8	7.1	0.001045	2.6494×10^{-2}	0.587	1.4888×10^{1}
6.8 - 6.3	6.5	0.000961	2.6502×10^{-2}	0.589	1.6240×10^{1}
6.3 - 5.8	6.0	0.000839	2.4425×10^{-2}	0.558	1.6231×10^{1}
5.8 - 5.3	5.5	0.000927	2.5090×10^{-2}	0.669	1.8107×10^{1}
5.3 - 5.0	5.2	0.000630	2.4337×10^{-2}	0.488	1.8851×10^{1}
5.0 - 4.6	4.8	0.000795	2.3607×10^{-2}	0.660	1.9606×10^{1}
4.6 - 4.4	4.5	0.000683	2.4282×10^{-2}	0.608	2.1635×10^{1}
4.4 - 4.1	4.2	0.000599	2.2133×10^{-2}	0.569	2.1012×10^{1}
4.1 - 3.9	4.0	0.000601	2.3008×10^{-2}	0.607	2.3219×10^{1}
3.9 - 3.6	3.7	0.000639	2.5162×10^{-2}	0.684	2.6942×10^{1}
3.6 - 3.4	3.5	0.000625	2.5259×10^{-2}	0.709	2.8651×10^{1}
3.4 - 3.2	3.3	0.000549	2.2375×10^{-2}	0.660	2.6862×10^{1}
3.2 - 3.1	3.2	0.000545	2.2825×10^{-2}	0.692	2.8971×10^{1}
3.1 - 2.7	2.9	0.001026	2.1345×10^{-2}	1.420	2.9562×10^{1}
2.7 - 2.5	2.6	0.000988	2.1045×10^{-2}	1.526	3.2509×10^{1}
2.5 - 2.0	2.2	0.001946	1.9977×10^{-2}	3.617	3.7130×10^{1}
2.0 - 1.5	1.7	0.002434	2.0687×10^{-2}	5.862	4.9836×10^{1}
1.5 - 1.2	1.3	0.002090	2.5950×10^{-2}	6.208	7.7080×10^{1}
1.2 - 0.9	1.0	0.006179	4.4005×10^{-2}	24.518	1.7460×10^{2}

Figure S12: BJH desorption pore distribution plot for 1:1-Co/Mel@SiO_2.

Summary Report

Surface Area

Single point surface area at P/Po = 0.200441730: 40.4746 m^2/g

BET Surface Area: 41.0911 m^2/g

Pore Volume

BJH Desorption cumulative volume of pores
between 1.0000 nm and 100.0000 nm width: 0.104774 cm^3/g

Pore Size

BJH Desorption average pore width (4V/A): 10.3936 nm

Figure S13: BET summary report for 1:5-Co/Mel@SiO_2.

Sample: Co/melamine/SiO2(1:5), V200
Operator: eck
Submitter: Bourriquen
File: C:\2020\DATA\2022\22_129.SMP

Started: 18.07.2022 17:30:28
Completed: 19.07.2022 9:14:14
Report Time: 21.07.2022 9:10:15
Sample Mass: 0.2010 g
Cold Free Space: 81.0000 cm³
Ambient Temperature: 22.00 °C
Automatic Degas: No

Analysis Adsorptive: N2
Analysis Bath Temp.: 77.447 K
Thermal Correction: No
Warm Free Space: 28.5000 cm³ Entered
Equilibration Interval: 10 s
Low Pressure Dose: None

BJH Desorption Pore Distribution Report

Faas Correction
Halsey
t = 3.54 [-5 / ln(P/Po)] ^ 0.333

Width Range: 1.0000 nm to 100.0000 nm
Adsorbate Property Factor: 0.95300 nm
Density Conversion Factor: 0.0015468
Fraction of Pores Open at Both Ends: 0.00

Pore Width Range (nm)	Average Width (nm)	Incremental Pore Volume (cm³/g)	dV/dlog(w) Pore Volume (cm³/g)	Incremental Pore Area (m²/g)	dA/dlog(w) Pore Area (m²/g)
83.7 - 40.7	48.6	0.046592	1.4868×10^{-1}	3.837	1.2244×10^{1}
40.7 - 25.9	30.0	0.017295	8.7916×10^{-2}	2.307	1.1726×10^{1}
25.9 - 20.1	22.2	0.006744	6.1222×10^{-2}	1.215	1.1030×10^{1}
20.1 - 16.3	17.8	0.004242	4.7110×10^{-2}	0.954	1.0599×10^{1}
16.3 - 13.5	14.6	0.003690	4.4152×10^{-2}	1.012	1.2104×10^{1}
13.5 - 11.8	12.5	0.001815	3.1251×10^{-2}	0.581	1.0007×10^{1}
11.8 - 10.3	11.0	0.001883	3.3361×10^{-2}	0.688	1.2184×10^{1}
10.3 - 9.1	9.7	0.001628	3.0229×10^{-2}	0.675	1.2528×10^{1}
9.1 - 8.2	8.6	0.001333	2.8829×10^{-2}	0.619	1.3384×10^{1}
8.2 - 7.4	7.8	0.001205	2.8226×10^{-2}	0.619	1.4507×10^{1}
7.4 - 6.8	7.1	0.001043	2.6410×10^{-2}	0.589	1.4912×10^{1}
6.8 - 6.2	6.5	0.000928	2.5304×10^{-2}	0.572	1.5589×10^{1}
6.2 - 5.8	6.0	0.000872	2.5234×10^{-2}	0.583	1.6869×10^{1}
5.8 - 5.4	5.5	0.000757	2.3318×10^{-2}	0.546	1.6833×10^{1}
5.4 - 5.0	5.2	0.000766	2.4819×10^{-2}	0.595	1.9268×10^{1}
5.0 - 4.7	4.8	0.000694	2.3432×10^{-2}	0.578	1.9500×10^{1}
4.7 - 4.4	4.5	0.000659	2.3392×10^{-2}	0.586	2.0803×10^{1}
4.4 - 4.1	4.2	0.000646	2.3588×10^{-2}	0.613	2.2361×10^{1}
4.1 - 3.9	4.0	0.000645	2.4361×10^{-2}	0.651	2.4569×10^{1}
3.9 - 3.6	3.7	0.000732	2.8388×10^{-2}	0.784	3.0405×10^{1}
3.6 - 3.4	3.5	0.000686	2.7217×10^{-2}	0.779	3.0911×10^{1}
3.4 - 3.2	3.3	0.000596	2.4164×10^{-2}	0.716	2.9064×10^{1}
3.2 - 3.1	3.1	0.000613	2.5279×10^{-2}	0.780	3.2164×10^{1}
3.1 - 2.7	2.9	0.001023	2.1072×10^{-2}	1.421	2.9284×10^{1}
2.7 - 2.5	2.6	0.000966	2.0195×10^{-2}	1.499	3.1354×10^{1}
2.5 - 2.0	2.1	0.002088	2.0999×10^{-2}	3.914	3.9372×10^{1}
2.0 - 1.5	1.6	0.002519	2.0910×10^{-2}	6.158	5.1112×10^{1}
1.5 - 1.2	1.3	0.002113	2.4228×10^{-2}	6.450	7.3947×10^{1}

Figure S14: BJH desorption pore distribution plot for 1:5-Co/Mel@SiO_2.

Summary Report

Surface Area

Single point surface area at P/Po = 0.151650141: 34.8807 m²/g

BET Surface Area: 35.7797 m²/g

Pore Volume

BJH Desorption cumulative volume of pores
between 1.0000 nm and 100.0000 nm width: 0.170464 cm³/g

Pore Size

BJH Desorption average pore width (4V/A): 12.1184 nm

Figure S15: BET summary report for 1:10-Co/Mel@SiO_2.

BJH Desorption Pore Distribution Report

Faas Correction
Halsey
t = 3.54 [-5 / ln(P/Po)] ^ 0.333

Width Range: 1.0000 nm to 100.0000 nm
Adsorbate Property Factor: 0.95300 nm
Density Conversion Factor: 0.0015468
Fraction of Pores Open at Both Ends: 0.00

Pore Width Range (nm)	Average Width (nm)	Incremental Pore Volume (cm³/g)	dV/dlog(w) Pore Volume (cm³/g)	Incremental Pore Area (m²/g)	dA/dlog(w) Pore Area (m²/g)
194.3 - 81.7	98.1	0.052385	1.3920×10^{-1}	2.137	5.6785×10^{0}
81.7 - 40.6	48.4	0.063738	2.0975×10^{-1}	5.269	1.7340×10^{1}
40.6 - 24.9	29.0	0.021030	9.9267×10^{-2}	2.897	1.3673×10^{1}
24.9 - 20.0	21.9	0.006227	6.5288×10^{-2}	1.138	1.1930×10^{1}
20.0 - 13.5	15.5	0.006549	3.8502×10^{-2}	1.694	9.9581×10^{0}
13.5 - 11.7	12.4	0.001845	2.8648×10^{-2}	0.593	9.2136×10^{0}
11.7 - 10.2	10.8	0.001418	2.3997×10^{-2}	0.525	8.8847×10^{0}
10.2 - 6.8	7.8	0.003034	1.7420×10^{-2}	1.559	8.9511×10^{0}
6.8 - 4.9	5.6	0.001590	1.1465×10^{-2}	1.145	8.2568×10^{0}
4.9 - 3.8	4.2	0.000864	7.7695×10^{-3}	0.818	7.3517×10^{0}
3.8 - 3.1	3.3	0.000703	7.1229×10^{-3}	0.842	8.5337×10^{0}
3.1 - 2.5	2.7	0.000445	4.6993×10^{-3}	0.665	7.0245×10^{0}
2.5 - 2.0	2.1	0.000634	6.5737×10^{-3}	1.182	1.2261×10^{1}
2.0 - 1.5	1.7	0.001367	1.1588×10^{-2}	3.304	2.8007×10^{1}
1.5 - 1.2	1.3	0.002008	2.4093×10^{-2}	6.012	7.2137×10^{1}
1.2 - 0.9	1.0	0.006627	4.7644×10^{-2}	26.486	1.9042×10^{2}

Figure S16: BJH desorption pore distribution plot for 1:10-Co/Mel@SiO_2.

S4 Lindlar Catalysed DIP Hydrogenation

The general procedure for hydrogenation using the catalysts prepared in this work is available in the main manuscript.

The catalytic activity tests were performed in a 300 ml stainless steel autoclave advanced with an internal aluminium plate to include eight uniform reaction glass vials (4 ml) with cap, septum, and

needle. 3,7,11,15-tetramethylhexadec-1-yn-3-ol (DIP, 0.25 mmol), Lindlar catalyst (1 mol% Pd) and heptane (2 mL) were placed in a 4 mL vial. A cap with a septum punctured by a needle, to allow entry of H2, was fitted. The vial was placed in an aluminium plate which was inserted into a 300 mL stainless steel autoclave. The autoclave was sealed and flushed twice with N_2 (5 bar) and then charged with H_2 (2 bar). The autoclave was placed in an aluminium block at room temperature (25 °C) with a stir rate of 750 ppm for 1 hour. Following the reaction, the stirring was stopped and the pressure released. Dodecane (40 µL) was added as an internal standard and the reaction mixture diluted with chloroform (1 mL). The catalyst and reaction mixture were separated *via* centrifugation (5000 RPM, 2 minutes). The reaction mixture was filtered through a celite plug and the product composition analysed *via* GC-FID.

S5 Catalyst Screening

Table S5: Screening different metal/melamine catalysts for the hydrogenation of DIP.

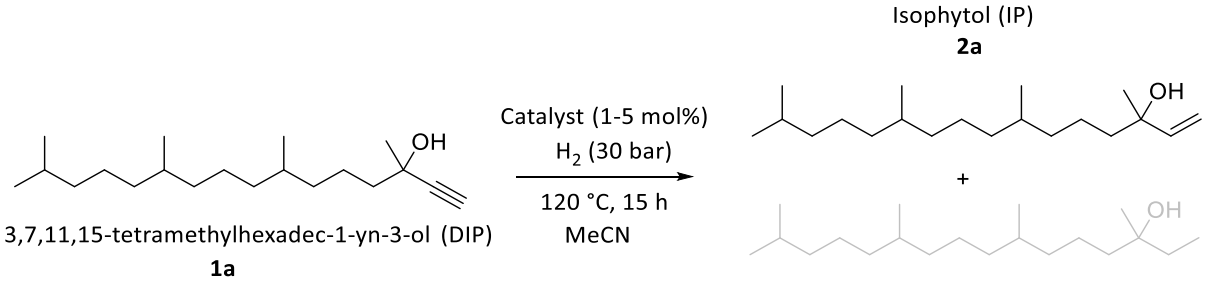

Entry	Catalyst	Conversion / %[a] (SD ±)[b]	IP Selectivity / %[a] (SD ±)[b]
1	1:1-Co/Mel@SiO_2	>99 (0)	67 (3)
2	1:1-Fe/Mel@SiO_2	0 (0)	NA
3[c]	1:1-Fe/Mel@SiO_2	44 (8)	70 (3)
4[d]	1:1-Fe/Mel@SiO_2	35 (1)	56 (1)
5[c,e]	1:1-Fe/Mel@SiO_2	87 (4)	72 (1)
6	1:1-Mn/Mel@SiO_2	0 (0)	NA
7[c]	1:1-Mn/Mel@SiO_2	0 (0)	NA
8	1:1-Cu/Mel@SiO_2	0 (0)	NA
9[c]	1:1-Cu/Mel@SiO_2	0 (0)	NA

Reaction conditions: Substrate (0.25 mmol), Catalyst (1 mol% metal), MeCN (2 mL), (120 °C, stir rate 750 RPM, 30 bar H_2, 15 h). [a]Determined by GC-FID using a known amount of dodecane. [b]Standard deviation of three reactions. [c]5 mol% catalyst. [d]10 mol% catalyst. [e]72 h.

The poor performance of iron, manganese, and copper catalysts at 5 mol% (Table S5 entries 3, 7, 9) is not due to diffusion limitations as 1 mol% of these metals also showed no activity for the reaction (Table S5 entries 2, 6, 8). 1:1-Fe/Mel@SiO_2 had good selectivity, but after 72 h the conversion was only 87 % (Table S5, entry 5).

Table S6: Screening cobalt catalysts with different nitrogen sources for the hydrogenation of DIP.

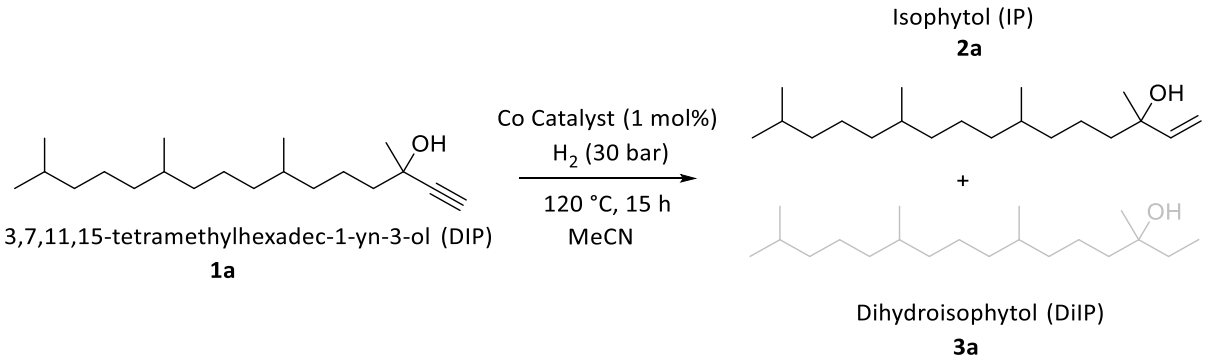

Entry	Catalyst	Conversion / %[a] (SD ±)[b]	IP Selectivity / %[a] (SD ±)[b]
1	1:1-Co/Phenanthroline@SiO_2	98 (1)	78 (3)
2	1:1-Co/Mel@SiO_2	>99 (0)	67 (3)
3	Co/Chitin@SiO_2	89 (5)	75 (0)

Reaction conditions: Substrate (0.25 mmol), Co catalyst (1 mol% Co), MeCN (2 mL), (120 °C, stir rate 750 RPM, 30 bar H_2, 15 h). [a]Determined by GC-FID using a known amount of dodecane, the remaining product is DiIP. [b]Standard deviation of three reactions.

Table S7: A comparison of 1:1-Co/Mel@SiO_2 and 1:1-Co/Phenanthroline@SiO_2 catalysts for DIP hydrogenation under milder conditions than the initial screening (Table S6).

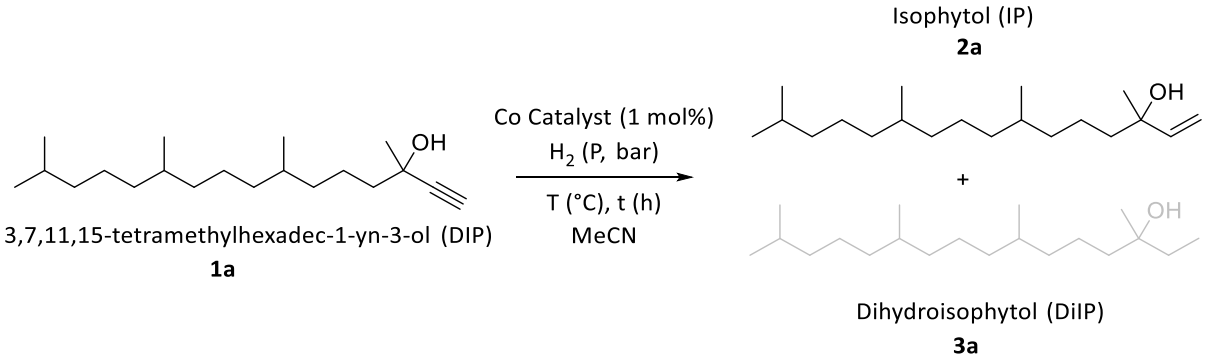

		1:1-Co/Mel@SiO_2		1:1-Co/Phenanthroline@SiO_2	
Entry	Variable Conditions	Conversion / %[a] (SD ±)[b]	IP Selectivity / %[a] (SD ±)[b]	Conversion / %[a] (SD ±)[b]	IP Selectivity / %[a] (SD ±)[b]
1	**8 h**, 120 °C, 30 bar H_2	>99 (0)	71 (1)	32 (4)	76 (2)
2	15 h, 120 °C, **20 bar H_2**	97 (2)	74 (3)	37 (1)	80 (0)
3	15 h, **100 °C**, 30 bar H_2	78 (0)	74 (3)	28 (3)	69 (7)

Fixed reaction conditions: Substrate (0.25 mmol), Co catalyst (1 mol% Co), MeCN (2 mL), stir rate 750 RPM. [a]Determined by GC-FID using a known amount of dodecane, the remaining product is DiIP. [b]Standard deviation of three reactions.

Under harsher conditions the phenanthroline catalyst achieves the highest selectivity (Table S6), however when the reaction time, pressure, or temperature are reduced then the melamine catalyst is shown to be the best performing (Table S7).

Table S8: A comparison of 1:1-Co/Mel@SiO_2 and 1:0.5-Co/Mel@SiO_2 catalysts for DIP hydrogenation.

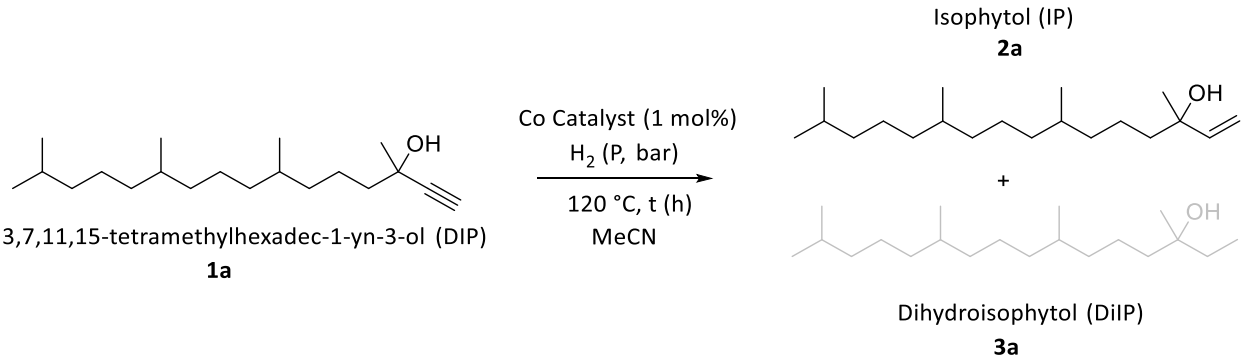

		1:1-Co/Mel@SiO_2		1:0.5-Co/Mel@SiO_2	
Entry	**Variable Conditions**	**Conversion / %[a] (SD ±)[b]**	**IP Selectivity / %[a] (SD ±)[b]**	**Conversion / %[a] (SD ±)[b]**	**IP Selectivity / %[a] (SD ±)[b]**
1	15 h, 120 °C, 30 bar H_2	>99 (0)	67 (3)	>99 (0)	66 (3)
2	**8 h**, 120 °C, 30 bar H_2	>99 (0)	71 (1)	62 (16)	65 (0)
3	15 h, 120 °C, **20 bar H_2**	97 (2)	74 (3)	54 (1)	77 (1)

Fixed reaction conditions: Substrate (0.25 mmol), 1:0.5-Co/Mel@SiO_2 (1 mol % Co), MeCN (2 mL), stir rate 750 RPM. [a]Determined by GC-FID using a known amount of dodecane, the remaining product is DiIP. [b]Standard deviation of three reactions.

As the cobalt species (Figure S1 Figure S2), and the species in the nitrogen doped carbon layer (Figure S3) are similar, the poor performance of 1:0.5-Co/Mel@SiO_2 could result from its low surface nitrogen content (Table S3) which is known to influence the behaviour of metal nanoparticles.[3,4]

Table S9: Control reaction with different catalyst variations.

Entry	**Catalyst**	**Conversion / %[a] (SD ±)[b]**	**IP Selectivity / %[a] (SD ±)[b]**
1	1:1-Co@SiO_2	63 (14)	79 (1)
2	1:1-Co/Mel@SiO_2 (Unpyrolyzed)	0 (0)	0 (0)
3[c]	Mel@SiO_2	0 (0)	0 (0)

Reaction conditions: Substrate (0.25 mmol), Co catalyst (1 mol% Co), MeCN (2 mL), (120 °C, stir rate 750 RPM, 30 bar H_2, 15 h). [a]Determined by GC-FID using a known amount of dodecane, the remaining product is DiIP. [b]Standard deviation of three reactions. [c]4.50 mg catalyst.

Table S10: Solvent screening at 30 bar for DIP hydrogenation using 1:1-Co/Mel@SiO_2.

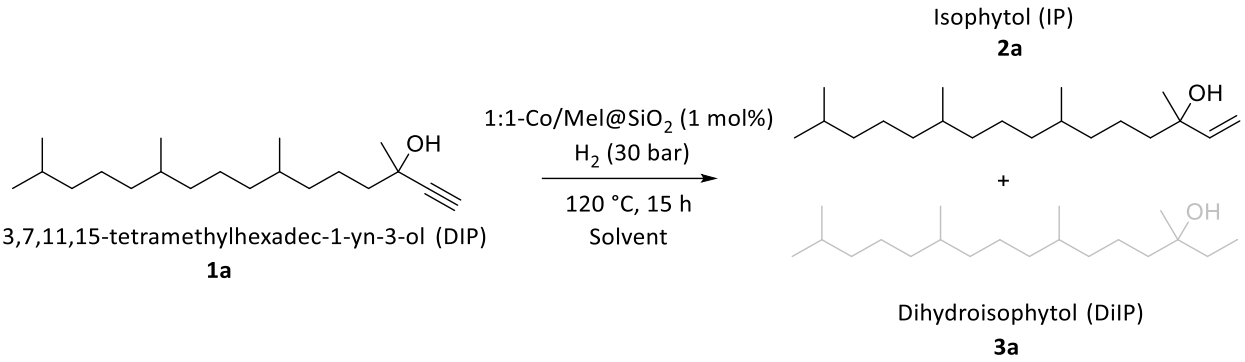

Entry	Solvent	Conversion / %[a] (SD ±)[b]	IP Selectivity / %[a] (SD ±)[b]
1	MeCN	99 (0)	65 (5)
2	Heptane	91 (8)	63 (13)
3	Toluene	99 (0)	61 (1)
4[c]	EtOH	99	75
5[c]	EtOH	99	40
6	MeOH	99 (0)	0 (0)

Reaction Conditions: Substrate (0.25 mmol), 1:1-Co/Mel@SiO_2 (1 mol % Co), solvent (2 mL) 120 °C, 30 bar H_2, stir rate 750 RPM. [a]Determined by GC-FID using a known amount of dodecane, the remaining product is DiIP. [b]Standard deviation of three reactions. [c]The results in EtOH exhibited poor reproducibility.

Table S11: The effect of catalyst loading for 1:1-Co/Mel@SiO_2 in the hydrogenation of DIP.

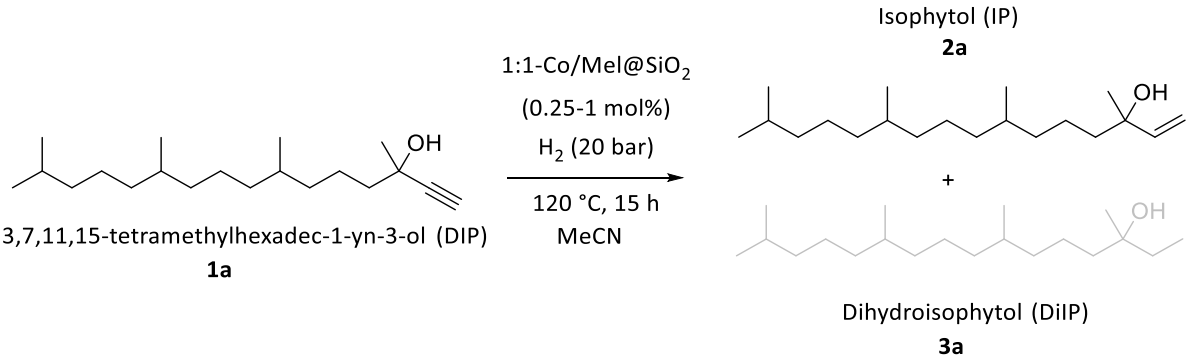

Entry	Catalyst loading / mol%	Conversion / %[a] (SD ±)[b]	IP Selectivity / %[a] (SD ±)[b]
1	1.0	97 (2)	74 (0)
2	0.75	99 (0)	82 (0)
3	0.5	53 (1)	84 (9)
4	0.25	24 (7)	81 (1)

Reaction conditions: Substrate (0.25 mmol), 1:1-Co/Mel@SiO_2 (0.25-1.0 mol % Co), MeCN (2 mL), (120 °C, stir rate 750 RPM, 20 bar H_2, 15 h). [a]Determined by GC-FID using a known amount of dodecane, the remaining product is DiIP. [b]Standard deviation of three reactions.

Table S12: The effect of catalyst loading for 1:1-Co/Mel@SiO_2 in the hydrogenation of 1,2-diphenylacetylene.

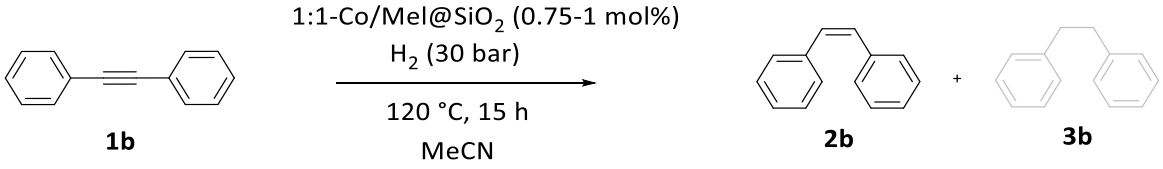

Entry	Catalyst loading / mol %	Conversion / %[a] (SD ±)[b]	Z Olefin Selectivity / %[a] (SD ±)[b]
1	1.0	>99 (0)	97 (2)
2	0.75	66 (1)	93 (0)

Reaction conditions: Substrate (0.25 mmol), 1:1-Co/Mel@SiO_2 (0.75-1.0 mol % Co), MeCN (2 mL), (120 °C, stir rate 750 RPM, 30 bar H_2, 15 h). [a]Determined by GC-FID using a known amount of dodecane. [b]Standard deviation of three reactions.

S6 Reaction Characterisation

The optimum conditions and reaction composition are displayed along with the corresponding NMR of the reaction mixture in order to easily evaluate the performance of the catalyst. Residual alkyne, and over-hydrogenation products are marked with dots in the NMR spectra, as in the reaction scheme.

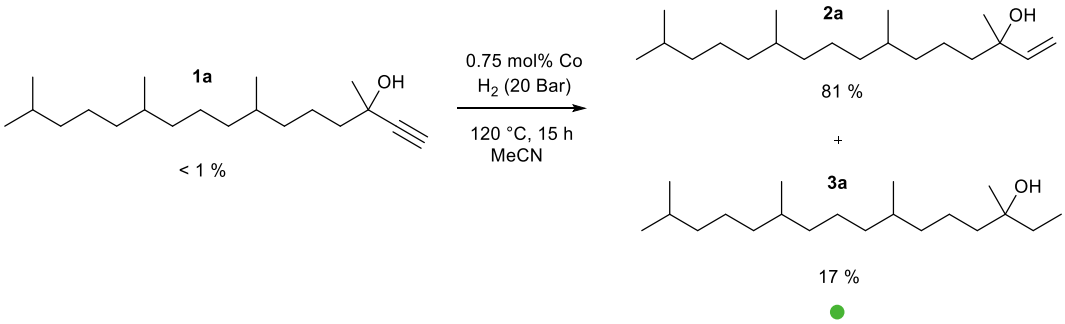

2a

^{1}H NMR (300 MHz, $CDCl_3$) δ = 5.93 (dd, *J* = 17.3, 10.7, 1H), 5.21 (dd, *J* = 17.4, 1.3, 1H), 5.05 (dd, *J* = 10.7, 1.3, 1H), 1.61 – 1.03 (m, 26H), 0.87 (t, *J* = 6.6, 12H). ^{13}C NMR (75 MHz, $CDCl_3$) δ = 145.3, 111.5, 73.3, 42.7, 39.4, 37.5, 37.4, 37.4, 37.3, 32.8, 27.98, 27.7, 24.8, 24.5, 22.7, 22.6, 21.4, 19.8, 19.7.

The proton aliphatic region contains too many protons due to overlap with the over-hydrogenated product. These have not been precisely assigned.

MS (EI, 70 eV): *m/z* (%) 123 (15), 95 (14), 83 (11), 82 (16), 81 (14), 57 (16), 55 (17).

Literature Mass Characterisation[5]

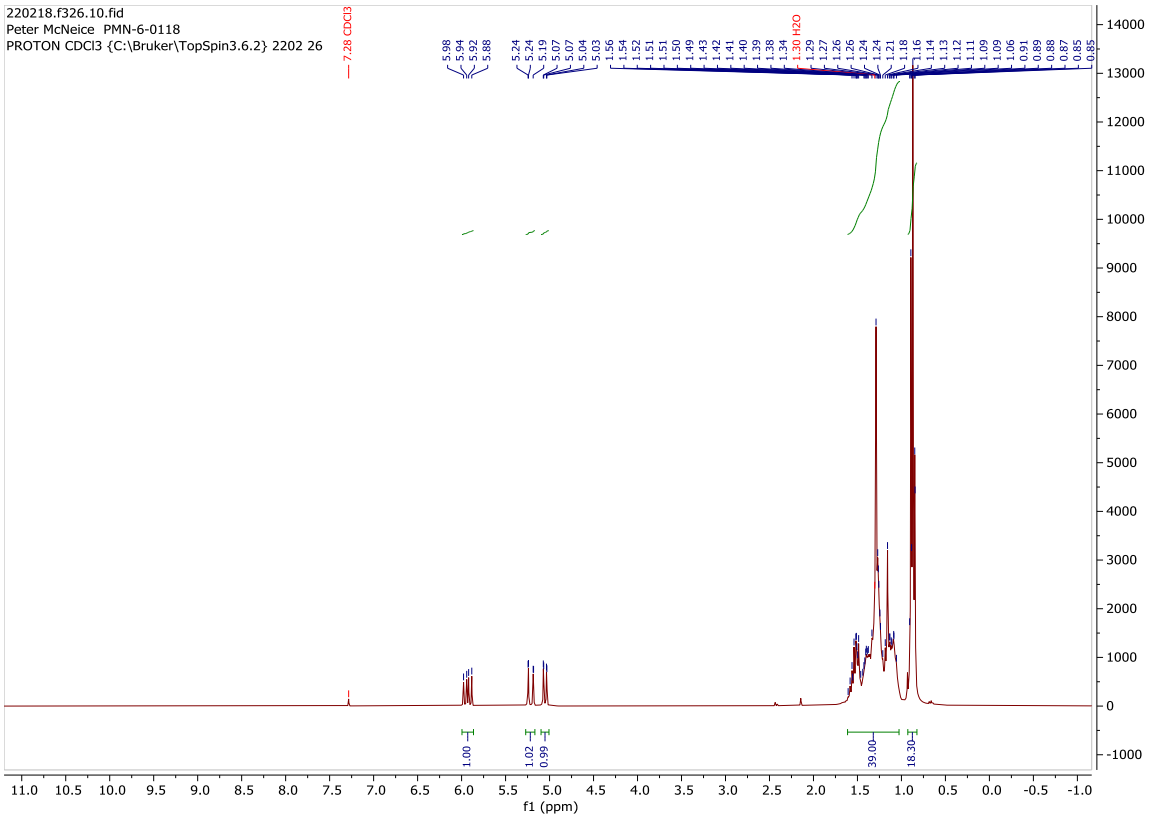

Figure S17: ^{1}H spectrum of the reaction mixture for 3,7,11,15-tetramethylhexadec-1-yn-3-ol (DIP, **1a**) hydrogenation to 3,7,11,15-tetramethylhexadec-1-en-3-ol (IP, **2a**).

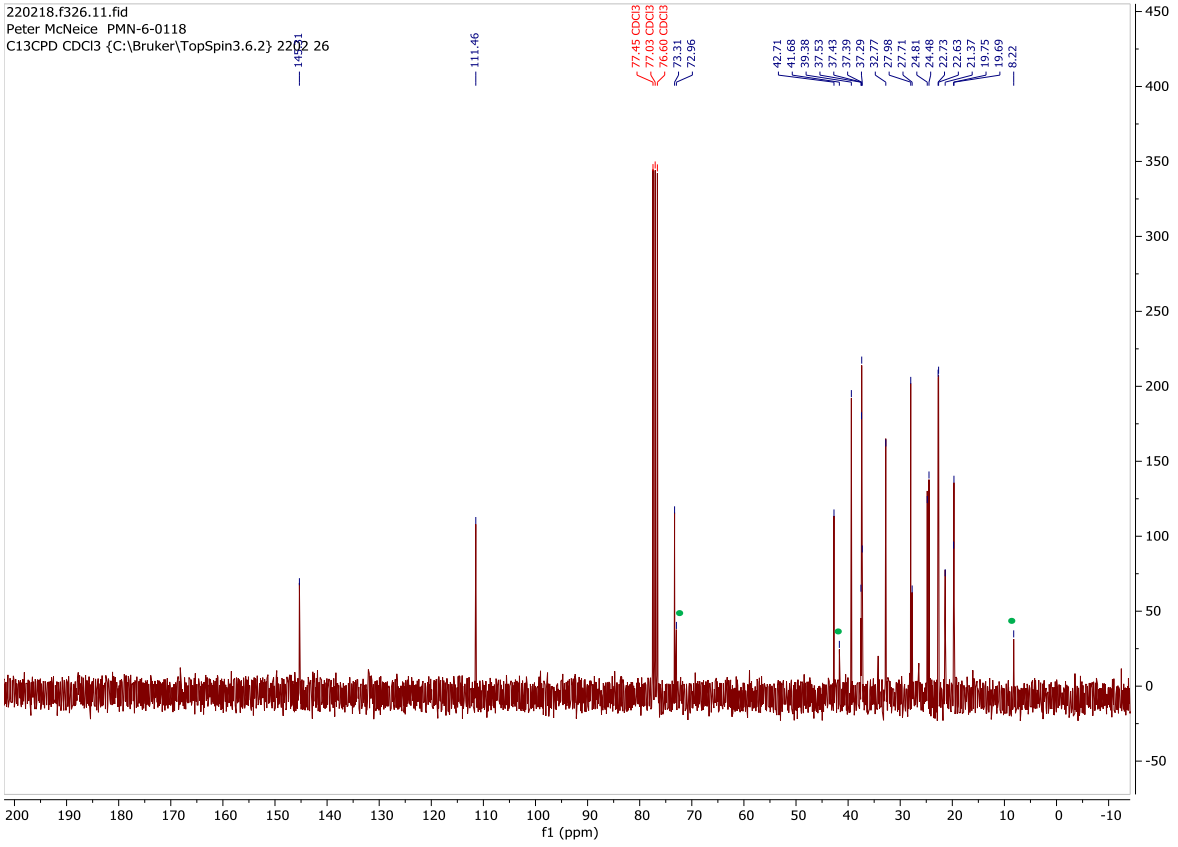

Figure S18: ^{13}C spectrum of the reaction mixture for 3,7,11,15-tetramethylhexadec-1-yn-3-ol (DIP, **1a**) hydrogenation to 3,7,11,15-tetramethylhexadec-1-en-3-ol (IP, **2a**).

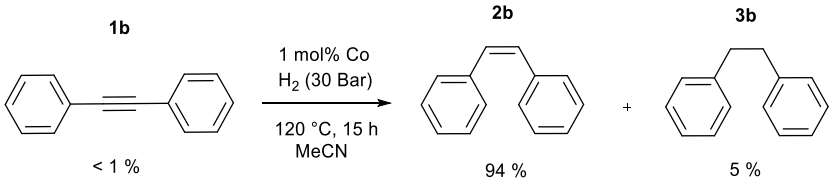

2b

^{1}H NMR (300 MHz, $CDCl_3$) δ = 7.36 – 7.19 (m, 10H), 6.66 (s, 2H). ^{13}C NMR (75 MHz, $CDCl_3$) δ = 137.3, 130.3, 128.9, 128.3, 127.1.

MS (EI, 70 eV): *m/z* (%) 180 (M^+, 100), 165 (64), 152 (20), 102 (11), 89 (19), 76 (14), 51 (8).

Literature Characterisation[6]

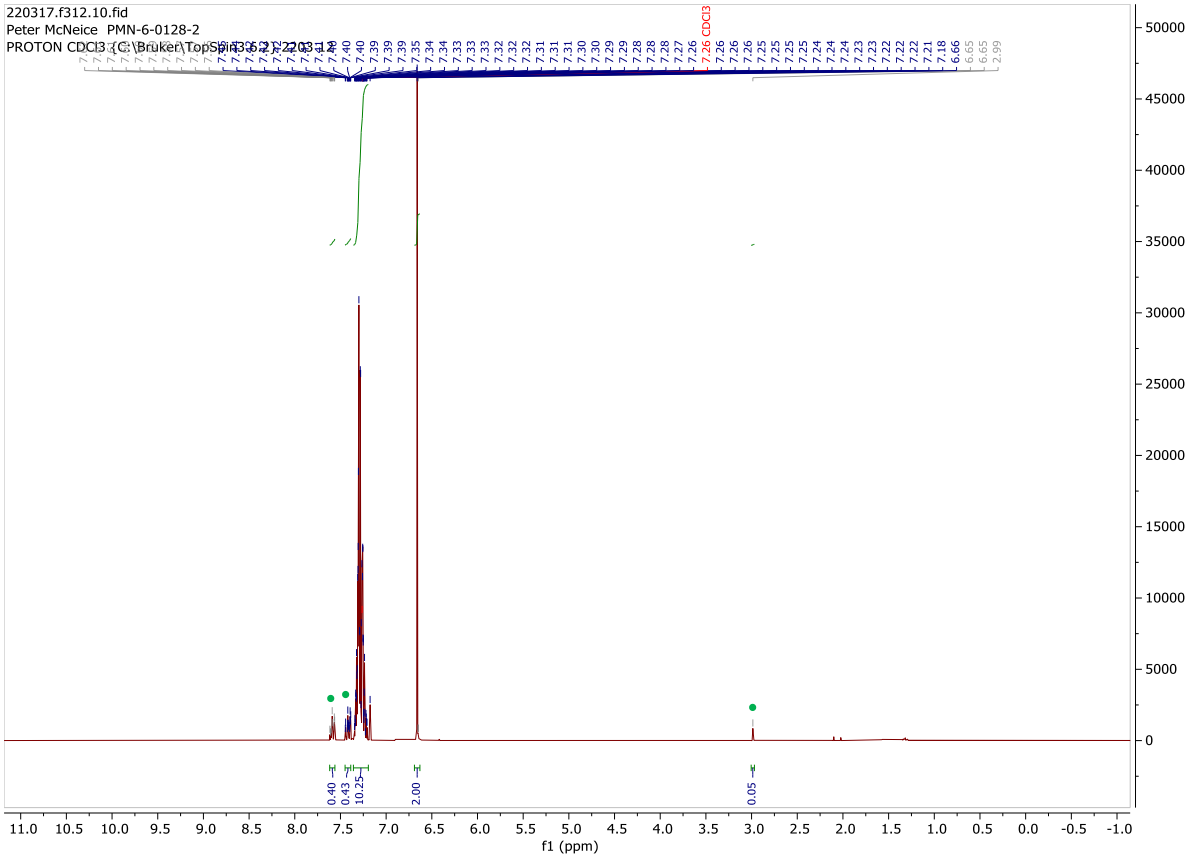

Figure S19: ^{1}H spectrum of the reaction mixture for 1,2-diphenylacetylene (**1b**) hydrogenation to (*Z*)-1,2-diphenylethene (**2b**).

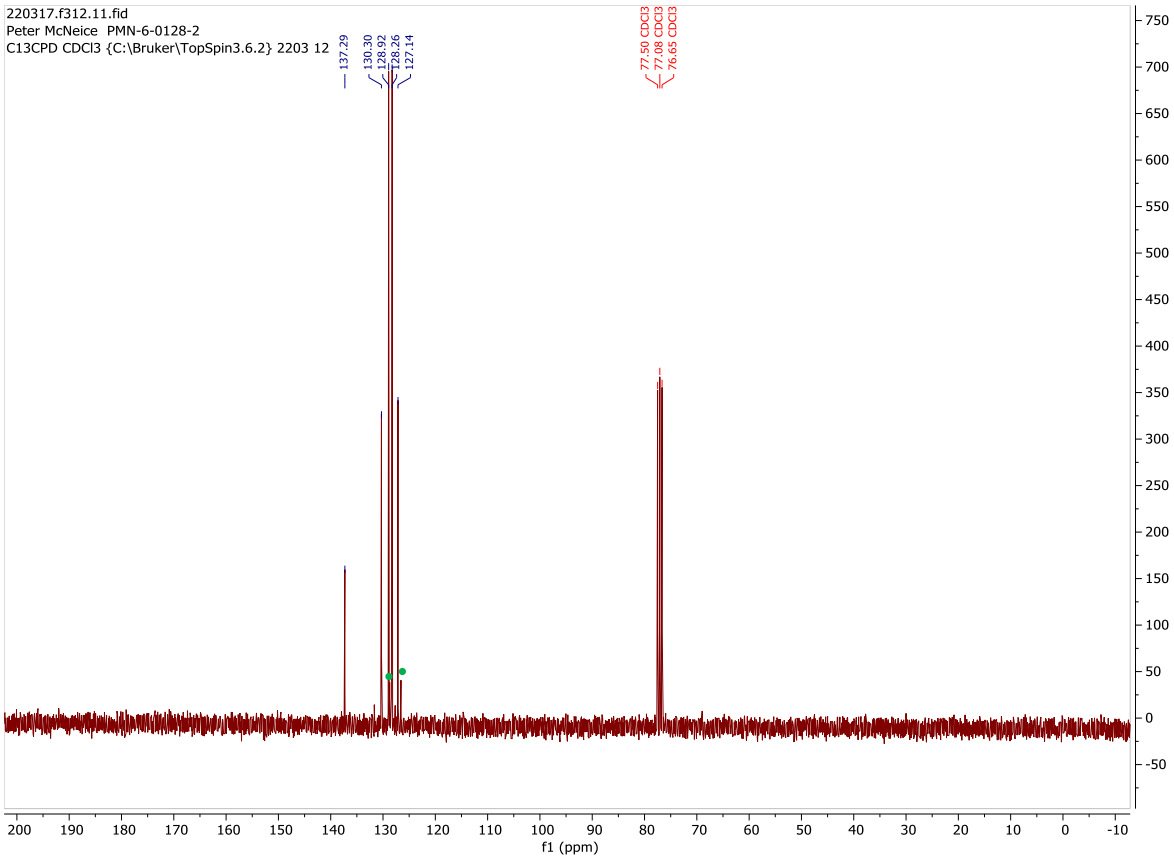

Figure S20: ^{1}H spectrum of the reaction mixture for 1,2-diphenylacetylene (**1b**) hydrogenation to (*Z*)-1,2-diphenylethene (**2b**).

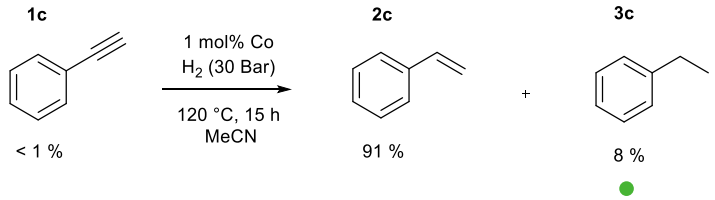

2c

^{1}H NMR (300 MHz, $CDCl_3$) δ = 7.49 – 7.22 (m, 5H), 6.76 (dd, *J* = 17.6, 10.9, 1H), 5.79 (dd, *J* = 17.6, 1.0, 1H), 5.28 (dd, *J* = 10.9, 1.0, 1H). ^{13}C NMR (75 MHz, $CDCl_3$) δ = 137.6, 136.90 128.5, 127.8, 126.2, 113.8.

MS (EI, 70 eV): *m/z* (%) 104 (M^+, 100), 103 (47), 102 (8), 78 (37), 77 (16), 63 (4), 51 (11), 50 (5).

MeCN is visible at 2.02 ppm due to the volatility of **2c** making its isolation difficult.

Literature Characterisation[7]

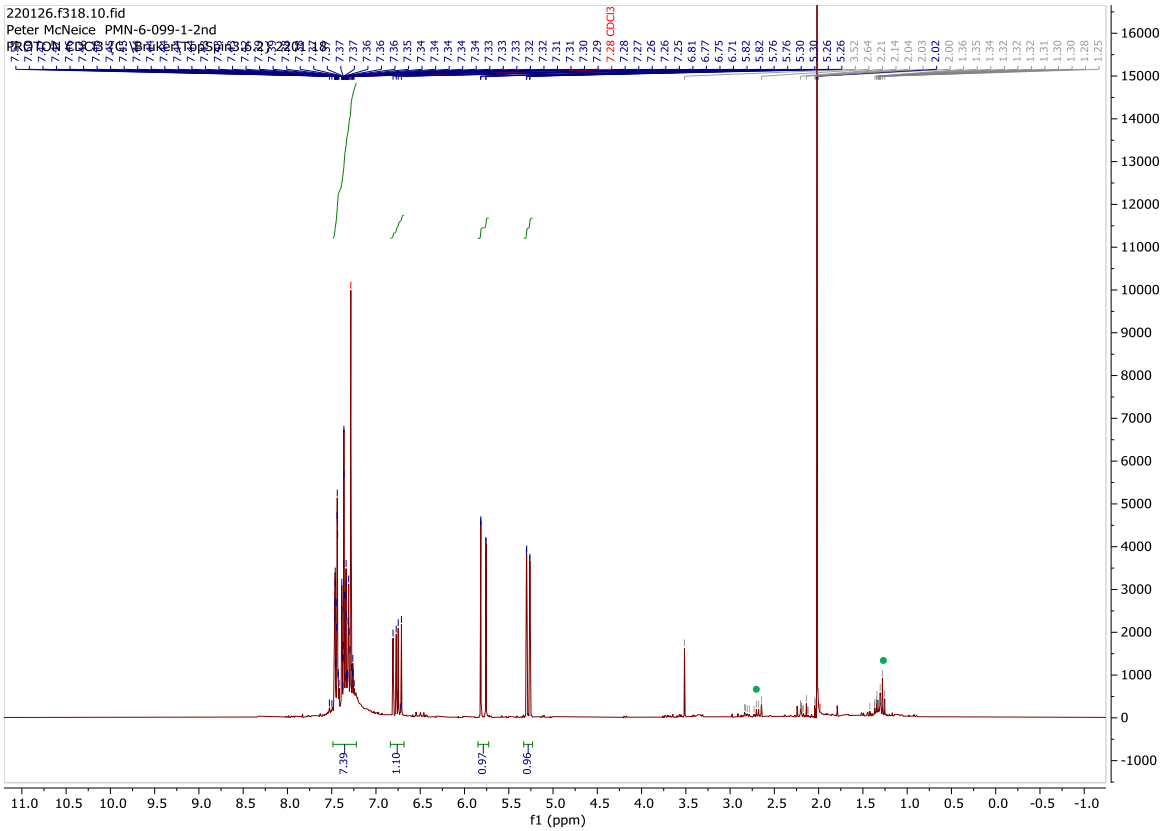

Figure S21: ^{1}H spectrum of the reaction mixture for phenylacetylene hydrogenation (**1c**) to styrene (**2c**).

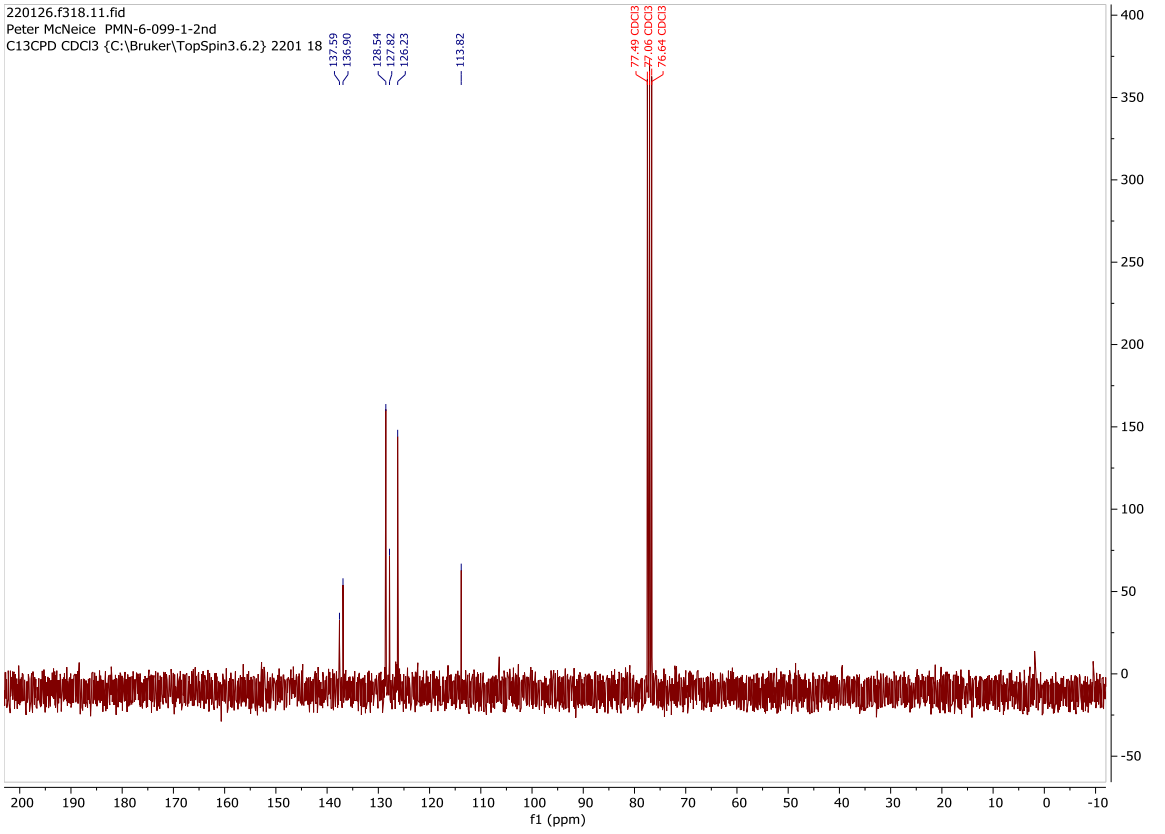

Figure S22: ^{13}C spectrum of the reaction mixture for phenylacetylene hydrogenation (**1c**) to styrene (**2c**).

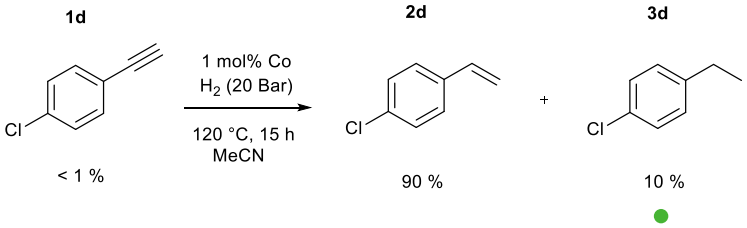

2d

^{1}H NMR (300 MHz, $CDCl_3$) δ = 7.39 – 7.25 (m, 4H), 6.70 (dd, *J* = 17.6, 10.9, 1H), 5.75 (dd, *J* = 17.6, 0.8, 1H), 5.30 (dd, *J* = 10.9, 0.8, 1H). ^{13}C NMR (75 MHz, $CDCl_3$) δ = 136.1, 135.69, 133.5, 128.7, 127.5, 114.5.

MeCN is visible at 2.02 ppm due to the volatility of **2d** making its isolation difficult.

MS (EI, 70 eV): *m/z* (%) 140 (M^+ + 2, 42), 138 (M^+, 100), 77 (Ph, 27).

Literature Characterisation[8]

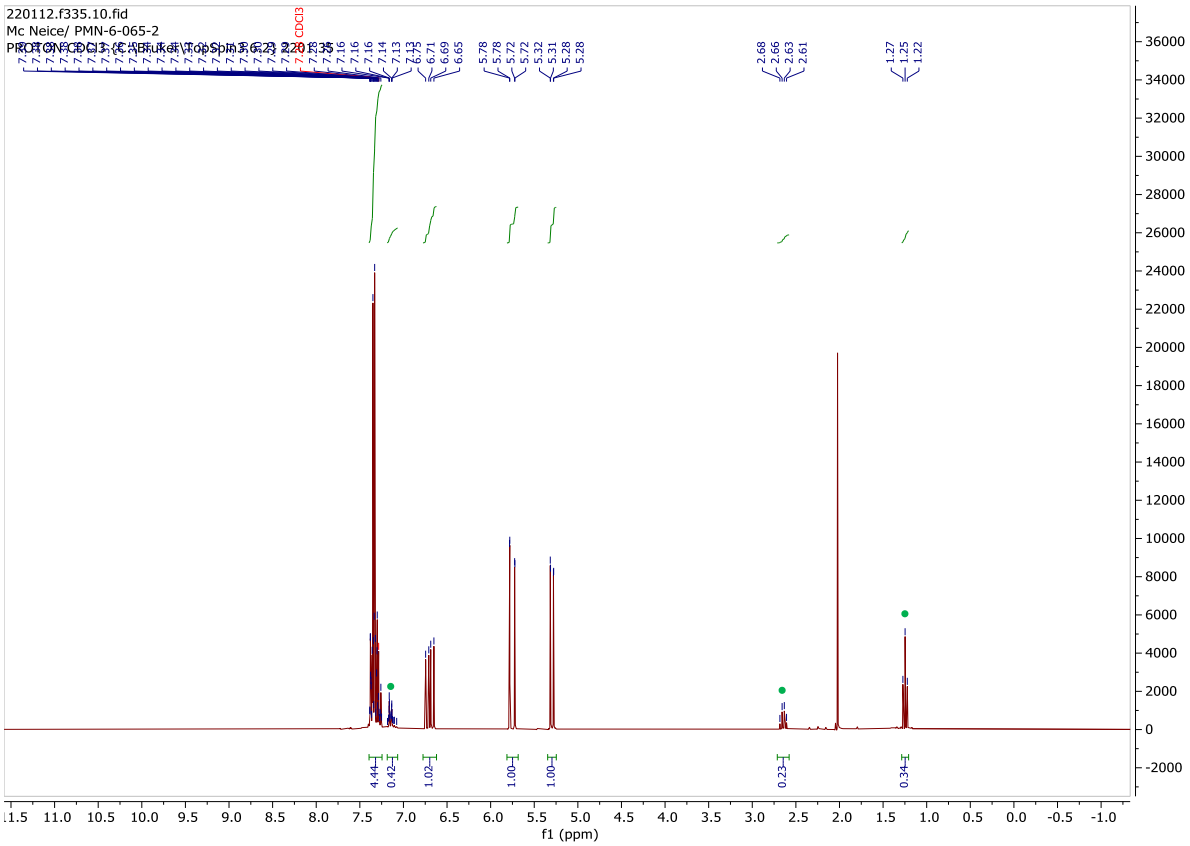

Figure S23: ^{1}H spectrum of the reaction mixture for 1-chloro-4-ethynylbenzene (**1d**) hydrogenation to 4-chlorostyrene (**2d**).

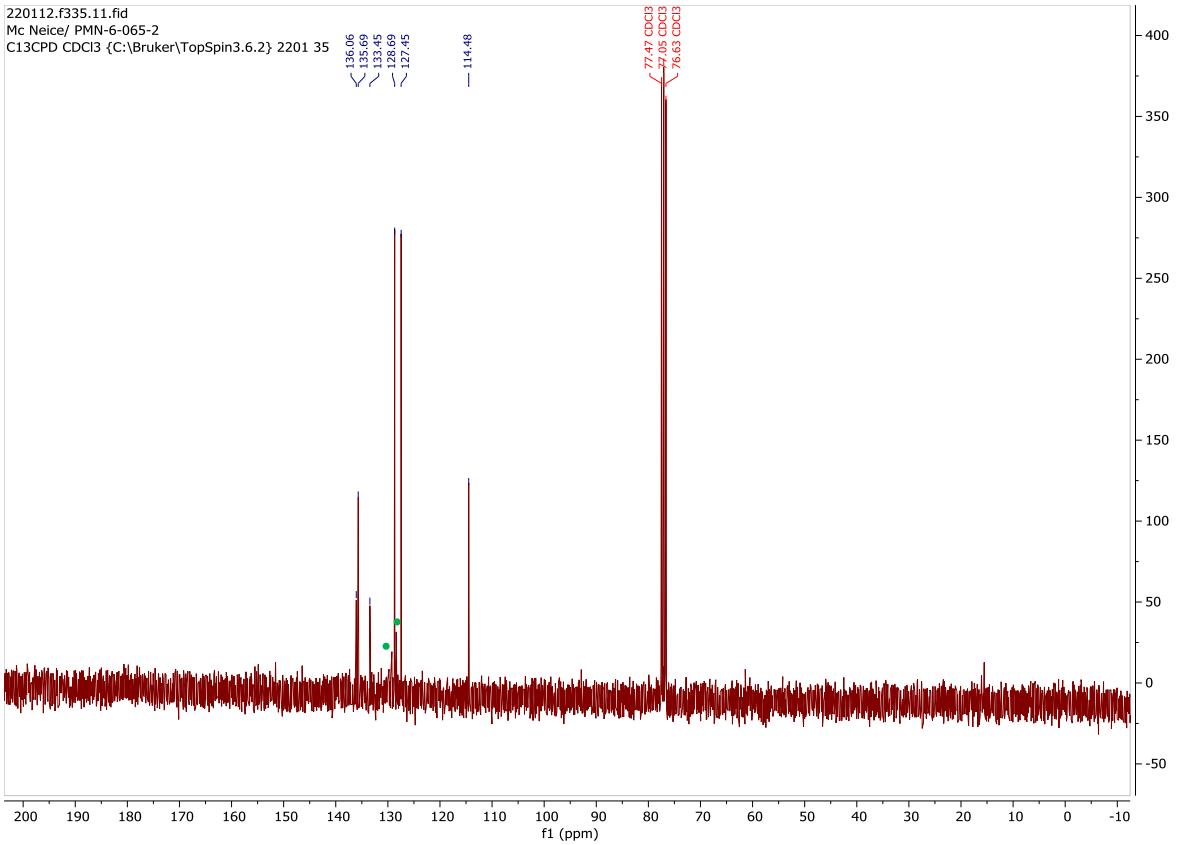

Figure S24: ^{13}C spectrum of the reaction mixture for 1-chloro-4-ethynylbenzene (**1d**) hydrogenation to 4-chlorostyrene (**2d**).

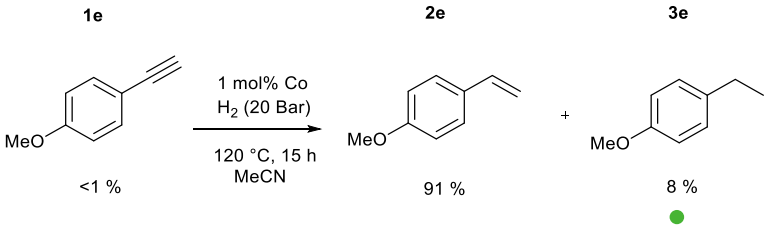

2e

^{1}H NMR (300 MHz, $CDCl_3$) δ = 7.43 – 7.34 (m, 2H), 6.94 – 6.86 (m, 2H), 6.72 (ddt, *J* = 17.6, 10.9, 0.5, 1H), 5.66 (dd, *J* = 17.6, 1.0, 1H), 5.18 (dd, *J* = 10.9, 1.0, 1H), 3.85 (s, 3H). ^{13}C NMR (75 MHz, $CDCl_3$) δ = 159.4, 136.3, 130.5, 128.7, 127.4, 113.95, 113.8, 111.6, 55.3.

MS (EI, 70 eV): *m/z* (%) 135 (M^+ + 1, 16), 134 (M^+, 100), 119 (70), 91 (67), 77 (9).

Literature Characterisation[8]

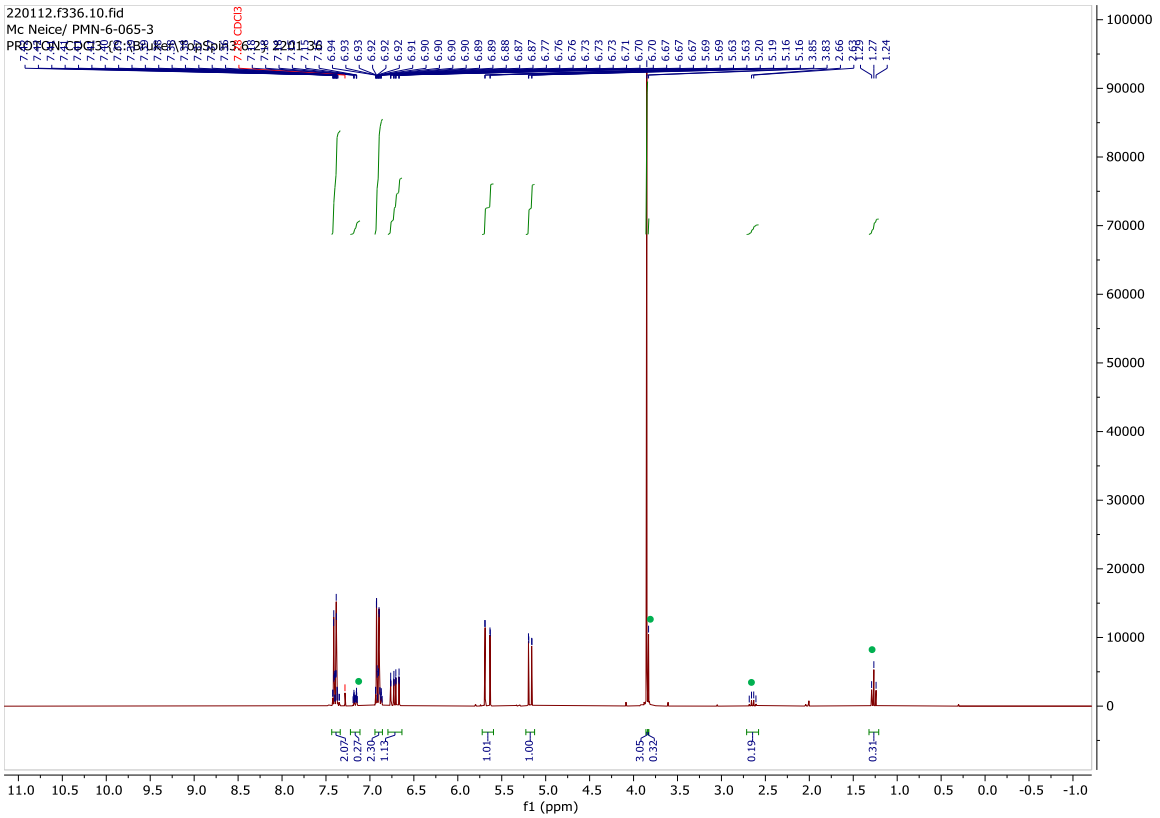

Figure S25: ^{1}H spectrum of the reaction mixture for 1-ethynyl-4-methoxybenzene (**1e**) hydrogenation to 4-methoxystyrene (**2e**).

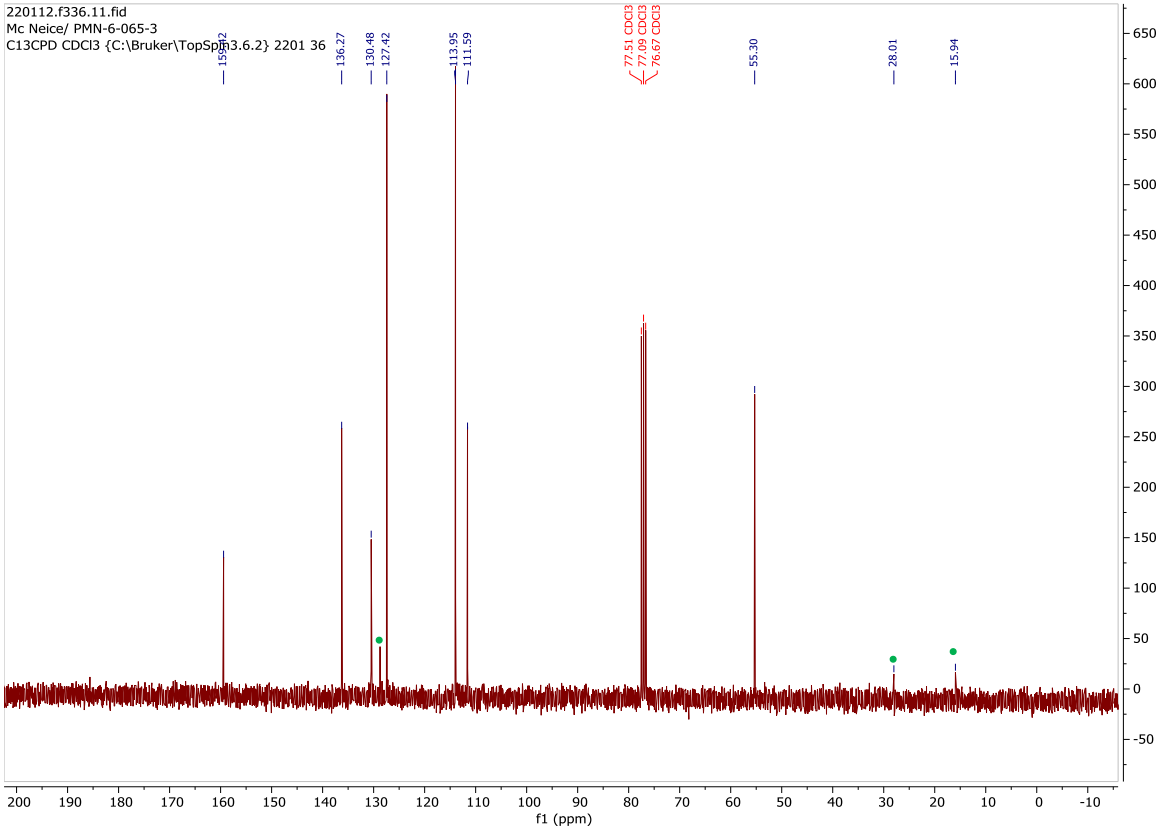

Figure S26: ^{13}C spectrum of the reaction mixture for 1-ethynyl-4-methoxybenzene (**1e**) hydrogenation to 4-methoxystyrene (**2e**).

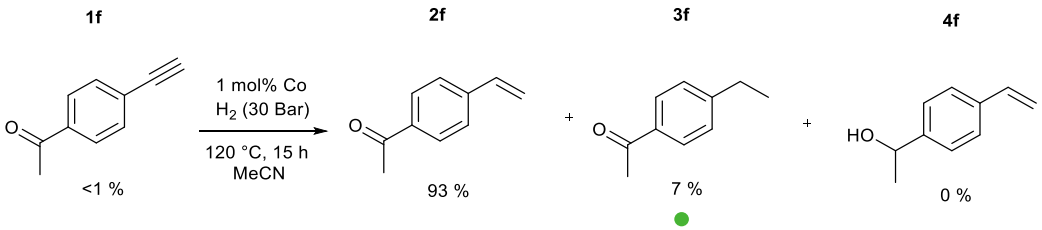

2f

^{1}H NMR (300 MHz, CDCl3) δ = 7.98 – 7.90 (m, 2H), 7.53 – 7.46 (m, 2H), 6.78 (dd, *J* = 17.6, 10.9, 1H), 5.89 (dd, *J* = 17.6, 0.7, 1H), 5.42 (dd, *J* = 10.9, 0.7, 1H), 2.61 (s, 3H). ^{13}C NMR (75 MHz, CDCl3) δ = 197.6, 142.1, 136.3, 135.9, 128.7, 126.3, 116.7.

MeCN is visible at 2.02 ppm due to the volatility of **2f** making its isolation difficult.

MS (EI, 70 eV): *m/z* (%) 146 (M^+, 57), 131 (100), 103 (58), 77 (34).

Literature Characterisation[8]

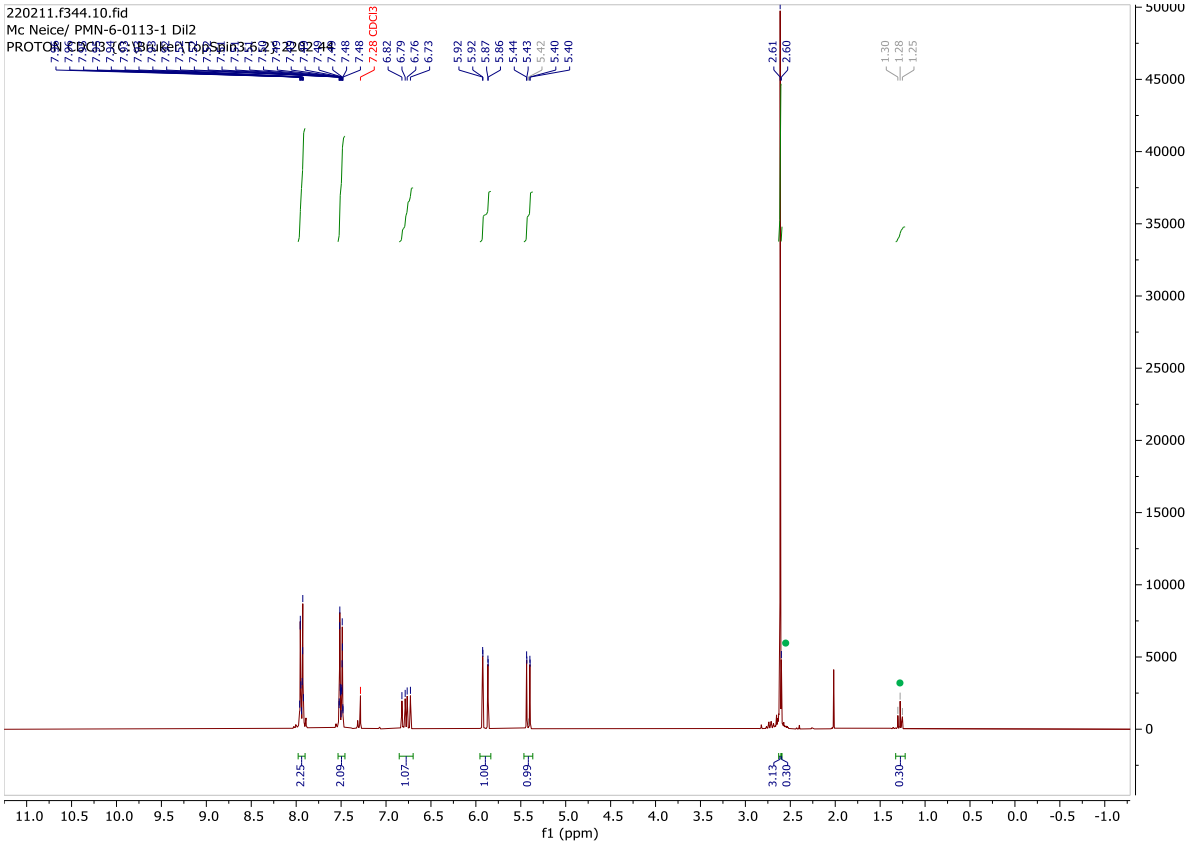

Figure S27: ^{1}H spectrum of the reaction mixture for 1-(4-ethynylphenyl)ethanone (**1f**) hydrogenation to 1-(4-ethenylphenyl)ethanone (**2f**).

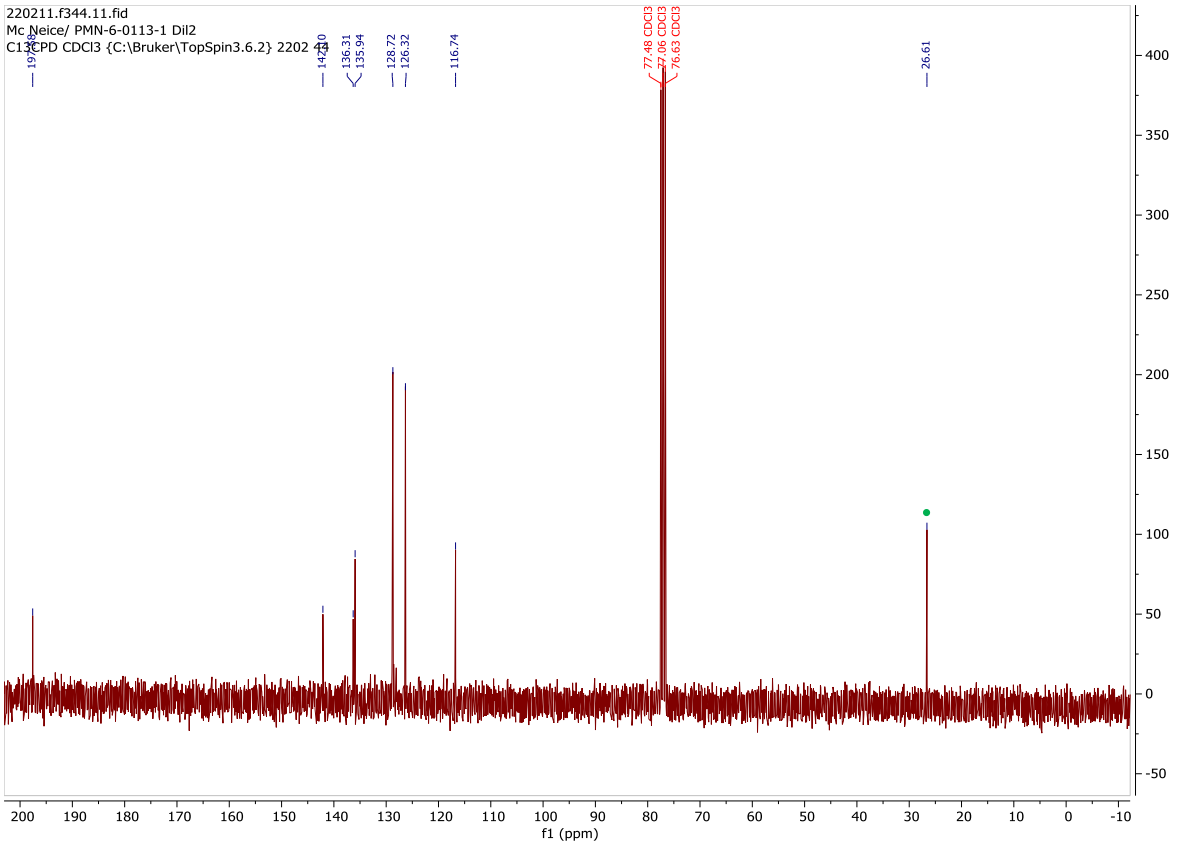

Figure S28: ^{13}C spectrum of the reaction mixture for 1-(4-ethynylphenyl)ethanone (**1f**) hydrogenation to 1-(4-ethenylphenyl)ethanone (**2f**).

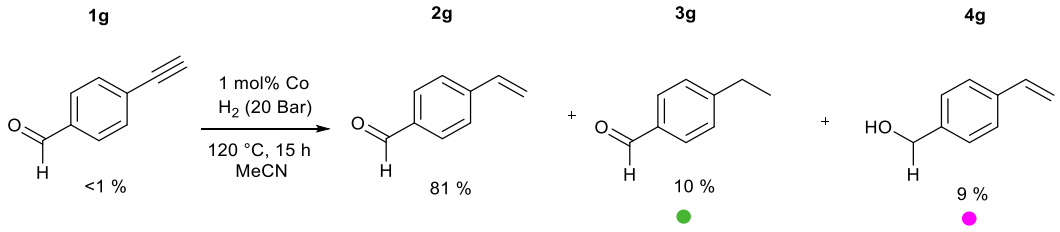

2g

^1H NMR (300 MHz, $CDCl_3$) δ = 9.99 (s, 1H), 7.93 – 7.74 (m, 2H), 7.65 – 7.50 (m, 2H), 7.50 – 7.31 (m, 1H), 6.78 (ddq, *J* = 17.6, 10.9, 0.5, 1H), 5.92 (dd, *J* = 17.6, 0.7, 1H), 5.45 (dd, *J* = 10.9, 0.7, 1H), 1.38 – 1.19 (m, 1H). ^{13}C NMR (75 MHz, $CDCl_3$) δ = 191.7, 135.9, 130.1, 126.7, 117.5.

MS (EI, 70 eV): *m/z* (%) 132 (M^+, 89), 102 (8), 78 (37), 77 (16), 51 (17).

Literature Characterisation[9]

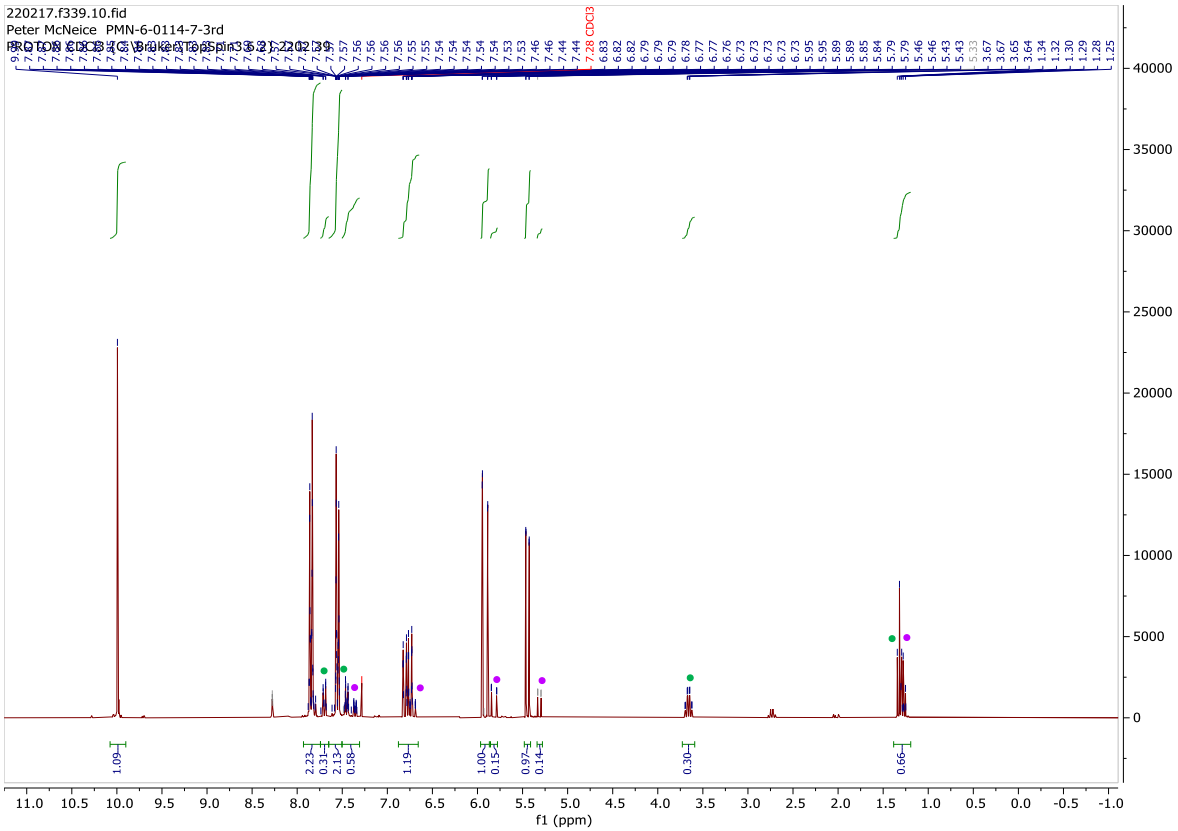

Figure S29: ^{13}C spectrum of the reaction mixture for 4-ethynylbenzaldehyde (**1g**) hydrogenation to 4-ethenylbenzaldehyde (**2g**).

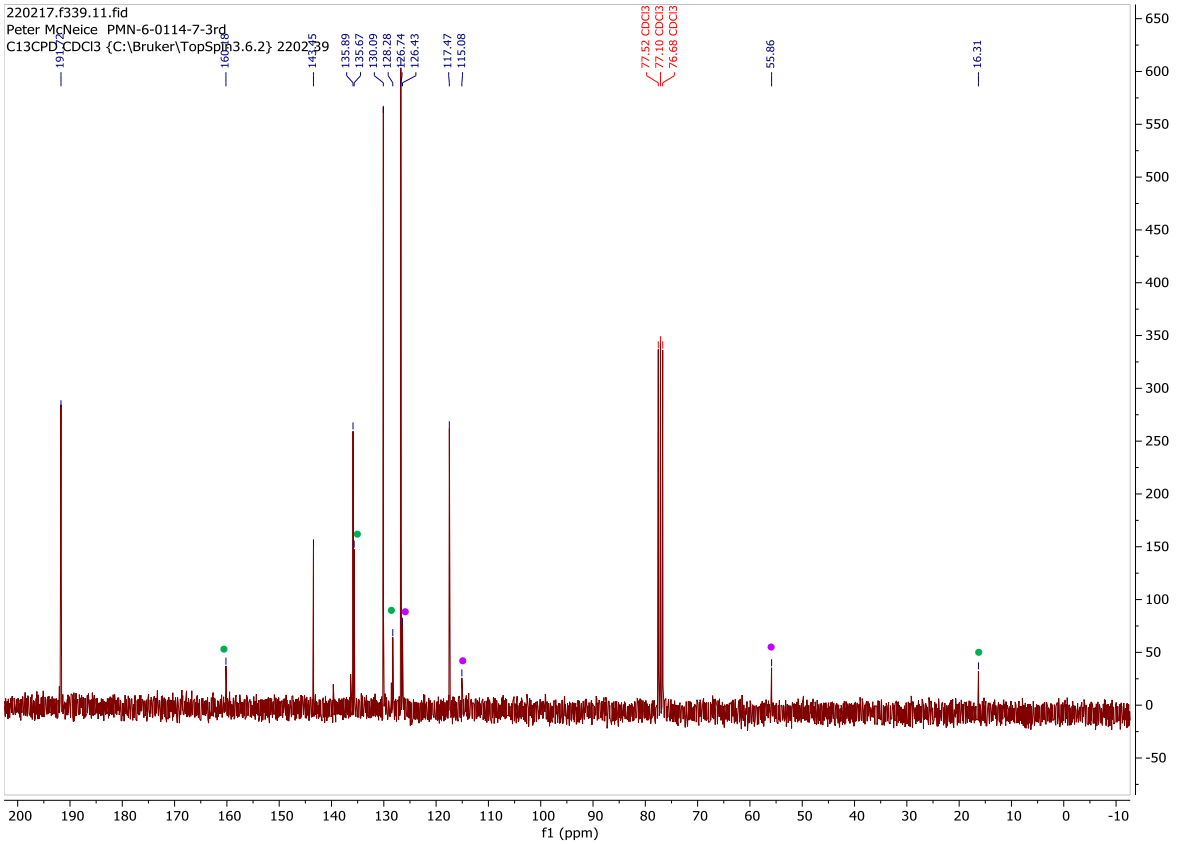

Figure S30: ^{13}C spectrum of the reaction mixture for 4-ethynylbenzaldehyde (**1g**) hydrogenation to 4-ethenylbenzaldehyde (**2g**).

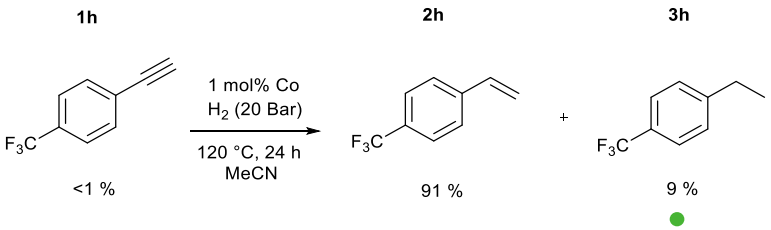

2h

^{1}H NMR (300 MHz, $CDCl_3$) δ = 7.61 – 7.47 (m, 4H), 6.75 (dd, *J* = 17.6, 10.9, 1H), 5.85 (d, *J* = 17.6, 1H), 5.39 (d, *J* = 10.9, 4H). ^{13}C NMR (75 MHz, $CDCl_3$) δ = 139.2, 133.8, 124.2 (q, *J* = 218 Hz), 114.7. ^{19}F NMR (282 MHz, $CDCl_3$) δ = -62.53.

The proton aromatic region contains too many protons due to overlap with the over-hydrogenated product. These have not been precisely assigned.

MeCN is visible at 2.02 ppm.

MS (EI, 70 eV): *m/z* (%) 172 (M^+, 100), 151 (21), 145 (7), 103 (33), 77 (7).

Literature Characterisation[10]

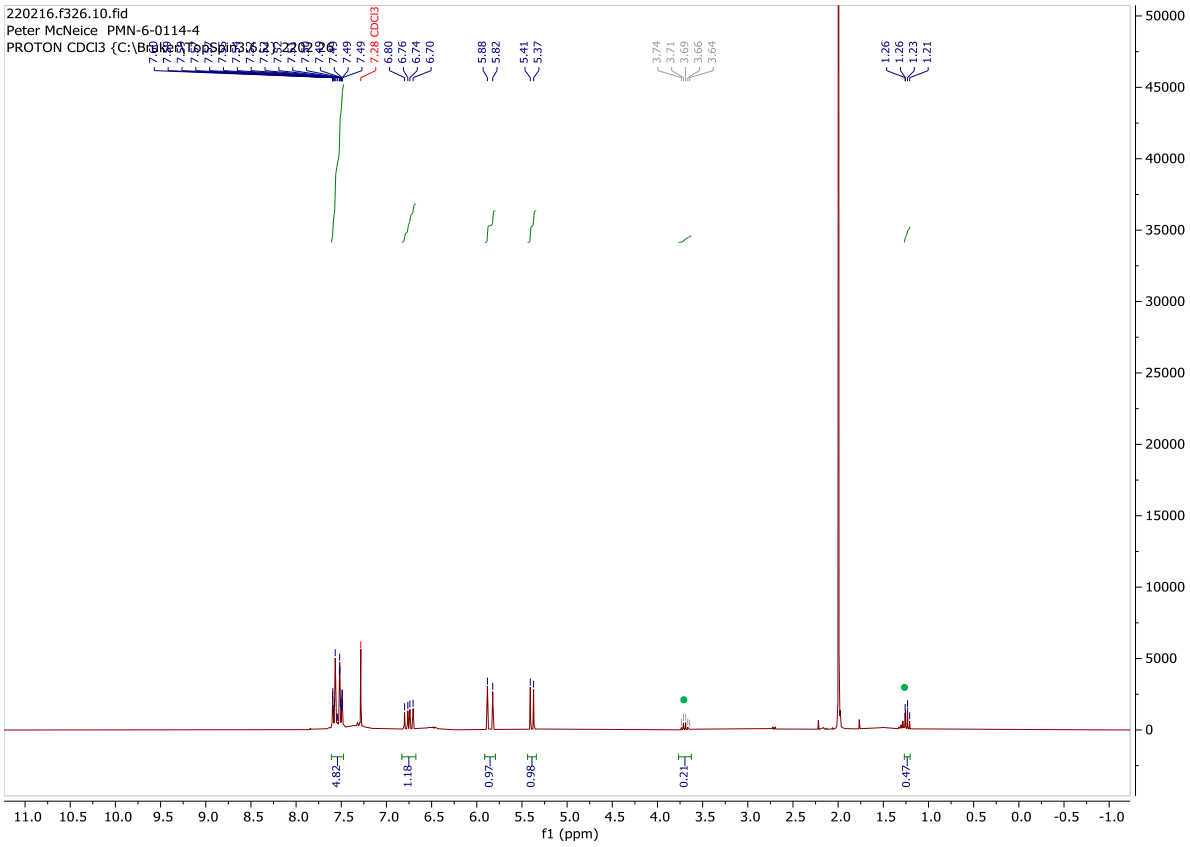

Figure S31: ^{1}H spectrum of the reaction mixture for 1-ethynyl-4-(trifluoromethyl)benzene (**1h**) hydrogenation to 1-ethenyl-4-(trifluoromethyl)benzene (**2h**).

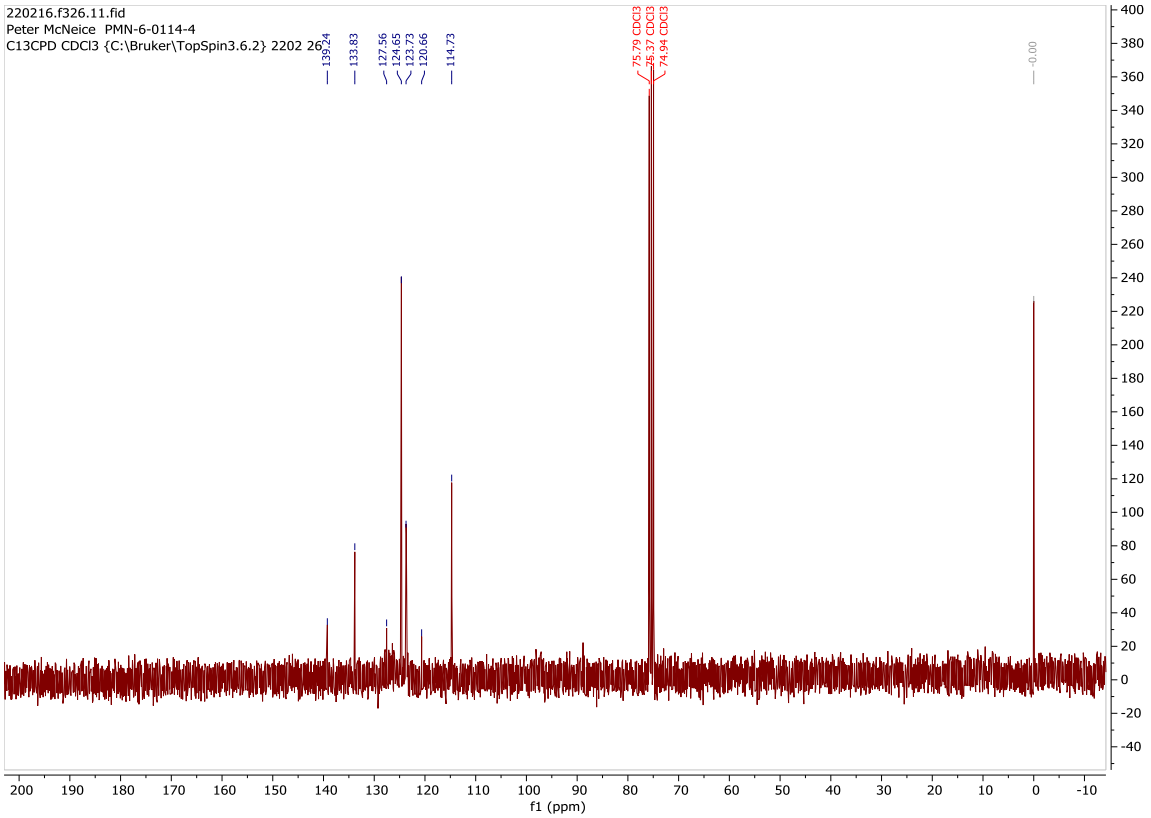

Figure S32: ^{13}C spectrum of the reaction mixture for 1-ethynyl-4-(trifluoromethyl)benzene (**1h**) hydrogenation to 1-ethenyl-4-(trifluoromethyl)benzene (**2h**).

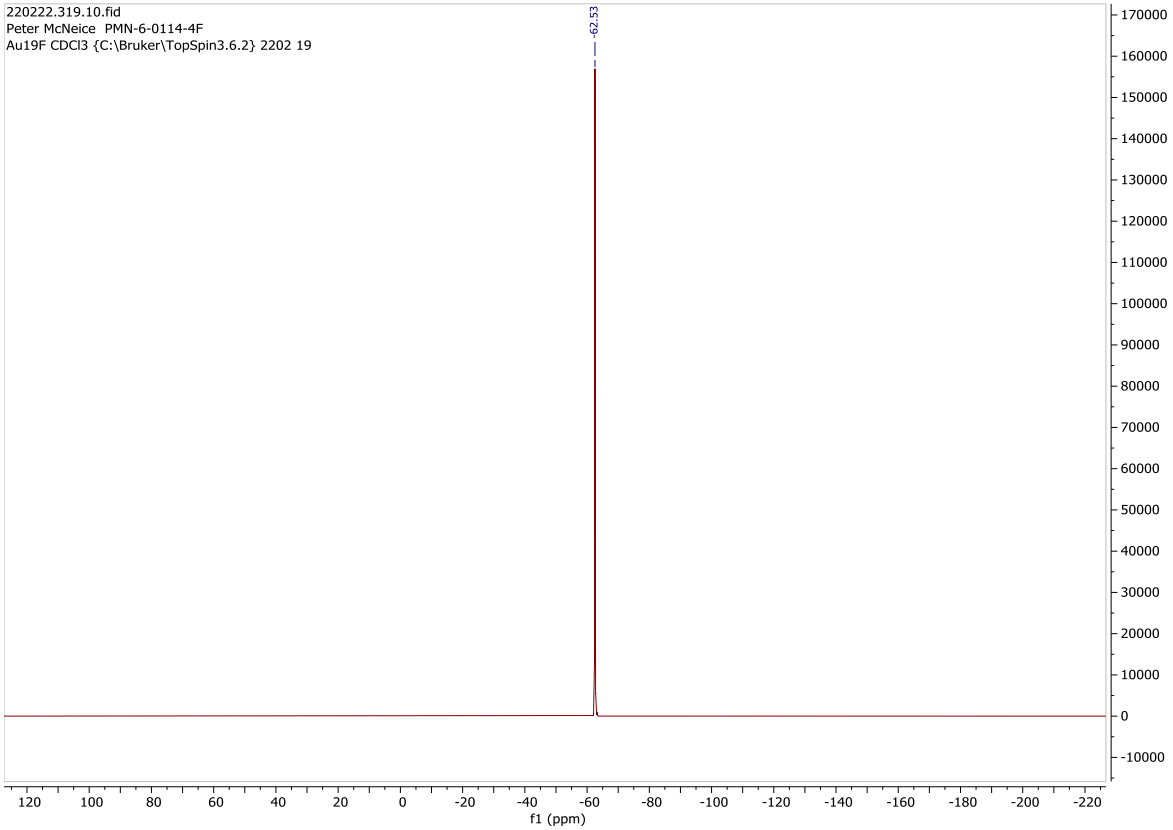

Figure S33: ^{19}F spectrum of the reaction mixture for 1-ethynyl-4-(trifluoromethyl)benzene (**1h**) hydrogenation to 1-ethenyl-4-(trifluoromethyl)benzene (**2h**).

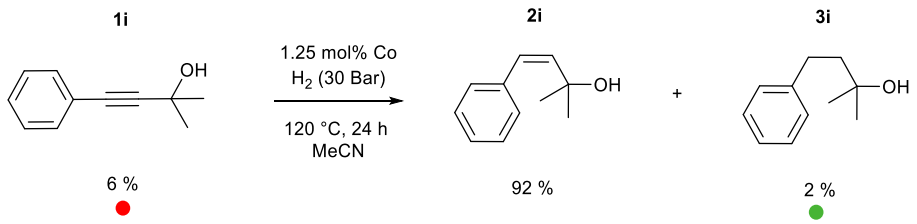

2i

^{1}H NMR (300 MHz, $CDCl_3$) δ = 7.29 – 7.20 (m, 5H), 6.41 – 6.34 (m, 1H), 5.67 (d, *J* = 12.7, 1H), 1.27 (s, 6H). ^{13}C NMR (75 MHz, $CDCl_3$) δ = 139.3, 137.5, 131.7, 129.0, 128.3, 128.1, 127.9, 126.98, 77.3, 71.98, 31.1.

Water from the NMR solvent is visible in the proton NMR at 1.53 ppm.

MS (EI, 70 eV): *m/z* (%) 162 (M^+, 23), 147 (100), 129 (79), 115 (13), 103 (15), 91 (68), 77 (22),

HRMS (ESI): *m/z* calc for $C_{11}H_{14}O$: 162.10392 (M^+), found: 162.10453 (M^+).

Literature Characterisation[11]

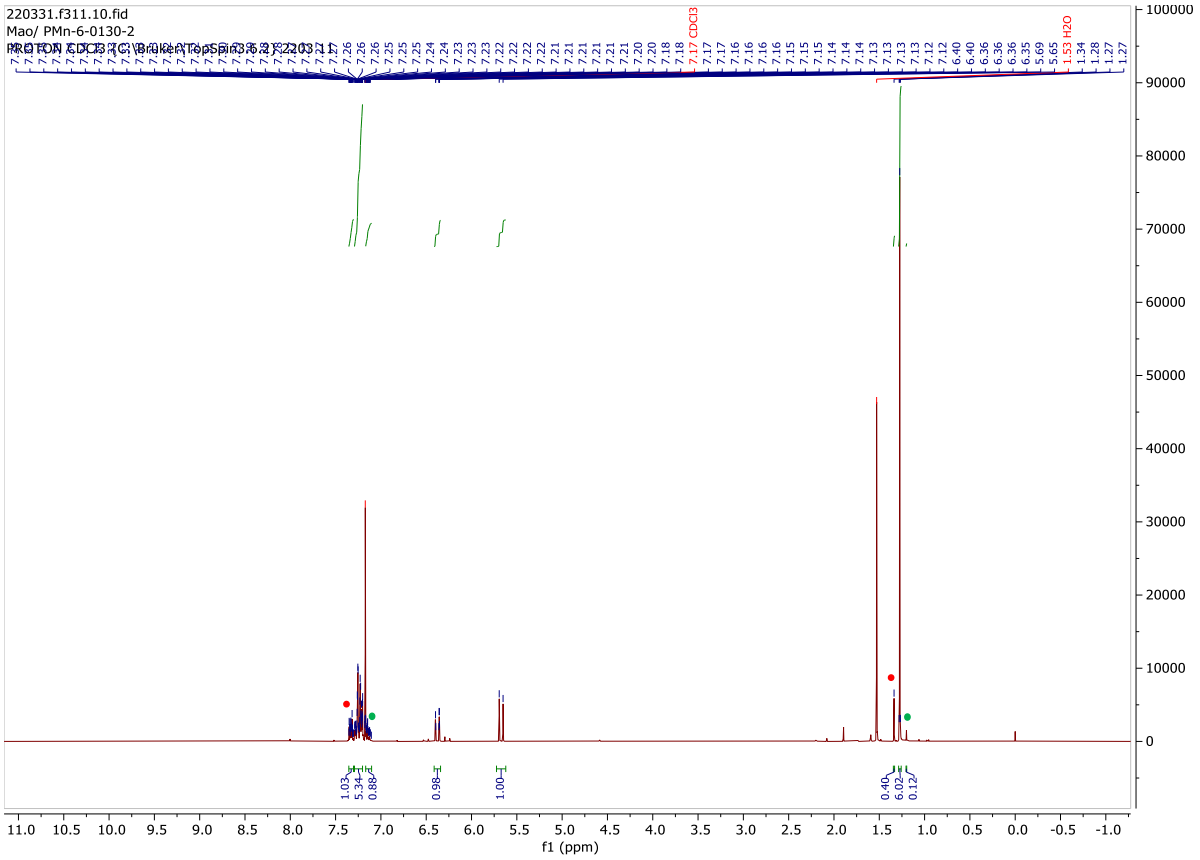

Figure S34: ^{1}H spectrum of the reaction mixture for 2-methyl-4-phenyl-3-butyn-2-ol (**1i**) hydrogenation to (*Z*)-2-methyl-4-phenyl-3-buten-2-ol (**2i**).

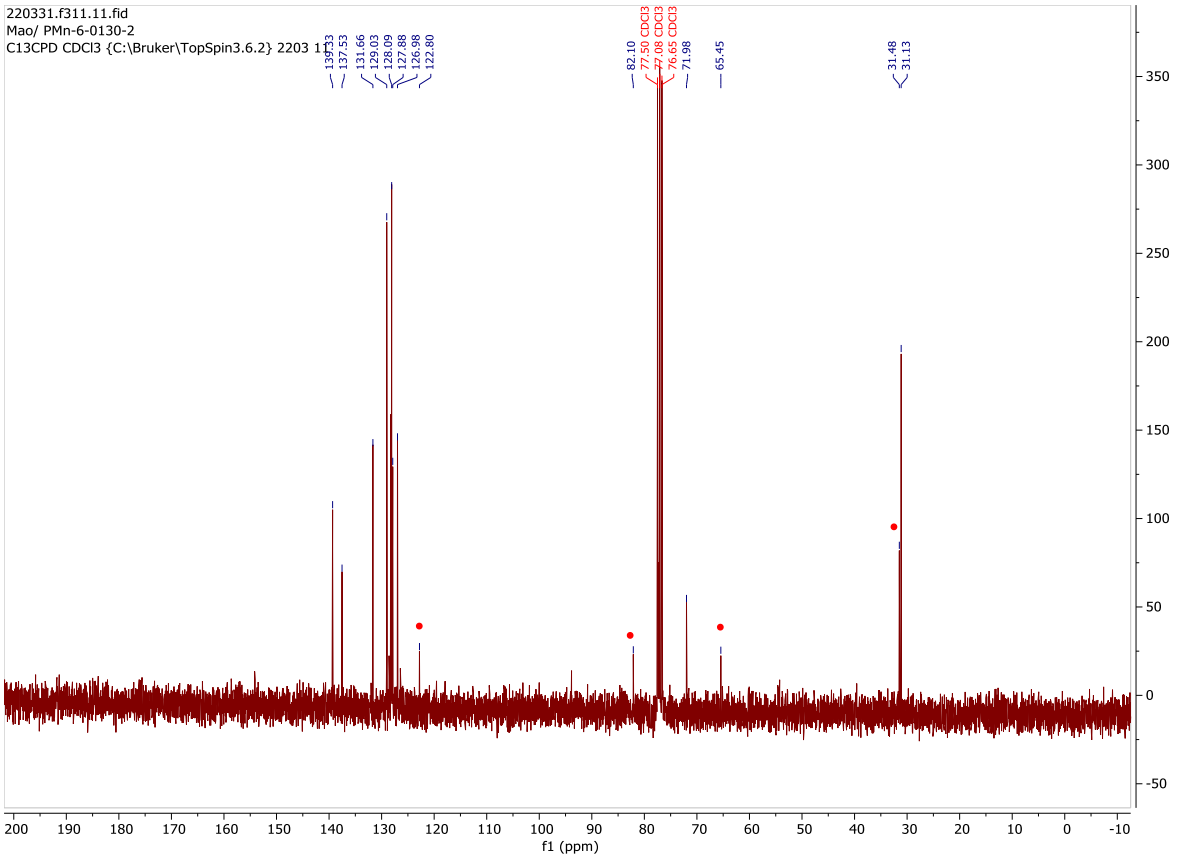

Figure S35: ^{13}C spectrum of the reaction mixture for 2-methyl-4-phenyl-3-butyn-2-ol (**1i**) hydrogenation to (*Z*)-2-methyl-4-phenyl-3-buten-2-ol (**2i**).

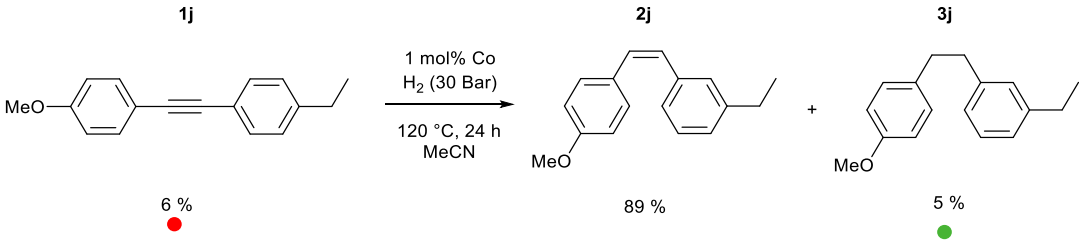

2j

^{1}H NMR (300 MHz, $CDCl_3$) δ = 7.37 – 7.24 (m, 4H), 7.24 – 7.02 (m, 2H), 6.93 – 6.80 (m, 2H), 6.57 (s, 2H), 3.86 (s, 3H), 2.71 (q, *J* = 7.6, 2H), 1.32 (t, *J* = 7.6, 3H). ^{13}C NMR (75 MHz, $CDCl_3$) δ = 158.7, 143.1, 134.9, 130.2, 130.0, 129.2, 128.9, 127.8, 113.7, 55.2, 28.7, 15.5.

MS (EI, 70 eV): *m/z* (%) 238 (M^+, 100), 224 (15), 223 (75), 209 (11), 178 (20), 165 (41), 152 (11)

Literature Characterisation[12]

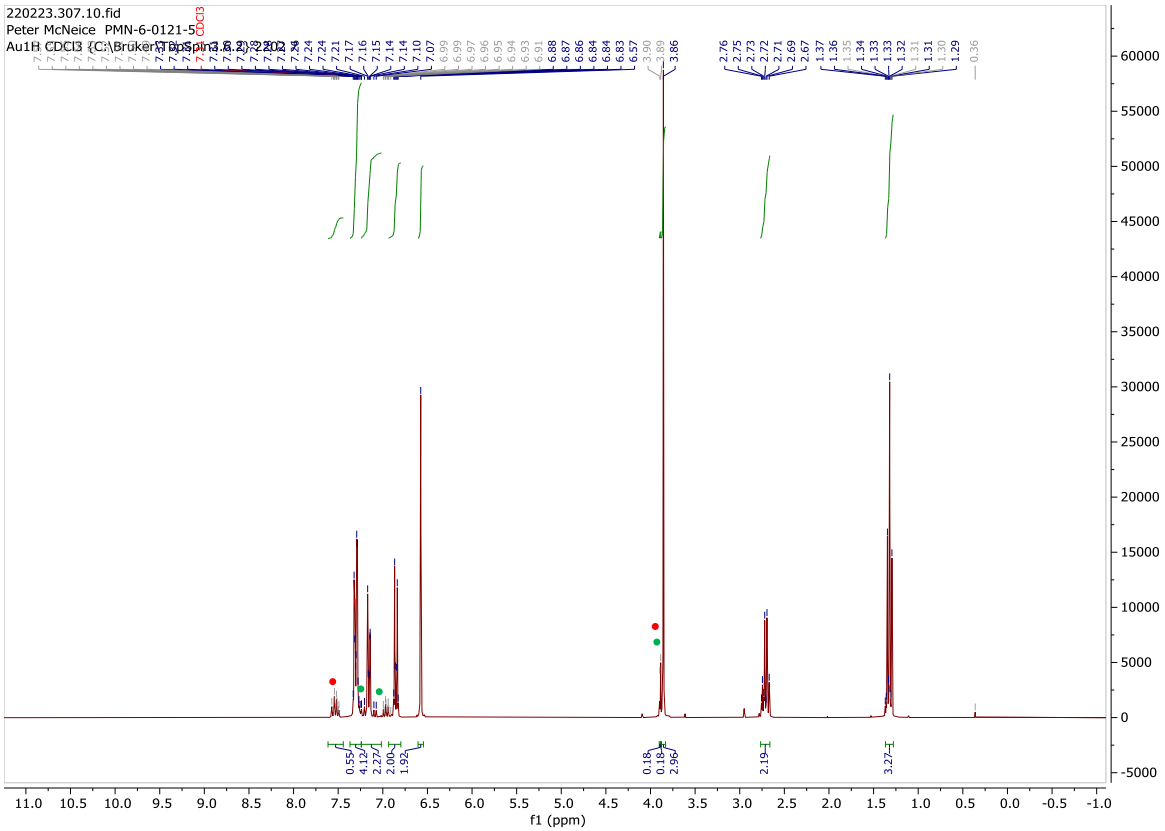

Figure S36: ^{1}H spectrum of the reaction mixture for 1-ethyl-4-[2-(4-methoxyphenyl)ethynyl]benzene (**1j**) hydrogenation to (*Z*)-1-ethyl-4-(4-methoxystyryl)benzene (**2j**).

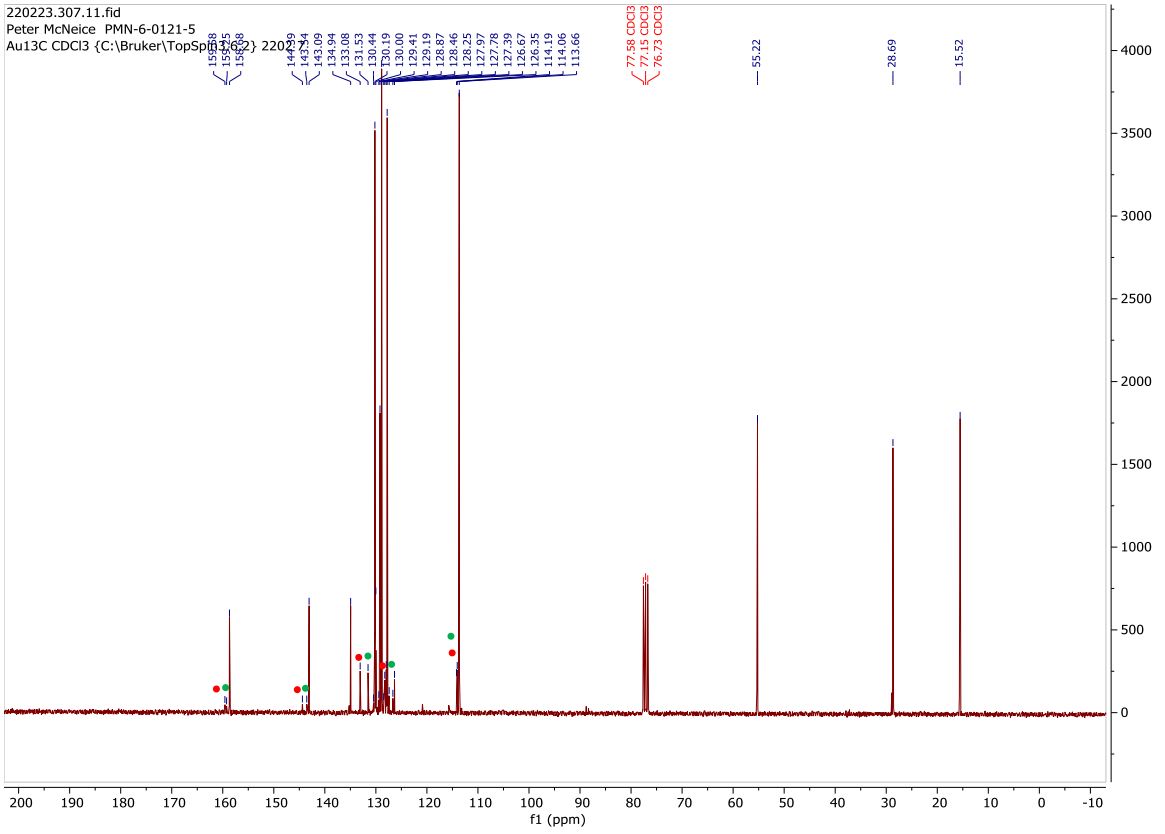

Figure S37: ^{1}H spectrum of the reaction mixture for 1-ethyl-4-[2-(4-methoxyphenyl)ethynyl]benzene (**1j**) hydrogenation to (*Z*)-1-ethyl-4-(4-methoxystyryl)benzene (**2j**).

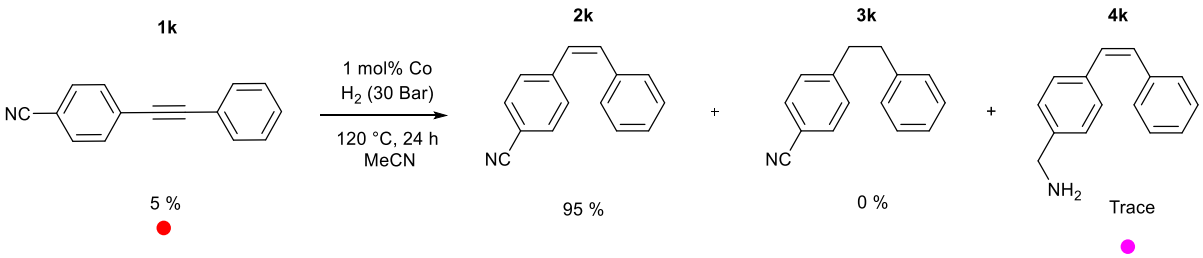

2k

^{1}H NMR (300 MHz, $CDCl_3$) δ = 7.71 – 7.47 (m, 2H), 7.35 (d, *J* = 8.1, 2H), 7.32 – 7.18 (m, 5H), 6.80 (d, *J* = 12.2, 1H), 6.60 (d, *J* = 12.1, 1H). ^{13}C NMR (75 MHz, $CDCl_3$) δ = 142.1, 136.3, 133.4, 132.1, 129.6, 128.8, 128.6, 128.4, 127.9, 118.98, 110.5.

MS (EI, 70 eV): *m/z* (%) 205 (M^+, 100), 190 (55), 177 (21), 165 (19), 151 (10), 115 (2), 102 (10), 89 (13), 76 (11).

Literature Characterisation[6]

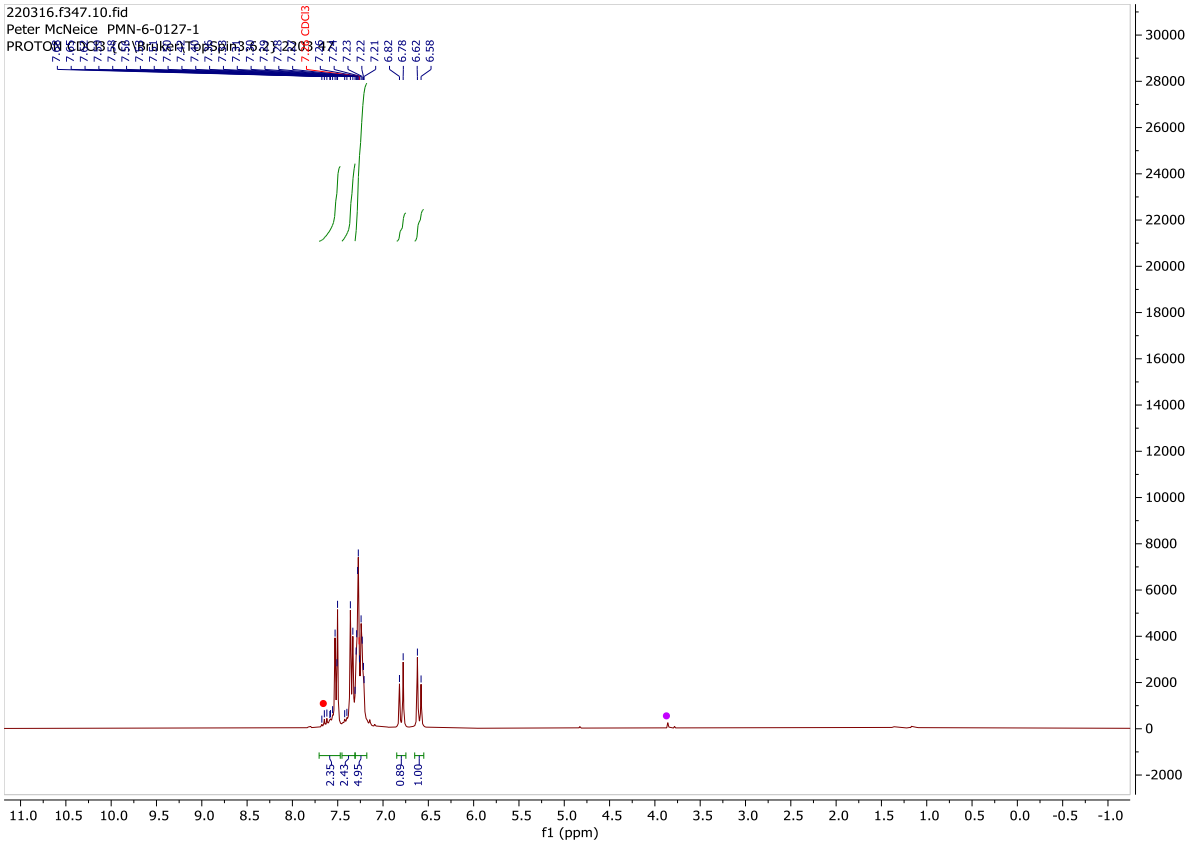

Figure S38: ^{1}H spectrum of the reaction mixture for 4-(2-phenylethynyl)benzonitrile (**1k**) hydrogenation to 4-[(*Z*)-2-phenylethenyl]benzonitrile (**2k**).

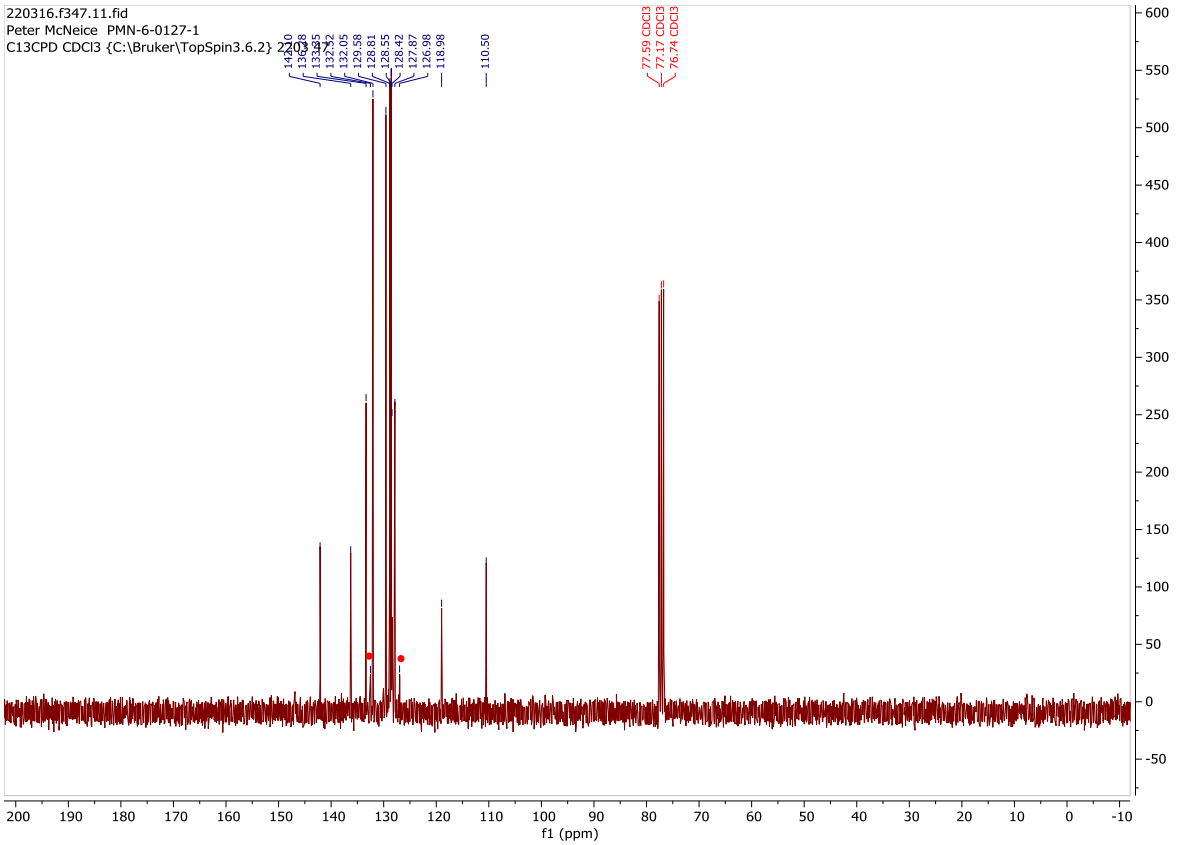

Figure S39: ^{13}C spectrum of the reaction mixture for 4-(2-phenylethynyl)benzonitrile (**1k**) hydrogenation to 4-[(*Z*)-2-phenylethenyl]benzonitrile (**2k**).

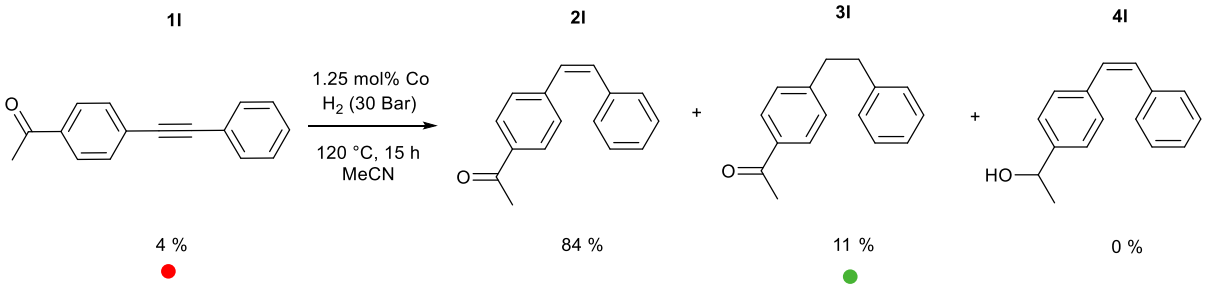

2l

^{1}H NMR (300 MHz, $CDCl_3$) δ = 7.72 – 7.67 (m, 2H), 7.49 – 7.38 (m, 1H), 7.24 – 7.17 (m, 2H), 7.14 – 7.08 (m, 5H), 6.61 (d, *J* = 12.1, 1H), 6.48 (d, *J* = 12.3, 1H), 2.44 (s, 3H). ^{13}C NMR (75 MHz, $CDCl_3$) δ = 197.6, 142.3, 136.7, 135.7, 132.5, 129.2, 129.1, 128.9, 128.4, 128.4, 127.6, 26.6.

MS (EI, 70 eV): *m/z* (%) 222 (M^+, 78), 178 (80), 152 (19), 89 (13), 77 (4), 76 (7).

HRMS (ESI): *m/z* calc for $C_{16}H_{14}O$: 222.10354 (M^+), found: 222.10392 (M^+).

Literature Characterisation[6]

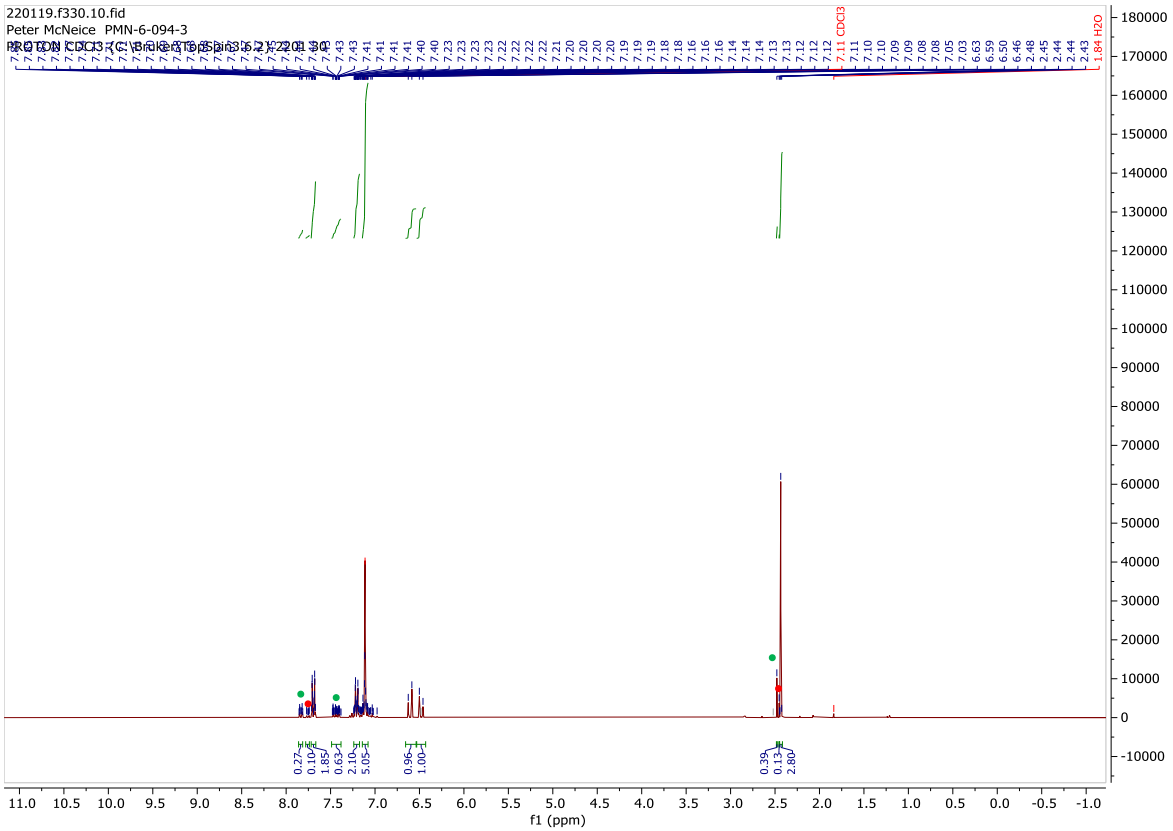

Figure S40: ^{1}H spectrum of the reaction mixture for 1-[4-(2-phenylethynyl)phenyl]ethanone (**1l**) hydrogenation to (*Z*)-1-acetyl-4-styrylbenzene (**2l**).

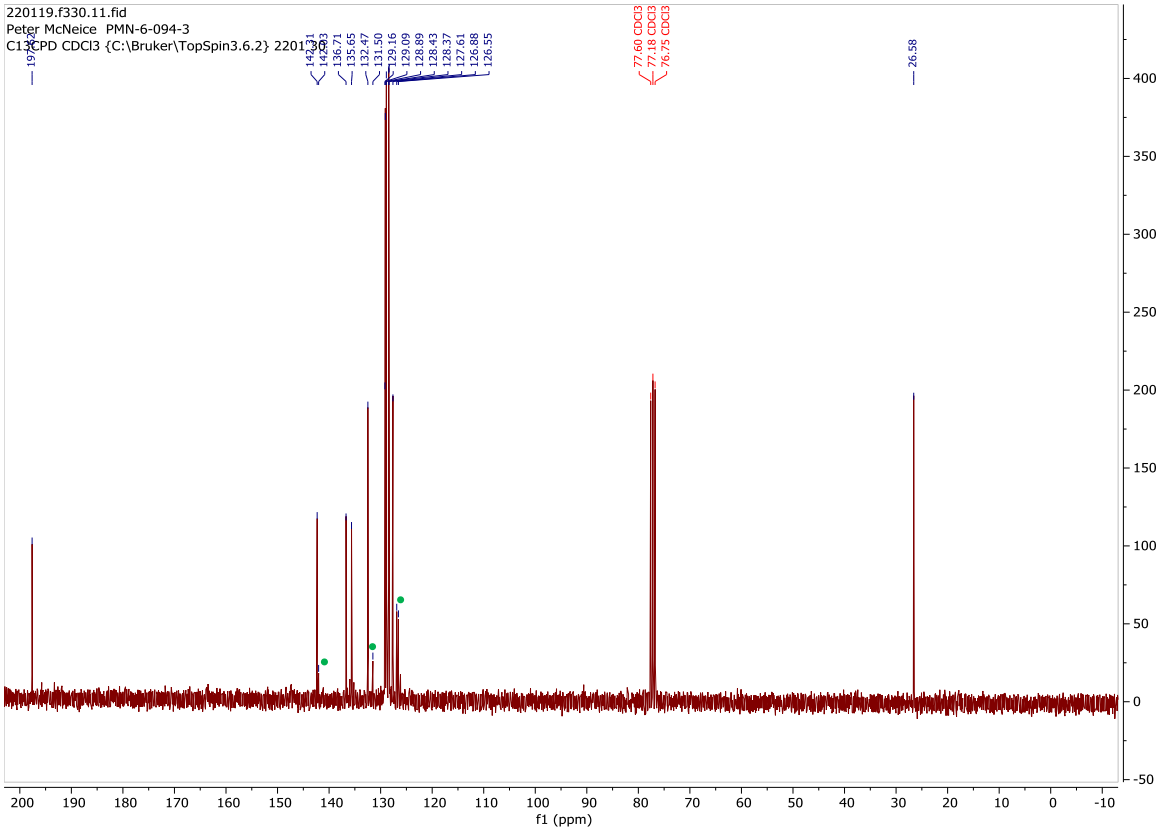

Figure S41: ^{13}C spectrum of the reaction mixture for 1-[4-(2-phenylethynyl)phenyl]ethanone (**1l**) hydrogenation to (*Z*)-1-acetyl-4-styrylbenzene (**2l**).

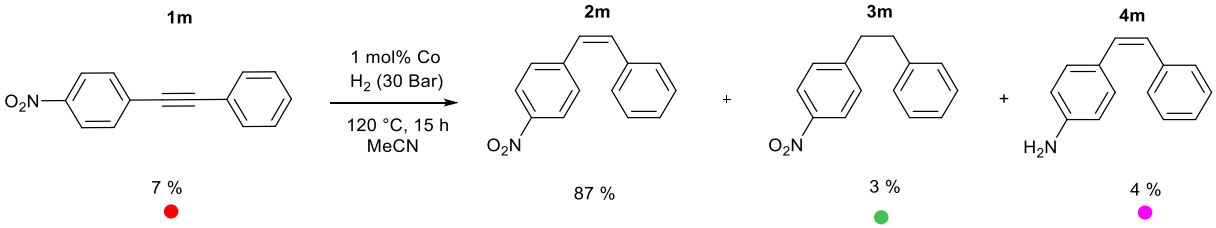

2m

^{1}H NMR (300 MHz, $CDCl_3$) δ = 8.02 – 7.95 (m, 2H), 7.32 – 7.26 (m, 2H), 7.20 – 7.09 (m, 5H), 6.81 – 6.67 (m, 1H), 6.53 (d, *J* = 12.2, 1H). ^{13}C NMR (75 MHz, $CDCl_3$) δ = 146.6, 144.2, 136.1, 133.97, 129.7, 128.8, 128.6, 128.0, 127.98, 123.6.

MS (EI, 70 eV): *m/z* (%) 225 (M^+, 100), 178 (98), 165 (9), 152 (21), 139 (3), 89 (7), 76 (6), 63 (2).

Literature characterisation[13]

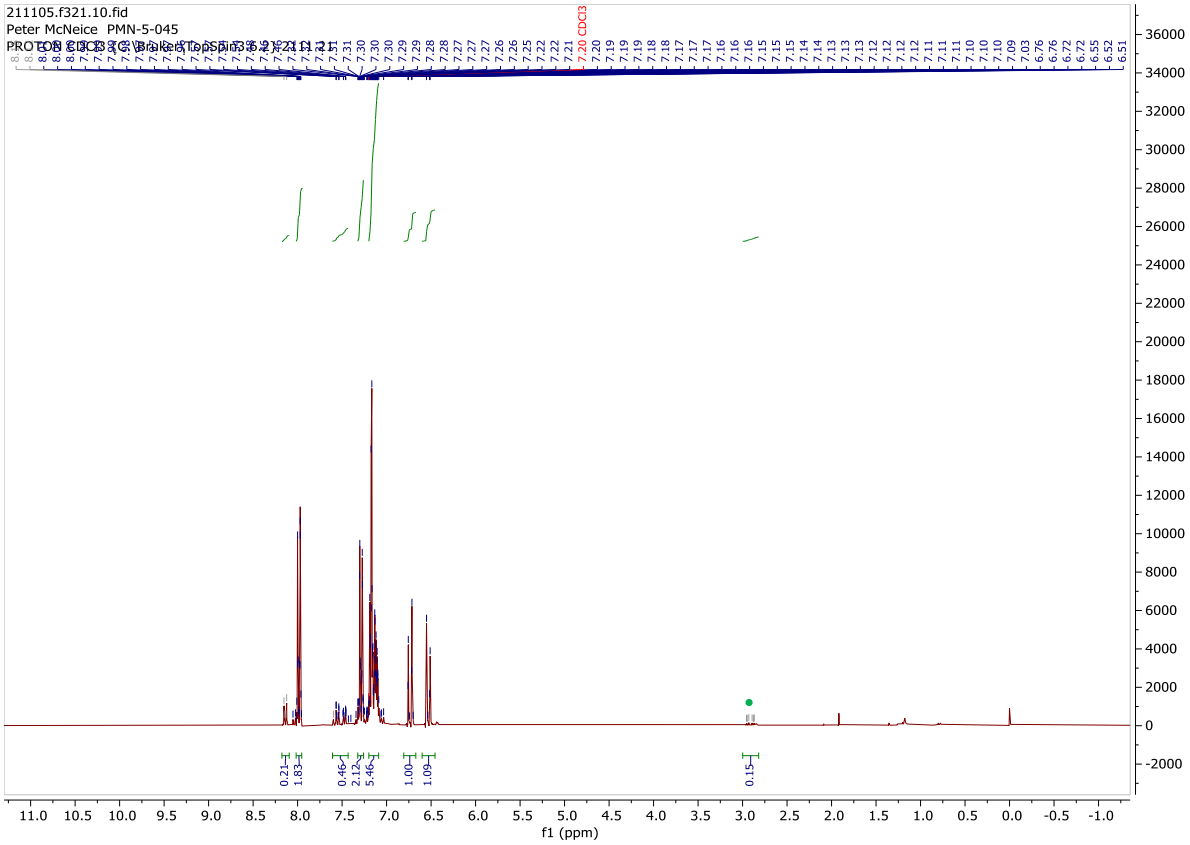

Figure S42: ^{1}H spectrum of the reaction mixture for 1-nitro-4-(2-phenylethynyl)benzene (**1m**) hydrogenation to 1-nitro-4-[(1*Z*)-2-phenylethenyl]benzene (**2m**).

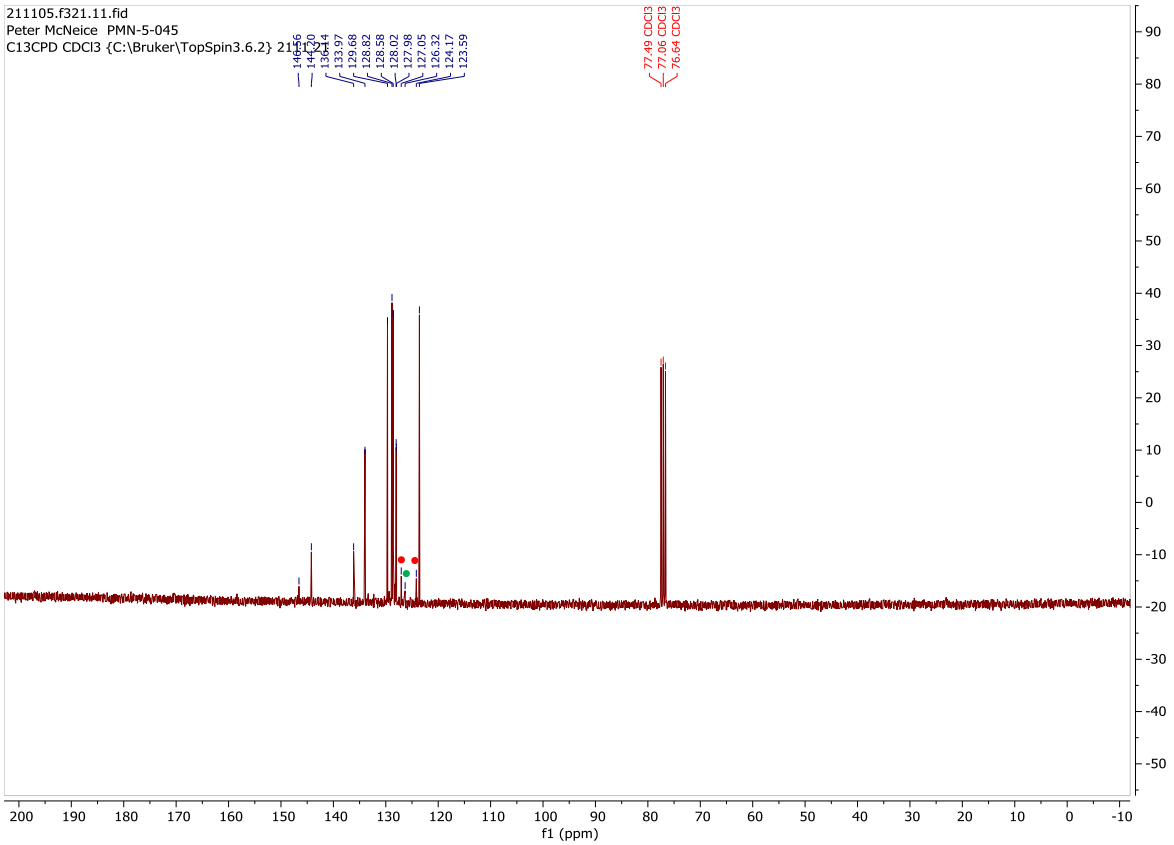

Figure S43: ^{13}C spectrum of the reaction mixture for 1-nitro-4-(2-phenylethynyl)benzene (**1m**) hydrogenation to 1-nitro-4-[(1*Z*)-2-phenylethenyl]benzene (**2m**).

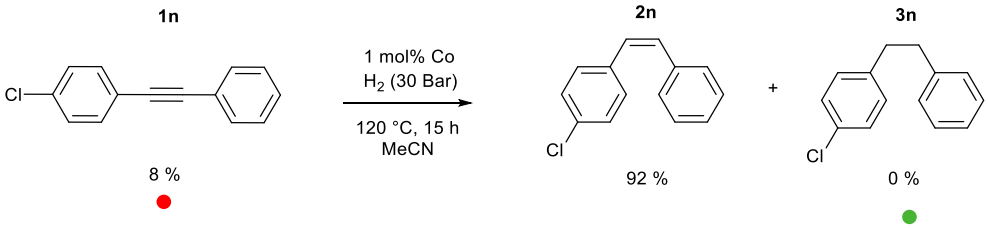

2n

^1H NMR (300 MHz, $CDCl_3$) δ = 7.44 – 7.20 (m, 1H), 7.17 – 7.04 (m, 9H), 6.54 (d, *J* = 12.2, 1H), 6.43 (d, *J* = 12.0, 1H). ^{13}C NMR (75 MHz, $CDCl_3$) δ = 136.9, 135.7, 132.8, 131.0, 130.3, 128.96, 128.85, 128.5, 128.4, 127.4.

MS (EI, 70 eV): *m/z* (%) 214 (M^+, 85), 178 (100), 152 (17), 89 (18), 76 (17), 51 (6).

HRMS (ESI): *m/z* calc for $C_{14}H_{11}Cl_1$: 214.05490 (M^+), found: 214.04967 (M^+).

Literature Characterisation[6]

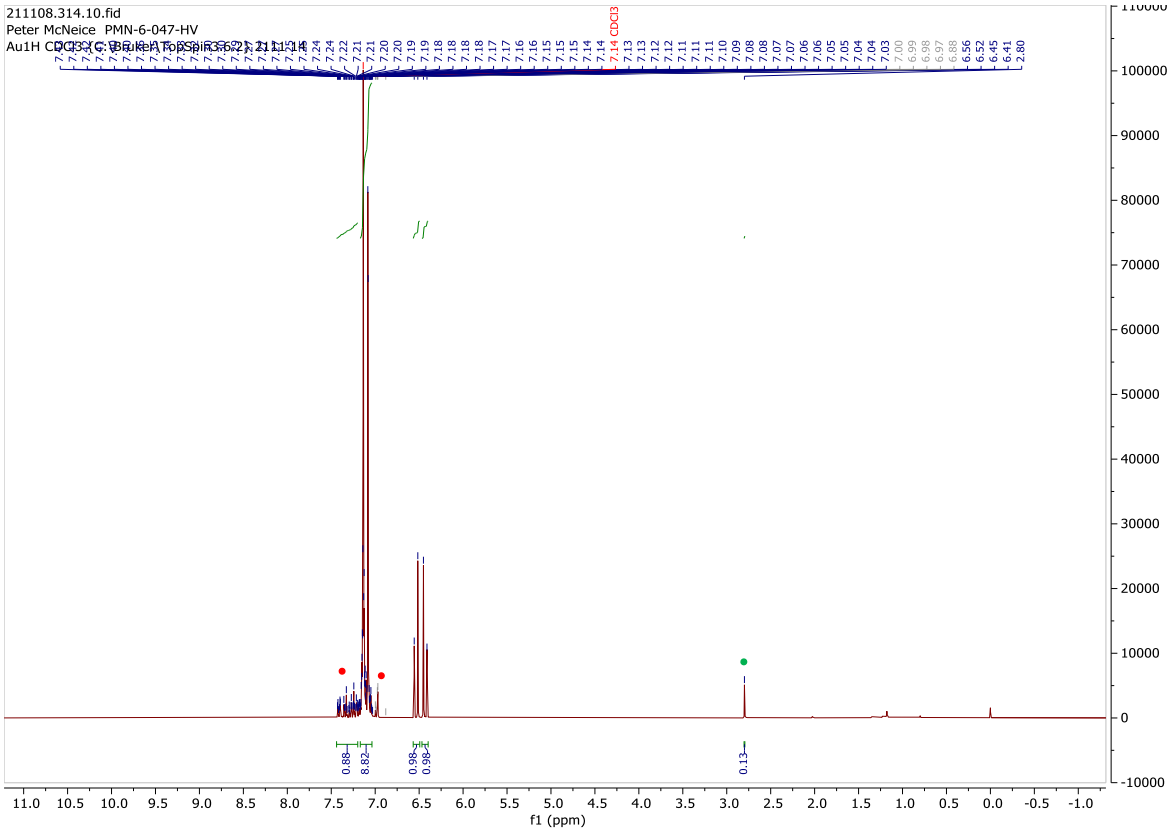

Figure S44: ^{1}H spectrum of the reaction mixture for 1-chloro-4-(2-phenylethynyl)benzene hydrogenation (**1n**) to (*Z*)-1-chloro-4-styrylbenzene (**2n**).

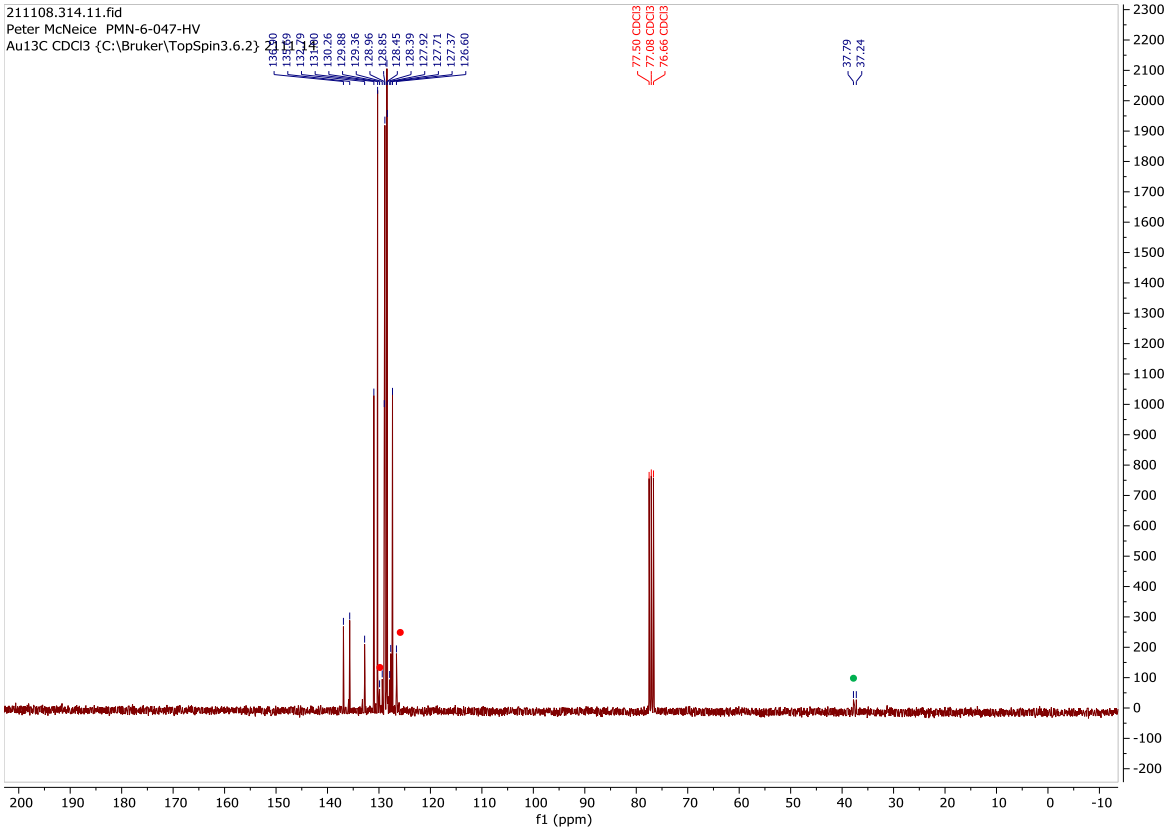

Figure S45: ^{13}C spectrum of the reaction mixture for 1-chloro-4-(2-phenylethynyl)benzene hydrogenation (**1n**) to (*Z*)-1-chloro-4-styrylbenzene (**2n**).

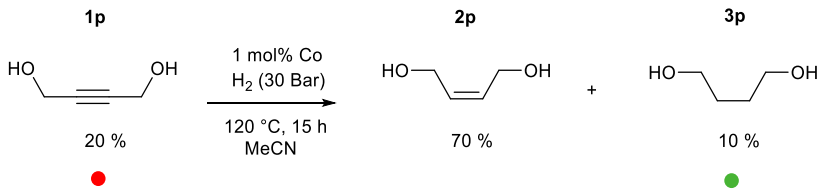

2p

^{1}H NMR (300 MHz, $CDCl_3$) δ = 5.81 (ddd, *J* = 4.9, 3.7, 1.2, 2H), 4.27 (d, *J* = 4.8, 4H). 13C NMR (75 MHz, CDCl3) δ = 131.1, 58.6.

MS (EI, 70 eV): *m/z* (%) 70 (76), 58 (10), 53 (7).

Literature Characterisation[14,15]

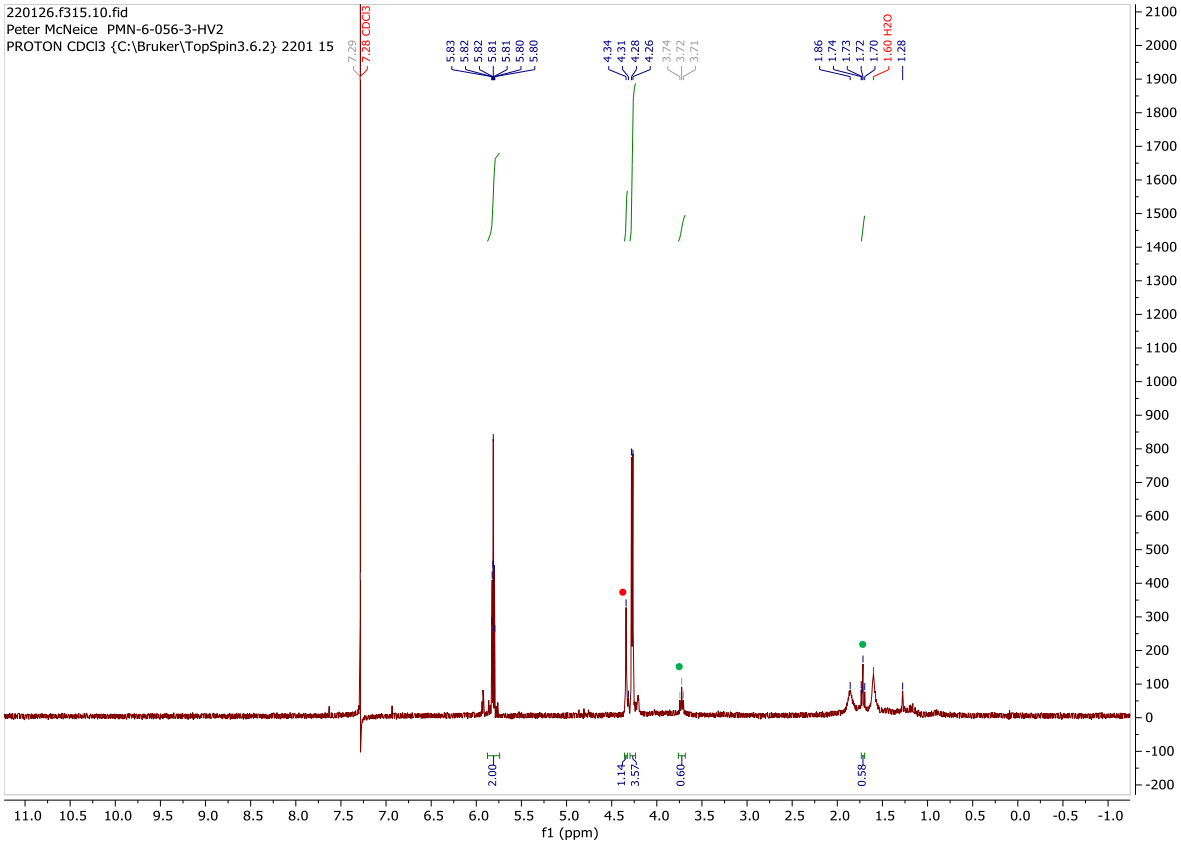

Figure S46: ^{1}H spectrum of the reaction mixture for 2-butyne-1,4-diol (**1p**) hydrogenation to (*Z*)-2-butene-1,4-diol (**2p**).

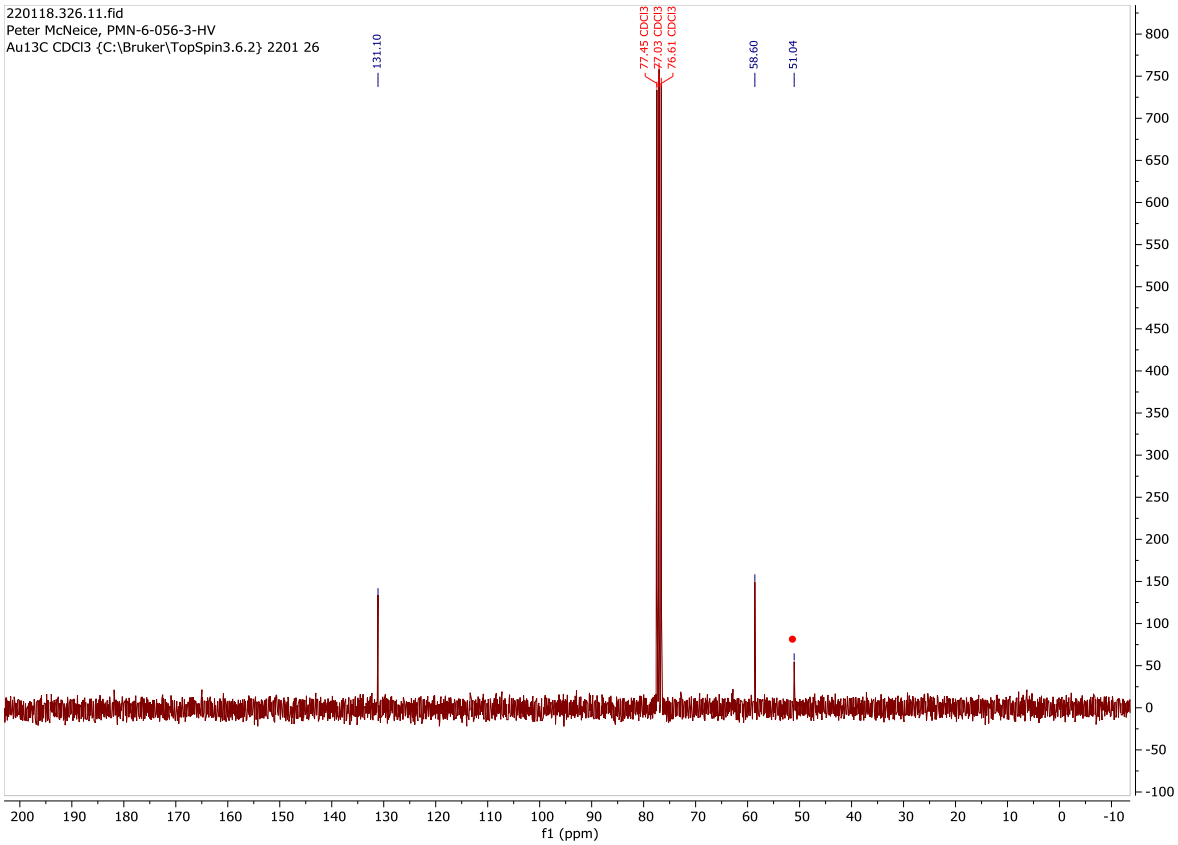

Figure S47: ^{13}C spectrum of the reaction mixture for 2-butyne-1,4-diol (**1p**) hydrogenation to (*Z*)-2-butene-1,4-diol (**2p**).

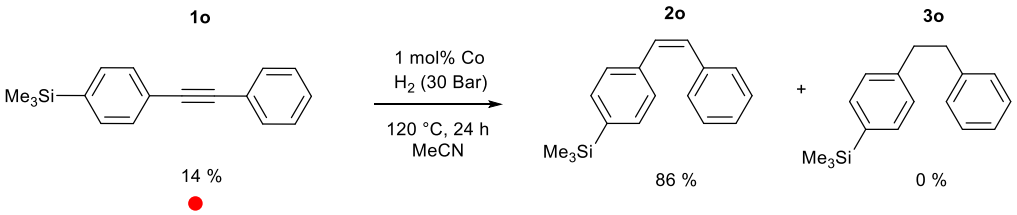

2o

^{1}H NMR (300 MHz, $CDCl_3$) δ = 7.36 – 7.29 (m, 2H), 7.28 – 7.08 (m, 7H), 6.60 – 6.45 (m, 2H), 0.23 (s, 1H), 0.20 (s, 9H). ^{13}C NMR (75 MHz, $CDCl_3$) δ = 140.4, 138.7, 138.5, 134.3, 131.5, 131.3, 129.9, 129.34, 129.25, 128.2, 0.0.

MS (EI, 70 eV): *m/z* (%) 252 (M^+, 63), 237 (100), 179 (9), 178 (21) 165 (5) 118 (7), 105 (5), 59 (6).

Literature characterisation[12]

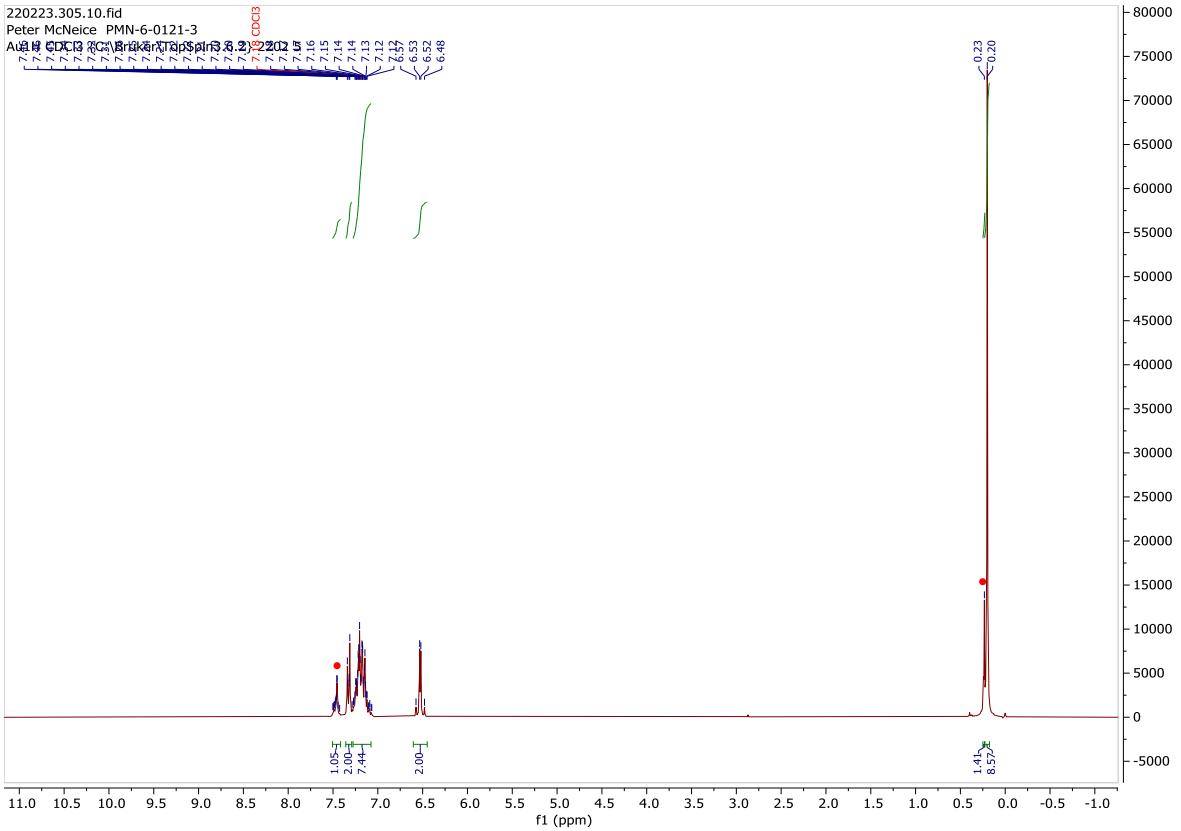

Figure S48: ^{1}H spectrum of the reaction mixture for 1-(2-phenylethynyl)-4-(trimethylsilyl)benzene (**1o**) hydrogenation to 1-[(1*Z*)-2-phenylethenyl]-4-(trimethylsilyl)benzene (**2o**).

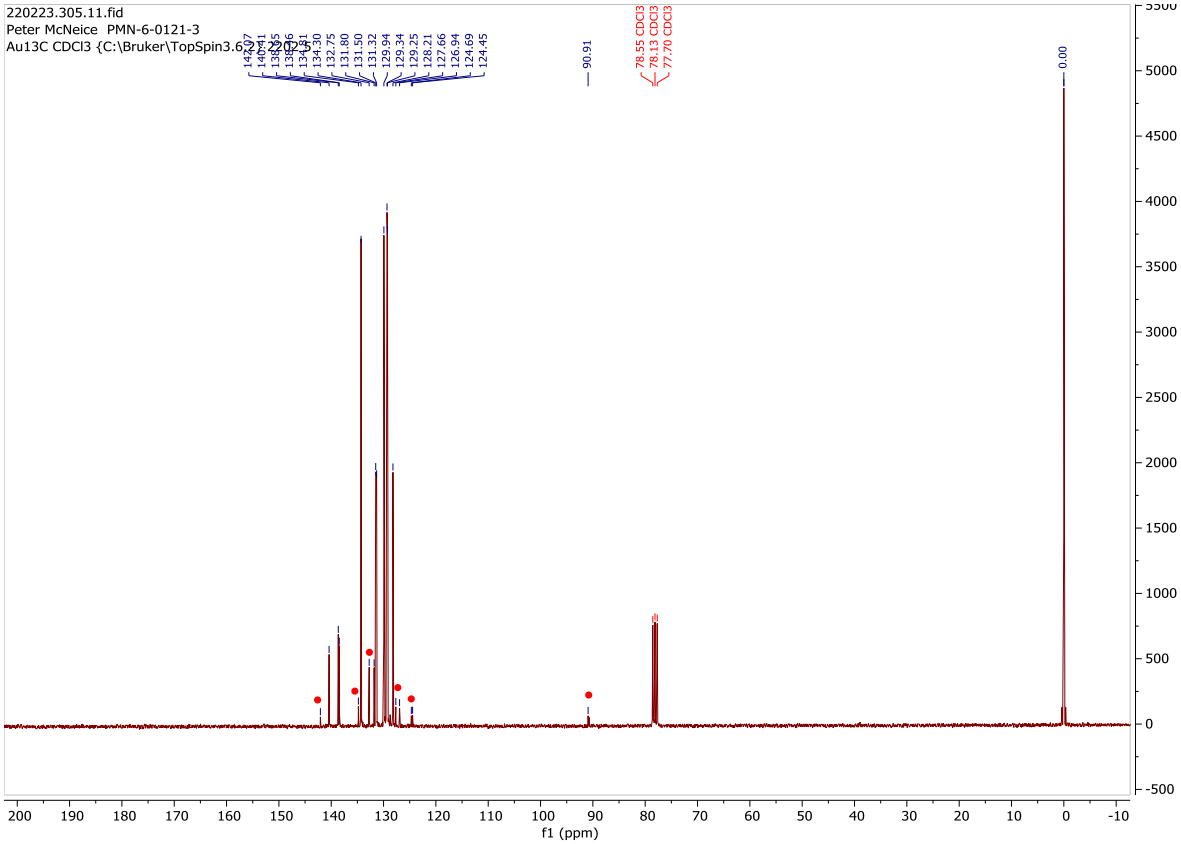

Figure S49: ^{13}C spectrum of the reaction mixture for 1-(2-phenylethynyl)-4-(trimethylsilyl)benzene (**1o**) hydrogenation to 1-[(1*Z*)-2-phenylethenyl]-4-(trimethylsilyl)benzene (**2o**).

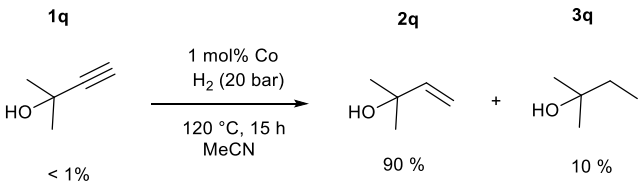

Structure **2q** was not analysed via NMR due to its volatility. Conversion and yield were determined using GC-FID with dodecane as an internal standard compared to commercial compounds.

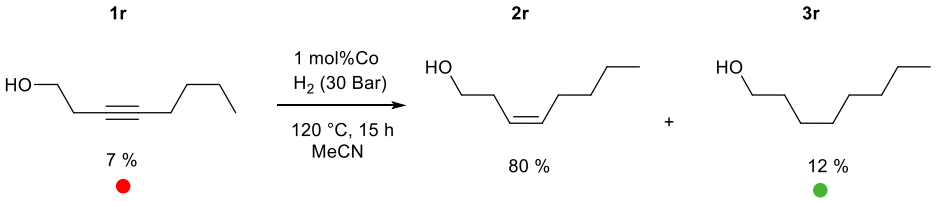

2r

^{1}H NMR (400 MHz, $CDCl_3$) δ = 5.60-5.53 (m, 1H), 5.42 – 5.32 (m, 1H), 3.64 (t, *J* = 8.0, 2H), 2.39 – 2.29 (m, 2H), 2.10 – 2.03 (m, 2H), 1.53 – 1.19 (m, 4H), 0.91 (dq, *J* = 7.0, 4.3, 3H). ^{13}C NMR (75 MHz, $CDCl_3$) δ = 133.4, 124.99, 62.3, 31.9, 30.8, 27.1, 22.3, 13.9.

MS (EI, 70 eV): *m/z* (%) 128 (M^+, 1), 110 (21), 82 (27), 81 (81), 79 (11), 69 (23), 68 61), 67 (50), 56 (25), 55 (100).

Literature characterisation[16]

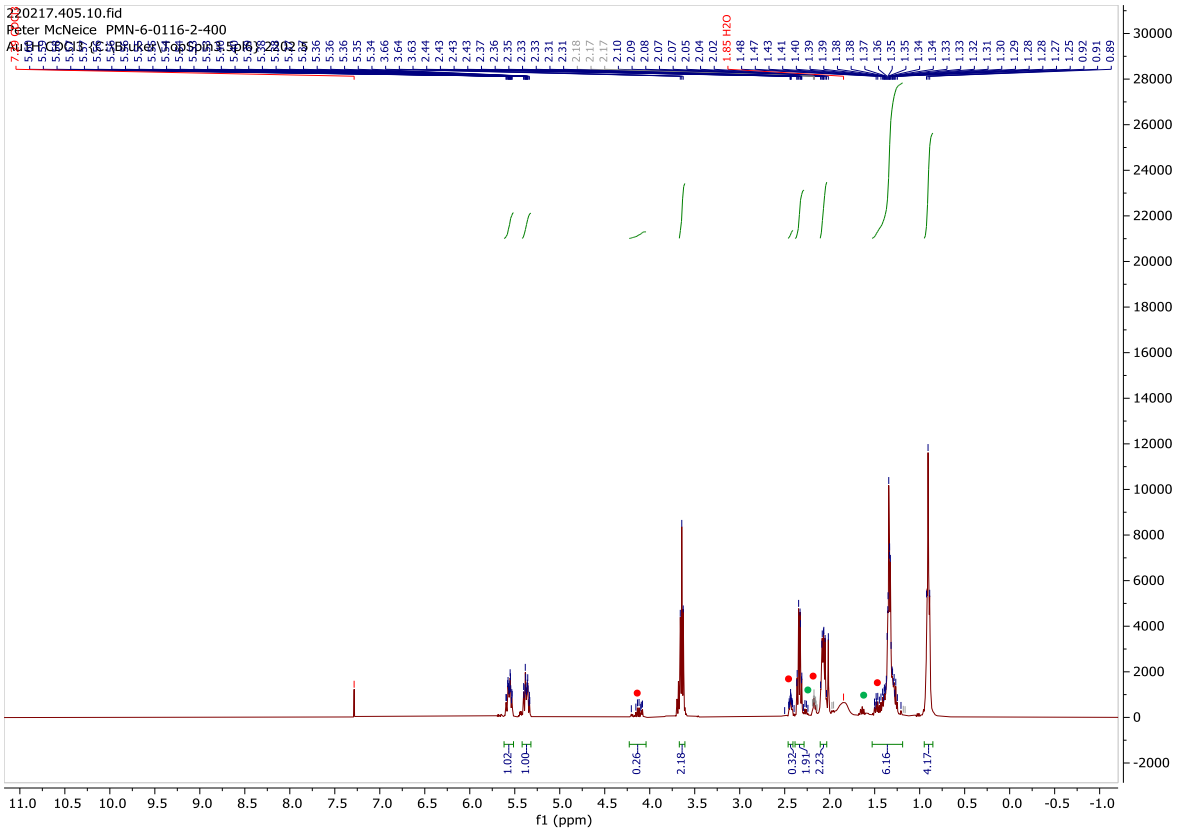

Figure S50: ^{1}H spectrum of the reaction mixture for 3-octyn-1-ol (**1r**) hydrogenation to (*Z*)-3-octen-1-ol (**2r**).

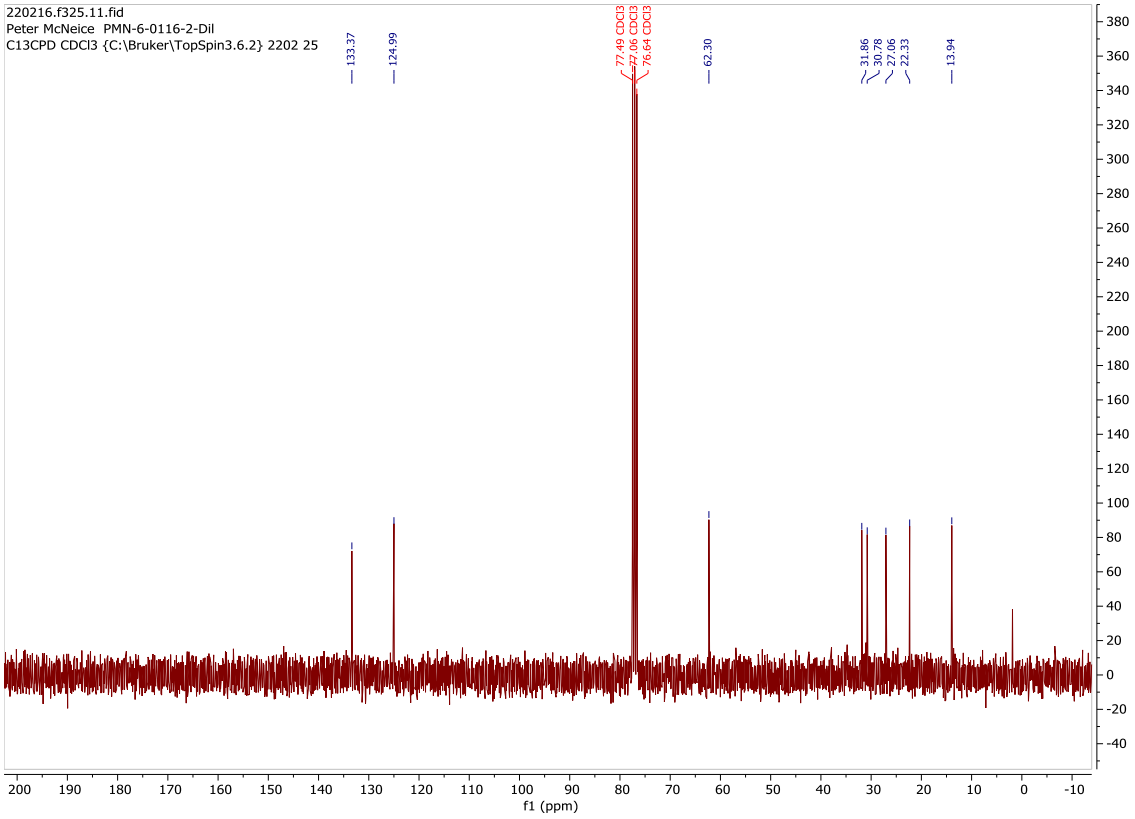

Figure S51: ^{13}C spectrum of the reaction mixture for 3-octyn-1-ol (**1r**) hydrogenation to (*Z*)-3-octen-1-ol (**2r**).

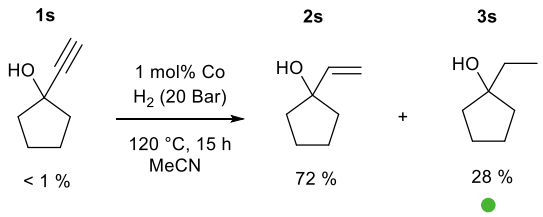

2s

^{1}H NMR (300 MHz, $CDCl_3$) δ = 6.04 (dd, *J* = 17.3, 10.7, 1H), 5.29 (dd, *J* = 17.2, 1.4, 1H), 5.05 (dd, *J* = 10.7, 1.4, 1H), 2.00 – 1.20 (m, 15H). ^{13}C NMR (75 MHz, $CDCl_3$) δ = 144.5, 111.1, 40.3, 33.9, 23.7. ^{13}C NMR (75 MHz, $CDCl_3$) δ = 144.5, 111.1, 82.2, 40.3, 33.9, 23.9, 23.7.

The proton aliphatic region contains too many protons due to overlap with the over-hydrogenated product. These have not been precisely assigned.

MS (EI, 70 eV): *m/z* (%) 112 (M^+, 7), 97 (62), 84 (38), 83 (100), 70 (25), 68 (48), 55 (74).

Literature Characterisation[17]

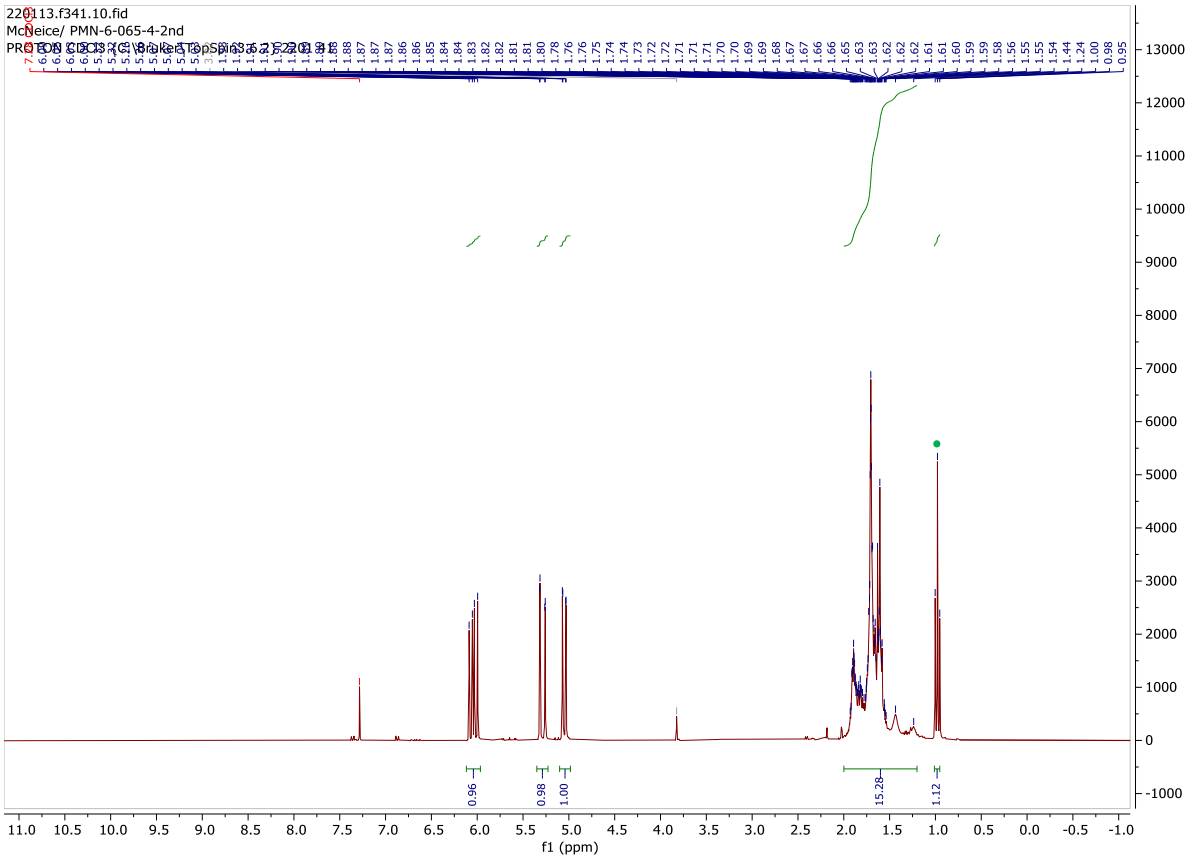

Figure S52: ^{1}H spectrum of the reaction mixture for 1-ethynylcyclopropanol (**1s**) hydrogenation to 1-vinylcyclopropanol (**2s**).

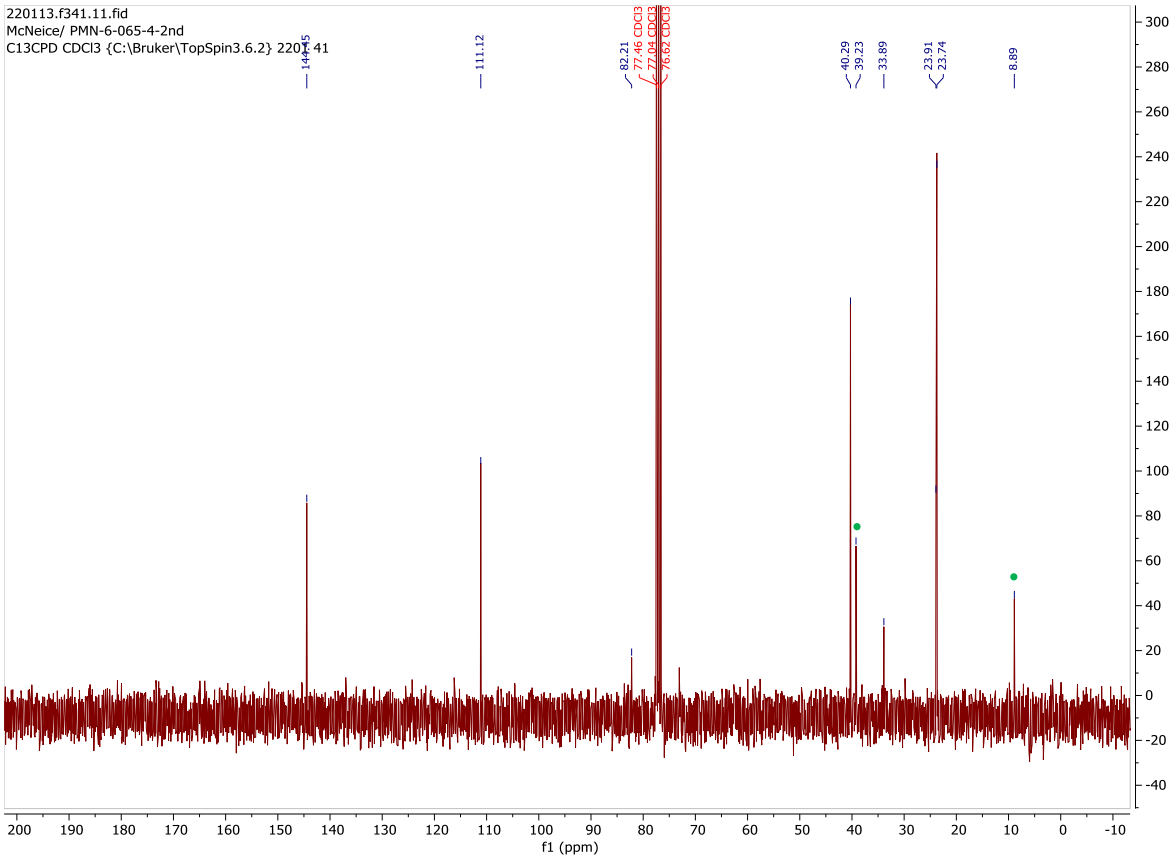

Figure S53: ^{1}H spectrum of the reaction mixture for 1-ethynylcyclopropanol (**1s**) hydrogenation to 1-vinylcyclopropanol (**2s**).

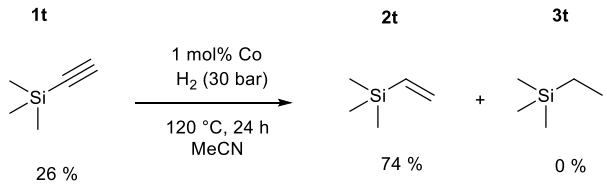

Structure **2t** was not analysed via NMR due to its volatility. Conversion and yield were determined using GC-FID with dodecane as an internal standard compared to commercial compounds.

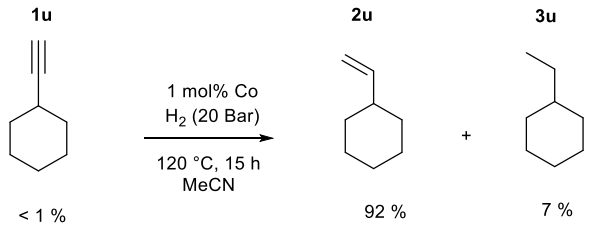

Structure **2u** was not analysed via NMR due to its volatility. Conversion and yield were determined using GC-FID with dodecane as an internal standard compared to commercial compounds.

MS (EI, 70 eV): *m/z* (%) 110 (M^+, 22), 95 (22), 81 (100), 79 (10), 67 (60), 54 (20).

Literature Characterisation[18]

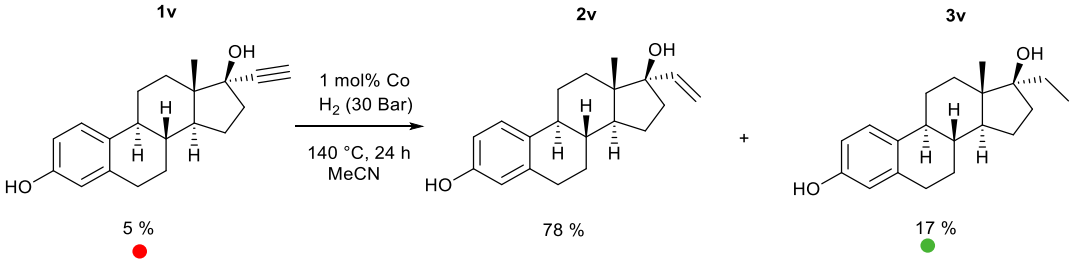

3v

^{1}H NMR (300 MHz, MeOD) δ = 7.05 (d, *J* = 8.5, 1H), 6.54 (dd, *J* = 8.4, 2.6, 1H), 6.48 (d, *J* = 2.7, 1H), 6.11 (dd, *J* = 17.3, 10.9, 1H), 5.23 – 5.06 (m, 2H), 2.89 – 2.66 (m, 3H), 2.25 (q, *J* = 6.1, 1H), 2.11 – 1.92 (m, 5H), 1.92 – 1.82 (m, 2H), 1.78 – 1.35 (m, 10H), 1.35 – 1.09 (m, 3H), 0.94 (s, 3H). ^{13}C NMR (75 MHz, MeOD) δ = 154.9, 143.2, 137.4, 131.0, 125.8, 114.8, 112.5, 110.9, 83.7, 48.8, 46.4, 43.8, 39.7, 35.0, 32.0, 29.4, 27.4, 26.2, 22.9, 13.4.

The proton aliphatic regions contain too many protons due to overlap with the alkyne and over-hydrogenated product. These have not been precisely assigned.

MS (EI, 70 eV): *m/z* (%) 298 (M^+, 30), 296 (33), 228 (41), 226 (28), 213 (100).

Literature Characterisation[19]

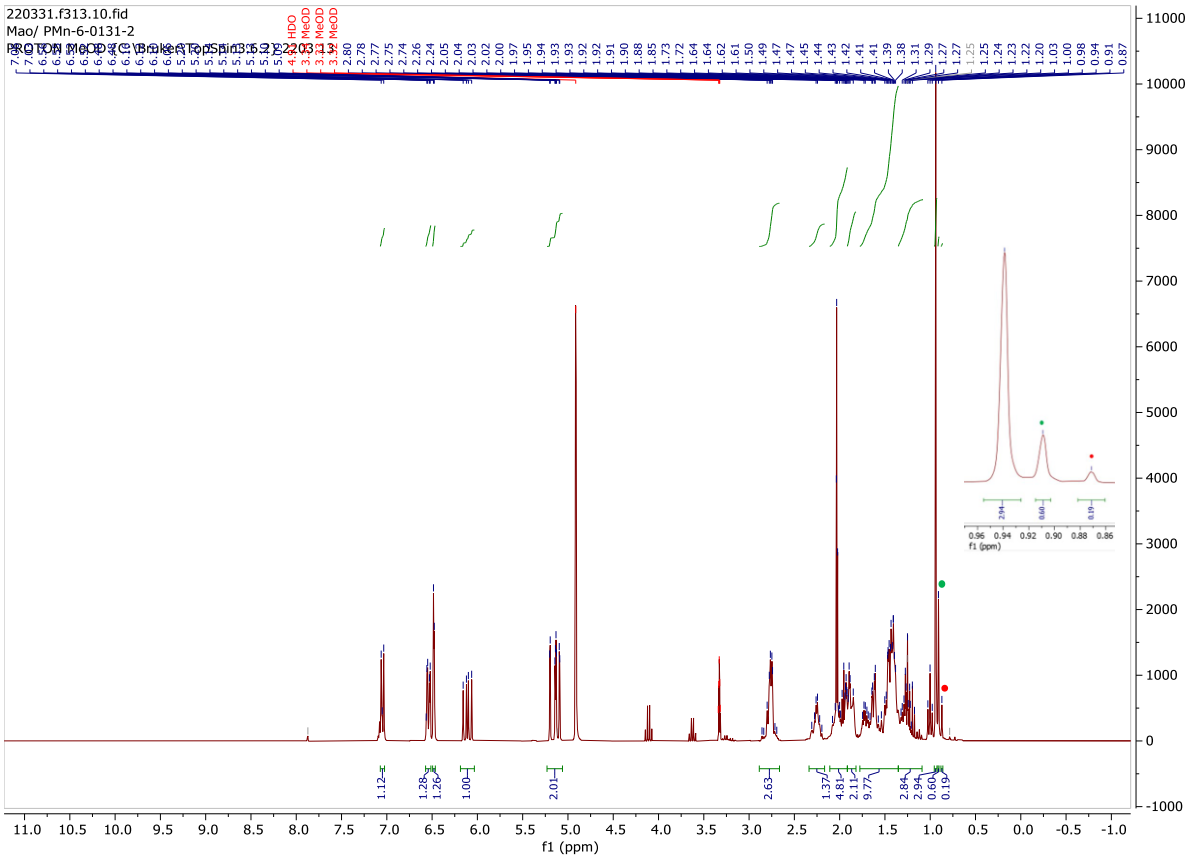

Figure S54: ^{1}H spectrum of the reaction mixture for 19-nor-17α-pregna-1,3,5(10)-trien-20-in-3,17-diol (17α-ethynylestradiol, **1v**) hydrogenation to 19-nor-17α-pregna-1,3,5(10)-tetraen-20-in-3,17-diol (17α-vinylestradiol, **2v**).

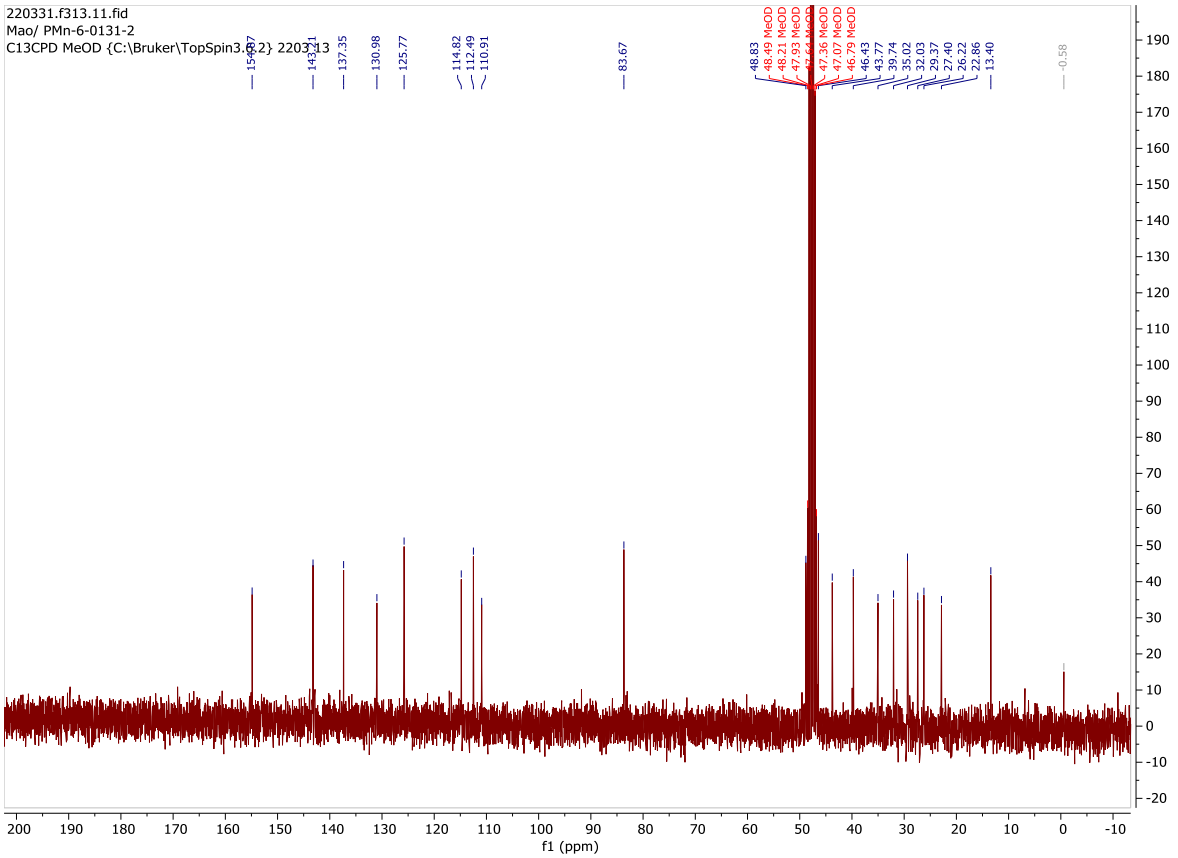

Figure S55: ^{13}C spectrum of the reaction mixture for 19-nor-17α-pregna-1,3,5(10)-trien-20-in-3,17-diol (17α-ethynylestradiol, **1v**) hydrogenation to 19-nor-17α-pregna-1,3,5(10)-tetraen-20-in-3,17-diol (17α-vinylestradiol, **2v**).

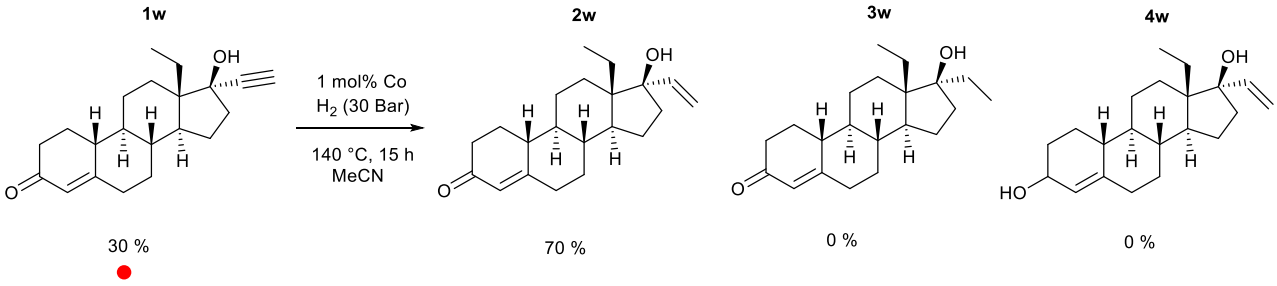

2w

^{1}H NMR (300 MHz, $CDCl_3$) δ = 5.97 (dd, *J* = 17.3, 10.7, 1H), 5.74 (s, 1H), 5.09 – 4.94 (m, 2H), 2.45 – 1.70 (m, 14H), 1.60 – 1.17 (m, 9H), 1.04 – 0.85 (m, 7H), 0.75 – 0.65 (m, 1H). ^{13}C NMR (75 MHz, $CDCl_3$) δ = 200.0, 167.0, 143.7, 124.4, 111.6, 85.6, 50.2, 49.1, 47.5, 42.4, 40.8, 36.4, 36.3, 35.5, 30.8, 28.1, 26.5, 26.2, 22.8, 20.1, 9.8.

The proton and carbon aliphatic regions contain too many protons due to overlap with the alkyne. These have not been precisely assigned.

HRMS (ESI): *m/z* calc for $C_{21}H_{30}O_2$: 314.22403 (M^+), found: 314.22407 (M^+).

Similar Literature characterisation:[20]

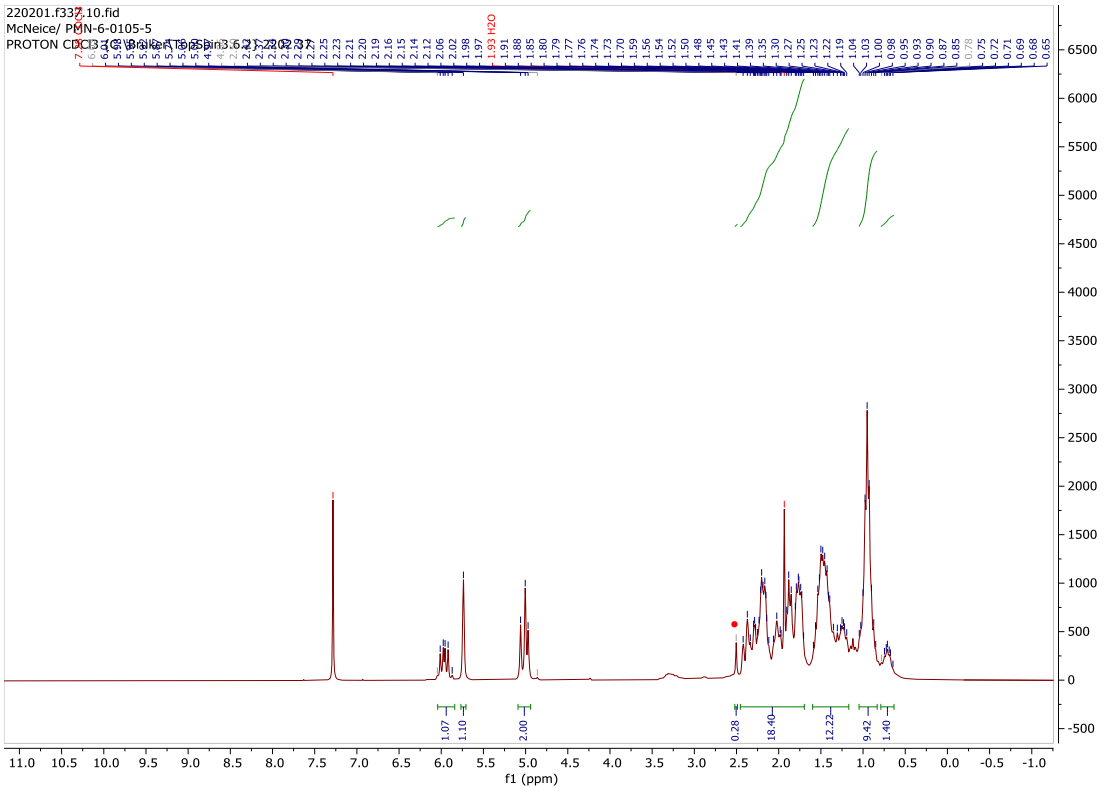

Figure S56: ^{1}H spectrum of the reaction mixture for (−)-17*β*-Hydroxy-18-methyl-19-nor-17*α*-pregn-4-en-20-in-3-on (Levonorgestrel, **1w**) hydrogenation to 18,19-Dinorpregna-4,20-dien-3-one, 13-ethyl-17-hydroxy-, (17α)-(±)- (9CI) (**2w**).

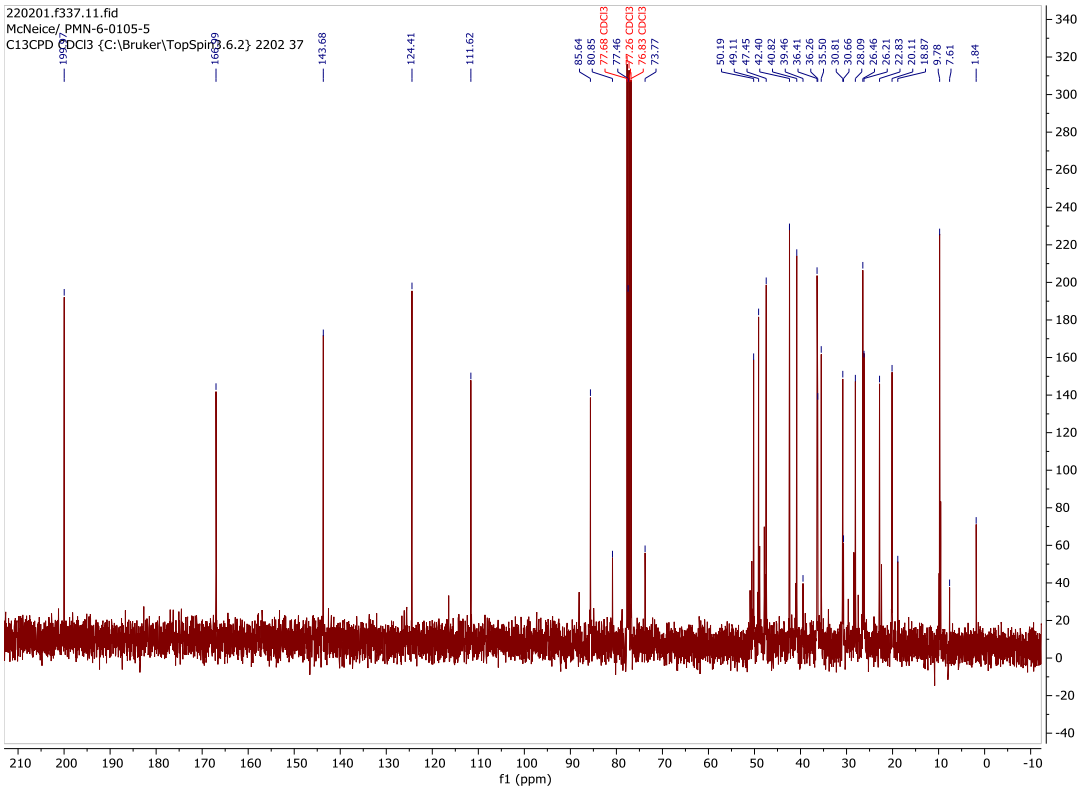

Figure S57: ^{13}C spectrum of the reaction mixture for (−)-17*β*-Hydroxy-18-methyl-19-nor-17*α*-pregn-4-en-20-in-3-on (Levonorgestrel, **1w**) hydrogenation to 18,19-Dinorpregna-4,20-dien-3-one, 13-ethyl-17-hydroxy-, (17α)-(±)- (9CI) (**2w**).

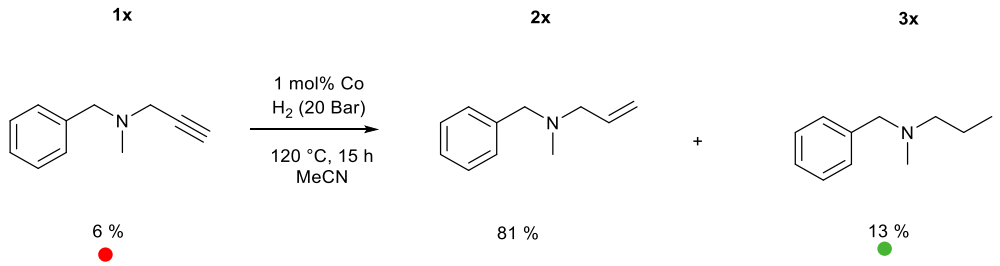

2x

^{1}H NMR (300 MHz, $CDCl_3$) δ = 7.37 – 7.32 (m, 5H), 5.94 (ddt, *J* = 17.2, 10.2, 6.4, 1H), 5.27 – 5.14 (m, 2H), 3.52 (s, 2H), 3.06 (dt, *J* = 6.5, 1.3, 2H), 2.22 (s, 3H). ^{13}C NMR (75 MHz, $CDCl_3$) δ = 137.3, 134.2, 127.3, 126.4, 125.1, 115.6, 59.9, 58.8, 40.3.

The proton aromatic region contains too many protons due to overlap with the alkyne and the over-hydrogenated product. These have not been precisely assigned. MeCN is visible at 1.98 ppm

Literature Characterisation[21]

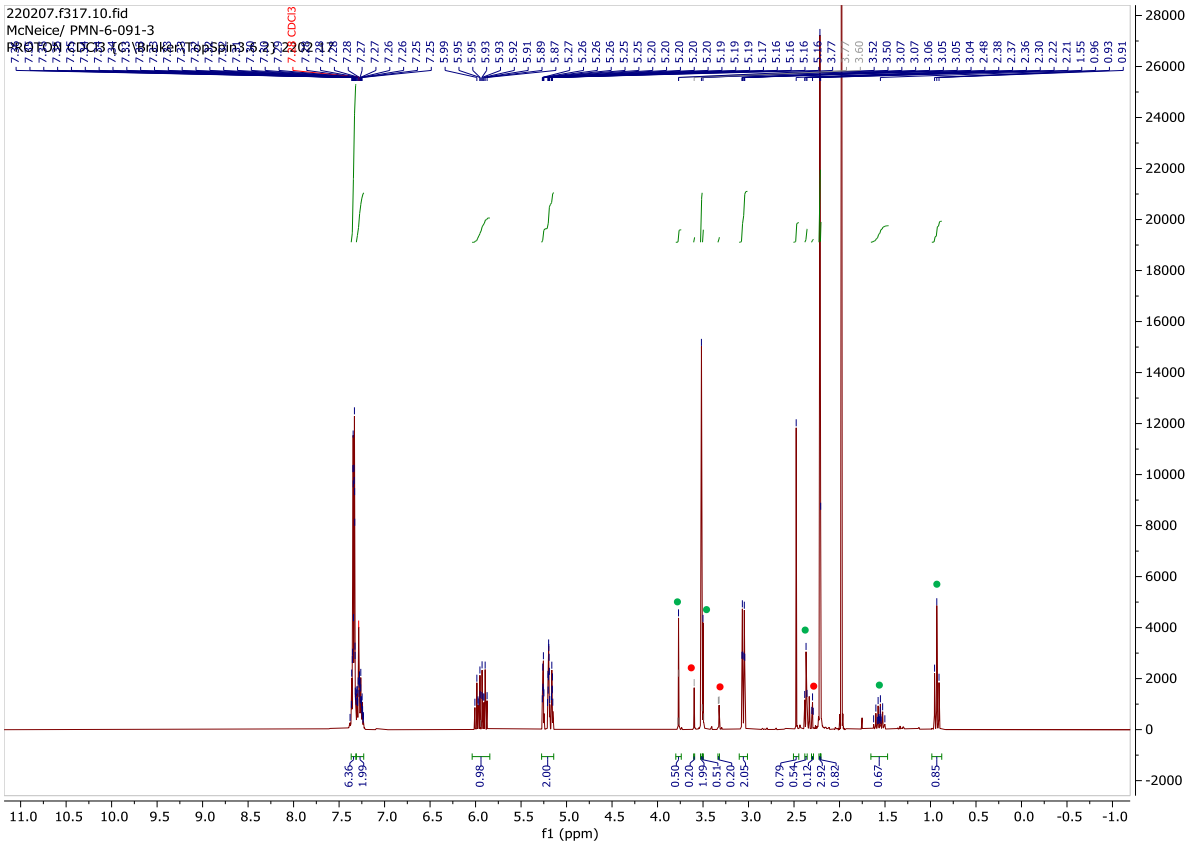

Figure S58: ^{1}H spectrum of the reaction mixture for *N*-ethynyl-*N*-methylbenzenemethanamine (**1x**) hydrogenation to *N*-ethenyl-*N*-methylbenzenemethanamine (**2x**).

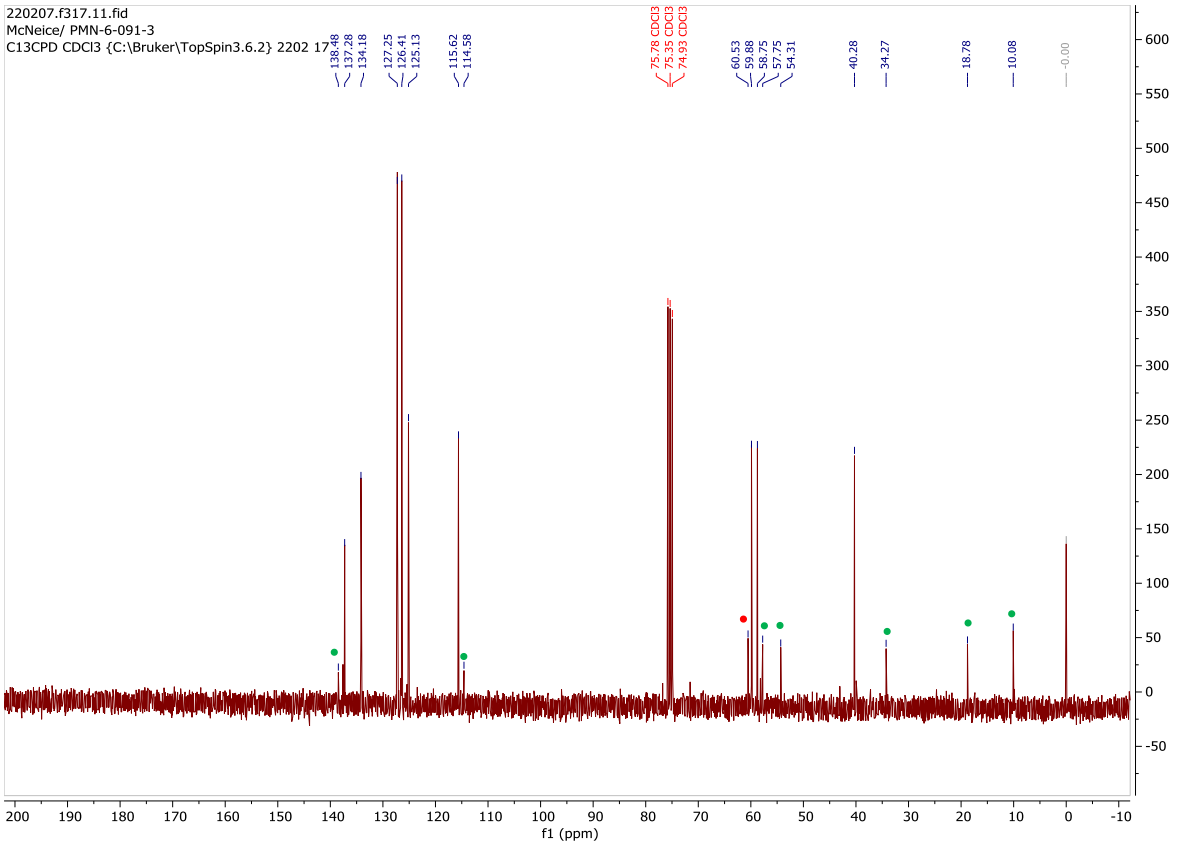

Figure S59: ^{13}C spectrum of the reaction mixture for *N*-ethynyl-*N*-methylbenzenemethanamine (**1x**) hydrogenation to *N*-ethenyl-*N*-methylbenzenemethanamine (**2x**).

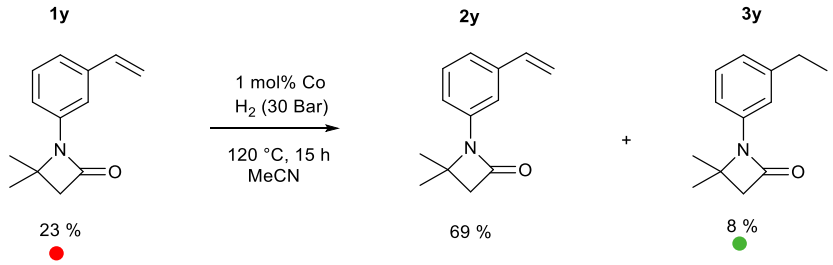

2y

^{1}H NMR (300 MHz, $CDCl_3$) δ = 7.42 – 7.39 (m, 1H), 7.32 – 7.11 (m, 4H), 6.70 (dd, *J* = 17.6, 10.9, 1H), 5.78 (dd, *J* = 17.5, 0.9, 1H), 5.28 (dd, *J* = 10.8, 0.9, 1H), 3.44 (s, 2H), 1.41-1.40 (m, 6H). ^{13}C NMR (75 MHz, $CDCl_3$) δ = 171.1, 138.96, 138.6, 136.4, 129.3, 127.4, 121.6, 115.8, 114.8, 114.0, 53.3, 49.8, 21.4.

HRMS (ESI): *m/z* calc for $C_{13}H_{15}NO$: 201.11482 (M^+), found: 201.11538 (M^+).

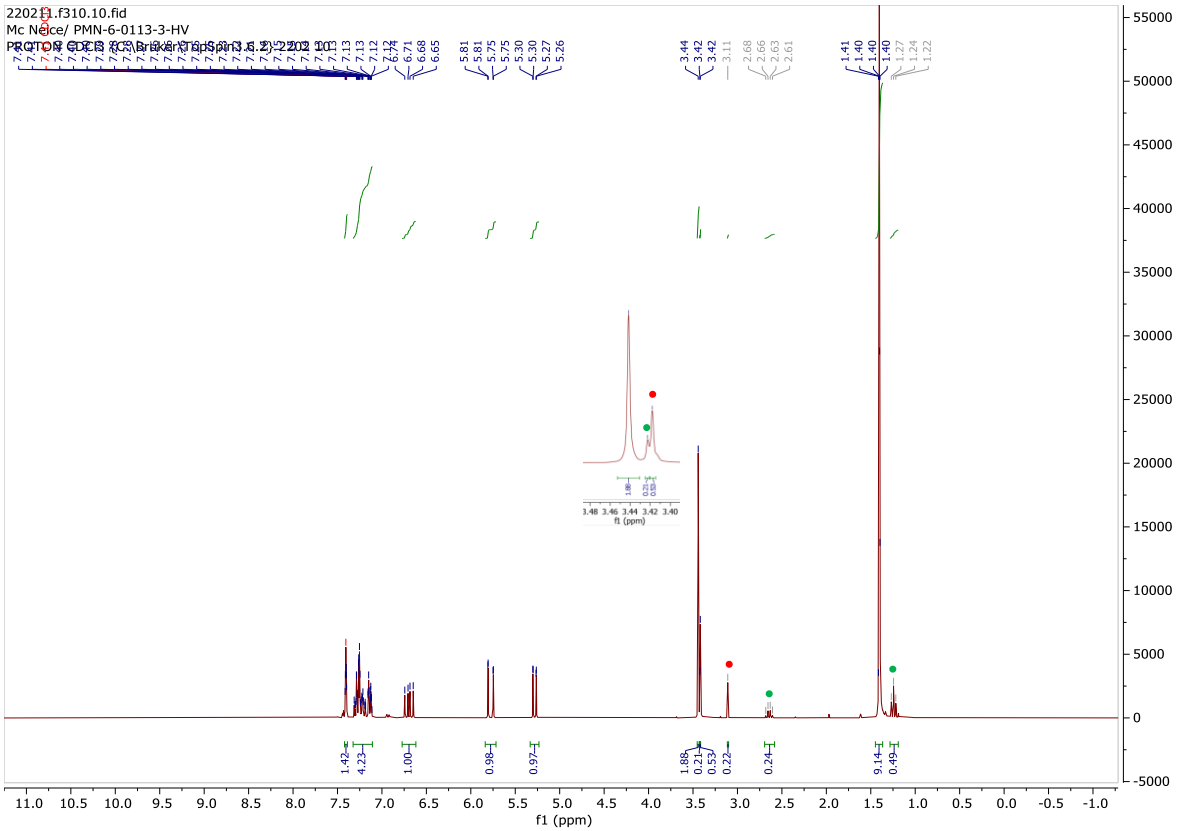

Figure S60: ^{1}H spectrum of the reaction mixture for 1-(3-ethynylphenyl)-3,3-dimethyl-2-azetidinone (**1y**) hydrogenation to 1-(3-ethenylphenyl)-3,3-dimethyl-2-azetidinone (**2y**).

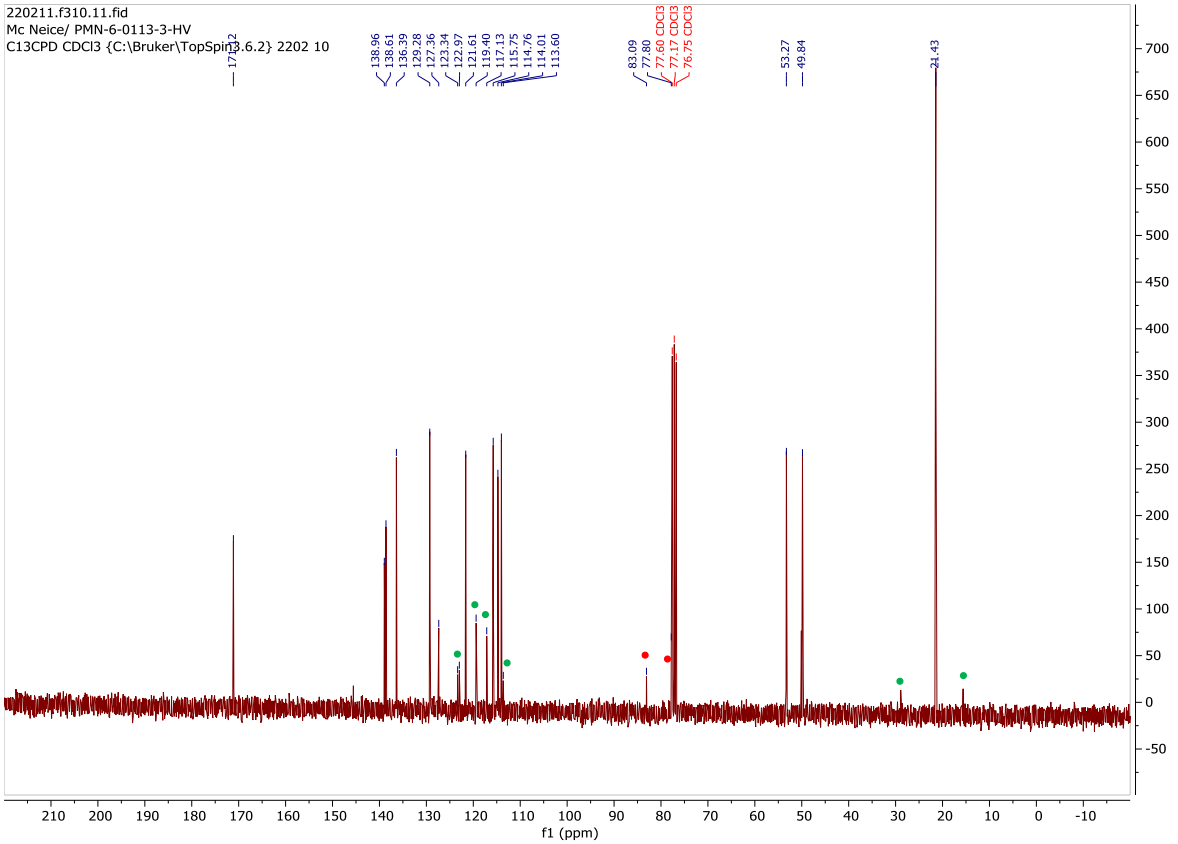

Figure S61: ^{13}C spectrum of the reaction mixture for 1-(3-ethynylphenyl)-3,3-dimethyl-2-azetidinone (**1y**) hydrogenation to 1-(3-ethenylphenyl)-3,3-dimethyl-2-azetidinone (**2y**).

S7 References

[1] D. H. Pearson, C. C. Ahn, B. Fultz, *Phys. Rev. B: Condens. Matter*, 1993, **47**, 8471-8478.
[2] G. M. Arzac, T. C. Rojas, A. Fernández, *ChemCatChem*, 2011, **3**, 1305-1313.
[3] H. Wang, T. Maiyalagan, X. Wang, *ACS Catal.*, 2012, **2**, 781-794.
[4] L. He, F. Weniger, H. Neumann, M. Beller, *Angew. Chem. Int. Ed.*, 2016, **55**, 12582-12594.
[5] I. G. Zenkevich, V. I. Babushok, P. J. Linstrom, E. White, S. E. Stein, *J. Chromatog. A*, 2009, **1216**, 6651-6661.
[6] T. Schabel, C. Belger, B. Plietker, *Org. Lett.*, 2013, **15**, 2858-2861.
[7] D. Srimani, Y. Diskin-Posner, Y. Ben-David, D. Milstein, *Angew. Chem. Int. Ed.*, 2013, **52**, 14131-14134.
[8] E. Alacid, C. Nájera, *J. Org. Chem.*, 2008, **73**, 2315-2322.
[9] T. M. Gøgsig, L. S. Søbjerg, A. T. Lindhart, K. L. Jensen, T. Skrydstrup, *J. Org. Chem.*, 2008, **73**, 3404-3410.
[10] L. Chu, F.-L. Qing, *Org. Lett.*, 2010, **12**, 5060-5063.
[11] Z.-Q. Liu, L. Sun, J.-G. Wang, J. Han, Y.-K. Zhao, B. Zhou, *Org. Lett.*, 2009, **11**, 1437-1439.
[12] W. Li, X. Cui, K. Junge, A.-E. Surkus, C. Kreyenschulte, S. Bartling, M. Beller, *ACS Catal*., 2019, **9**, 4302-4307.
[13] Y. Zhao, Q. Liu, J. Li, Z. Liu, B. Zhou, *Synlett*., 2010, **12**, 1870-1872.
[14] AIST Database, https://sdbs.db.aist.go.jp/sdbs/cgi-bin/landingpage?sdbsno=4007, (Accessed 18.02.22).
[15] S. Rej, M. Madasu, C.-S. Tan, C.-F. Hsia, M. H. Huang, *Chem. Sci.*, 2018, **9**, 2517-2524.
[16] R. B. Mitra, G. B. Reddy, *Synthesis*, 1989, **9**, 694-698.
[17] U. Albrecht, P. Langer, *Tetrahedron*, 2007, **63**, 4648-4654.
[18] S. Nagahara, K. Maruoka, Y. Doi, H. Yamamoto, *Chem. Lett.*, 1990, **19**, 1595-1598.
[19] Y. Yabe, T. Yamada, S. Nagata, Y. Sawama, Y. Monguchi, H. Sajiki, *Adv. Synth. Catal.*, 2012, **354**, 1264-1268.
[20] W.-F. Tian, Y.-Q. He, X.-R. Song, H.-X. Ding, J. Ye, W.-J. Guo, Q. Xiao, *Adv. Synth. Catal*., 2020, **362**, 1032-1038.
[21] A. R. Abreu, I. Costa, C. Rosa, L. M. Ferreira, Ana Lourenço, P. P. Santos, *Tetrahedron*, 2005, **61**, 11986-11990.